Dissertation
submitted to the
Combined Faculties for the Natural Sciences and for Mathematics
of the Ruperto-Carola University of Heidelberg, Germany
for the degree of
Doctor of Natural Sciences

presented by

MSc. Julian Peter Sefrin

Born in: Zweibrücken, Germany

Oral-examination: March 30th, 2017

Sensitization of tumor cells for T cell mediated eradication through targeted delivery of virus-derived immunogenic peptide epitopes

Referees: Prof. Dr. Rienk Offringa

Prof. Dr. Viktor Umansky

Table of contents

1. List of figures

2. Abbreviations

4-1BB	Tumor necrosis factor receptor superfamily member 9
Ab	Antibody
ADCC	Antibody-dependent cellular cytotoxicity
APC	Antigen presenting cell
ATPP	Antibody-targeted pathogen-derived peptide
B-ALL	B cell acute lymphoblastic leukemia
Bcl-2	B cell lymphoma-2 protein
Bcl-XL	B cell lymphoma-extra large protein
BiTE	Bispecific T cell engager
BMLF1	BamHI-M leftward reading frame 1
CAR-T	Chimeric antigen receptor T cell
CCR	Chemokine receptor
CD	Cluster of differentiation
CD40L	CD40 ligand
CD95L	CD95 ligand
CDC	Complement-dependent cellular cytotoxicity
CDCP1	CUB domain-containing protein 1
CDR	Complementarity determining region
CEA	Carcinoembryonic antigen
cFLIP	Cellular FLICE-inhibitory protein
C_H	Constant domain of the antibody heavy chain
C_L	Constant domain of the antibody light chain
CMV	Cytomegalovirus
CTL	Cytotoxic T lymphocyte
CTLA-4	Cytotoxic T lymphocyte-associated protein 4
DAMPs	Danger-associated molecular patterns
DC	Dendritic cell
DMF	Dimethylformamide
DMSO	Dimethyl sulfoxide

DNA	Deoxyribonucleic acid
EBV	Epstein-Barr virus
EDTA	Ethylenediaminetetraacetic acid
EGF	Epidermal growth factor
EGFR	Epidermal growth factor receptor
ELISA	Enzyme-linked immunosorbent assay
ELISPOT	Enzyme-Linked ImmunoSpot
EMT	Epithelial-mesenchymal transition
EpCAM	Epithelial cell adhesion molecule
ER	Endoplasmic reticulum
ERAP1/2	(ER)-associated aminopeptidases 1 or 2
ET-ratio	Effector-to-target ratio
Fab’	Fragment antigen binding
FACS	Fluorescence-activated cell screening/sorting
FBS	Fetal bovine serum
Fc	Fragment crystallizable
FcRn	Neonatal Fc-receptor
FcγR	Fc-gamma receptor
FDA	Food and Drug Administration
FELASA	Federation of Laboratory Animal Science Associations
FGF	Fibroblast growth factor
FRET	Fluorescence resonance energy transfer
GITR	Glucocorticoid-induced TNFR-related protein
GM-CSF	Granulocyte macrophage colony-stimulating factor
GvHD	Graft-versus-host disease
HER2	Human epidermal growth factor receptor 2
HLA	Human leukocyte antigen
HMGB1	High mobility group box 1
HPV	Human papillomavirus
i.p.	Intraperitoneal
i.v.	Intravenous

IDO	Indolamine-2,3-dioxygenase
IFNα	Interferon-α
IFNγ	Interferon-γ
IgG	Immunoglobulin G
IL	Interleukin
INF	Influenza A
iNOS	Inducible nitric oxide synthetase
LAG3	Lymphocyte-activation gene 3
LCL	Lymphoblastoid cell line
LCMV	Lymphochoriomeningitis Virus
LDH	Lactate dehydrogenase
LMP2	Latent membrane protein 2
mAb	Monoclonal antibody
MAGE	Melanoma-associated antigen
MCSP	Melanoma-associated chondroitin sulfate proteoglycan
MDSC	Myeloid-derived suppressor cell
MED	Minimum effective dose
MFI	Mean fluorescence intensity
MHC	Major histocompatibility complex
mRNA	Messenger ribonucleic acid
NK	Natural killer
NO	Nitric oxide
NP	Nucleoprotein
NSCLC	Non-small cell lung cancer
OVA	Ovalbumin
OX40	Tumor necrosis factor receptor superfamily, member 4
PAMPs	Pathogen-associated molecular patterns
PBMC	Peripheral blood mononuclear cell
PBS	Phosphate-buffered saline
PD1	Programmed cell death protein 1
PD-L1	Programmed cell death ligand 1

PDGF	Platelet-derived growth factor
PGE2	Prostaglandin E2
PI3K	Phosphatidylinositol-3-kinase
pRB	Retinoblastoma protein
PRR	Pattern recognition receptor
RAG-1/2	Recombinase activating gene 1 or 2
RAS	Rat sarcoma viral oncogene homolog
ROS	Reactive oxygen species
s.c.	Subcutaneous
scFv	Single-chain variable fragment
SPDP	N-Succinimidyl 3-(2-pyridyldithio)-propionate
TAM	Tumor-associated macrophage
TAP	Transporter associated with antigen processing
TCR	T cell receptor
TGFβ	Tumor growth factor-β
Th1	Type 1 T helper cell
Th17	Type 17 T helper cell
Th2	Type 2 T helper cell
TIL	Tumor infiltrating lymphocyte
TIM3	T-cell immunoglobulin and mucin-domain containing-3
TNFα	Tumor necrosis factor-α
TRAIL	TNF-related apoptosis-inducing ligand
Treg	Regulatory T cell
TRP-2	Tyrosinase-related protein 2
VEGF	Vascular endothelial growth factor
V_H	Variable domain of the antibody heavy chain
V_L	Variable domain of the antibody light chain
wt	Wild type
XIAP	X-linked inhibitor of apoptosis protein
Zap70	Zeta-chain-associated protein kinase 70

3. Summary

The work presented in this thesis aimed at the development of antibody immunoconjugates for the delivery in tumor cells of highly immunogenic T cell epitopes that mediate the antigen-specific recognition by tumoricidal T cells. For this purpose, antibody-targeted pathogen-derived peptides (ATPPs) were generated by conjugating immunodominant, cysteine-containing MHC class I peptides from Epstein-Barr or Influenza A virus to tumor antigen-specific antibodies via a disulfide bond. The integral membrane protein CUB domain-containing protein 1 (CDCP1) was chosen as proof of concept target, as it is upregulated on various cancer types and known to efficiently internalize after antibody binding.

After binding to the target and subsequent internalization of ATPPs, fluorescence resonance energy transfer (FRET) imaging revealed that delivered peptides are released upon disulfide reduction in an early endosomal compartment, where they can be loaded into recycling MHC class I complexes. Transport of these MHC-peptide complexes to the cell surface triggers activation of human peptide-specific cytotoxic $CD8^+$ T cells as revealed by interferon-γ ELISA and ELISPOT. Moreover, peptide-specific $CD8^+$ T cells from human donors efficiently lysed ATPP-treated tumor cell lines of various cancer types in a target-dependent manner *in vitro*. Importantly, targeting of different tumor antigens (e.g. CD138) was equally efficient. The possibility to utilize various peptides with differing HLA-restrictions further highlights the broad applicability of the ATPP approach for T cell mediated targeting of cancer. The usage of a non-cleavable construct or an extended peptide that can not bind to MHC class I molecules additionally revealed the importance of disulfide-dependent peptide release and epitope delivery independent of the classical MHC class I antigen processing pathway.

In vivo, ATPPs mediated approximately 60% tumor growth inhibition of established, PD-L1 expressing MDA-MB231 xenografts after 3 weeks of treatment in combination with αPD1-mAb therapy and adoptive transfer of human, peptide-specific $CD8^+$ T cells in NOG mice. These data indicate the potential of ATPPs as novel immunotherapeutic agents, which can be employed to redirect pre-existing virus-specific memory T cells against cancer. Since the immune response will be directed against an exogenous, viral antigen, ATPP therapy reduces the risk for autoimmune side effects as observed with other immunotherapies. Furthermore, the use of highly

immunogenic target epitopes circumvents the limitations of the T cell repertoire directed against tumor-associated auto-antigens. The flexible design of ATPPs allows development of an off-the-shelf repertoire of immunoconjugates comprising immunogenic T cell epitopes encoded by highly prevalent pathogens and presented by various high frequency HLA allotypes, thereby providing a means for T cell mediated tumor targeting in a broad patient population.

4. Zusammenfassung

Ziel dieser Doktorarbeit war die Evaluierung der Möglichkeit, immunogene, virale Peptide mittels tumorspezifischen Antikörpern in Krebszellen einzuschleusen, sodass diese durch virusspezifische, zytotoxische T Zellen erkannt und lysiert werden. Zu diesem Zweck wurden ATPP genannte (engl. antibody-targeted pathogen-derived peptides) Antikörper-Immunkonjugate hergestellt, indem immundominante, cysteinhaltige MHC-I Peptide aus dem Epstein-Barr oder Influenza A Virus über eine Disulfidbrücke an tumorspezifische Antikörper konjugiert wurden. Das Transmembranprotein CDCP1 (engl. CUB-domain-containing-protein-1) wurde als Zielantigen ausgewählt, da es in mehreren Krebsarten überexprimiert wird und weil es sehr schnell internalisiert nach Antikörperbindung.

Mittels Fluoreszenz-Resonanzenergietransfer (FRET)-basierter Bildgebung konnte gezeigt werden, dass die gekoppelten Peptide nach Bindung des ATPP Konjugats an das Antigen und folgender Internalisierung durch Reduktion der Disulfidbrücke in Endosomen freigesetzt werden. Dort binden die viralen Peptide an zelluläre MHC-I Moleküle. Im Folgenden werden diese Peptid-MHC Komplexe zur Zelloberfläche transportiert, wo sie von peptidspezifischen T Zellen erkannt werden können. Mittels Interferon-γ ELISA und ELISPOT wurde bewiesen, dass eine Behandlung mit ATPP zur Aktivierung von humanen, peptidspezifischen zytotoxischen T Zellen durch die entsprechenden Tumorzellen *in vitro* führt. Des Weiteren waren sowohl *in vitro* expandierte als auch frisch isolierte T Zellen aus humanem Blut in der Lage, ATPP behandelte Krebszellen von verschiedenen Tumorindikationen antigenabhängig zu lysieren. Dies konnte für verschiedene Zielantigene (z.B. CD138), als auch mit mehreren Peptiden mit unterschiedlichen HLA-Restriktionen gezeigt werden. Mithilfe eines nicht spaltbaren Konjugats wurde zudem die Notwendigkeit der disulfidabhängigen Spaltung aufgezeigt. Die Verwendung eines verlängerten Peptids, welches ohne intrazelluläre Prozessierung nicht auf MHC-I Komplexe geladen werden kann, bewies außerdem, dass die in den Endosomen freigesetzten Peptide nicht in den klassischen Weg der MHC-I abhängigen Antigenprozessierung eintreten.

Die *in vivo* Wirksamkeit der Immunkonjugate wurde anschließend im Tierversuch getestet. NOG Mäuse wurden subkutan mit der PD-L1 exprimierenden, humanen

Brustkrebszelllinie MDA-MB231 inokuliert und nach adoptivem Transfer von humanen peptidspezifischen T Zellen mit ATPP und αPD1 Antikörper behandelt, sobald die Tumore 70mm^3 erreicht hatten. Die Kombinationstherapie erzielte eine deutliche, ca. 60%ige Inhibition des Tumorwachstums nach 3 Wochen Behandlung. Diese Resultate suggerieren ein großes Potential des hier vorgestellten Ansatzes der Krebsimmuntherapie, welcher darauf abzielt, Tumorzellen mit bereits existierenden, virusspezifischen T-Gedächtniszellen zu bekämpfen. Dieses Konzept schließt somit die Entstehung von autoimmun assoziierten Nebenwirkungen aus, da die Immunantwort – im Gegensatz zu bestehenden Immuntherapien – gegen ein exogenes, virales Antigen gerichtet ist, welches zudem eine höhere Immunogenität als körpereigene Tumorantigene aufweist. Durch die Entwicklung von ATPP Konjugaten, welche mehrere Peptide von verschiedenen Viren mit hoher Seroprävalenz enthalten, die zudem an häufig vorkommende HLA Moleküle binden, könnte dieser Ansatz dem Großteil der Patienten zugänglich gemacht werden.

5. Introduction

5.1. Hallmarks of cancer development

Despite substantial advances in prevention, early diagnosis and therapy, as evidenced by a 23% drop in the cancer death rate from 1991 to 2012[1], cancer still remains one of the leading causes of death especially in developed countries[1,2]. In the United States about 1.7 million new cancer cases and 600,000 cancer-related deaths are assumed to be diagnosed in 2016[1], hence highlighting the need to further decipher the mechanisms of cancer formation and progression, in order to develop sophisticated treatment strategies.

In the last decades numerous molecular mechanisms underlying cancer development have been unraveled, with the major hallmark being genomic mutations. Especially functional disruption of tumor suppressor genes or hyperactivation of oncogenes plays a major role for cellular transformation. Accumulation and manifestation of these genetic variations eventually lead to alterations in cellular physiology and metabolism and acquisition of the hallmarks of cancer, as postulated by Hanahan and Weinberg[3,4].

The most obvious property of cancer cells involves their capacity to proliferate infinitely. While normal cells require mitogenic growth signals in order to grow and divide, tumor cells exhibit reduced dependence on exogenous growth stimulation, which can be achieved by upregulating growth receptors (such as epidermal growth factor receptor, EGFR) and/or production of growth factors (also by the tumor stroma) for autocrine stimulation[5-7]. Most importantly, mutations in oncogenic signaling molecules such as Rat sarcoma viral oncogene homolog (Ras) allow mitogenic downstream signaling without external stimuli[8,9]. On the other hand, evasion from growth suppressive mechanisms, e.g. downregulation of tumor growth factor-β (TGFβ) receptors, relieves the homeostatic growth control and further enhances cancer proliferation and cell cycle progression[10,11].

An important safeguard mechanism to prevent propagation of transformed cells represents the induction of apoptosis. Different pathways have evolved to sense cellular abnormality, such as excess DNA damage, hypoxia or oncogene hyperactivation, in turn triggering cell death of transformed cells[12,13]. Hence, incipient cancer cells must acquire abilities to evade apoptosis induction. Several

mechanisms have been unraveled, including upregulation of anti-apoptotic factors (such as the B cell lymphoma proteins Bcl-2, Bcl-XL), functional loss of pro-apoptotic molecules or apoptotic signaling components, as well as mutations in sensors of cellular transformation (e.g. p53)[12,14].

Having acquired growth signal autonomy, evasion/unresponsiveness to growth inhibitors and resistance to apoptosis, there is still another hurdle to take before tumor cells can grow infinitely. As revealed by Hayflick in 1997, cells have a limited replicative potential in culture[15]. At some point, accumulation of cellular stress due to reactive oxygen species (ROS) or oncogene activation leads to a state termed senescence that is induced by the activation of tumor suppressor genes, such as retinoblastoma protein (pRB) or p53[16,17]. After inactivation of these genes, cells will eventually progress until reaching the state of crisis, which ultimately limits their replicative potential[18,19]. This state bases on the progressive shortening of telomeres upon DNA replication until the point where the chromosomes end[20]. Unprotected telomeres eventually result in chromosomal fusions of their ends, in turn yielding karyotypic disorder and cell death. However, by acquiring expression of the gene telomerase, which is generally limited to stem cells, cancer cells counteract telomere shortening and prevent crisis induction[21,22].

As oxygen and nutrients supplied by the blood are essential for cell function and survival, neoplasms have to additionally acquire angiogenic ability, rendering it another important hallmark of cancer. Along this line, tumor cells trigger the release of pro-angiogenic factors (e.g. vascular endothelial growth factor, VEGF or fibroblast growth factor, FGF) within the microenvironment by either expressing them or inducing their release from stromal cells, while simultaneously downregulating inhibitors of angiogenesis such as thrombospondin-1[23,24].

The last and in most patients eventually lethal characteristic of cancer cells is their capability to invade the surrounding tissue and disseminate via the blood stream to generate metastasis in other organs. Enabling metastatic capacity is accompanied by the so-called epithelial-mesenchymal transition (EMT), which involves production of extracellular matrix proteases, loss of adhesion molecules such as E-cadherin and altered integrin expression, in turn allowing intravasation into the blood stream, traffic to distant sites, extravasation into the tissue and formation of new tumor tissue[25,26].

Besides the six mentioned and well-accepted hallmarks, four additional characteristics of cancer have been proposed and reviewed by Hanahan and

Weinberg[4]. In this respect, especially the finding that tumors employ mechanisms to evade recognition and/or destruction by the immune system has fostered the development of a novel, promising concept for the treatment of cancer: cancer immunotherapy.

5.2. Cancer immunosurveillance and immune tolerance

Although chronic inflammation is known as a risk factor for cancer development[27,28], immune cells also play a major role in the elimination of incipient cancer cells, as defined in the theory of cancer immunosurveillance[29-31].

In the late 1970s, Boon and colleagues have already proven the existence of antigens that can trigger immune rejection of mutagen-treated teratocarcinomas in C57BL/6 mice[32-34]. More detailed insights into the mechanisms of cancer immunosurveillance came from studies using mice that were genetically engineered to lack certain components of the immune system. For instance, abrogation of interferon-γ (IFNγ) signaling[35,36] or perforin[37,38] resulted in increased incidence of carcinogen-induced tumors. While IFNγ can upregulate major histocompatibility complexes (MHCs) on cancer cells[36], promote $CD4^+$ Th1 T helper cell and $CD8^+$ cytotoxic T cell generation as well as trigger cytocidal macrophage activity[39], perforin acts as an effector molecule in the cytolytic granules of natural killer (NK) and cytotoxic T cells[40,41].

On the cellular basis, the use of mice lacking the recombinase activating gene (RAG)-1 or RAG-2 revealed a major implication of lymphocytes in the prevention of sarcoma outgrowth following carcinogen encounter[36,42]. Since RAG-1 and -2 are indispensable mediators of somatic antigen receptor rearrangement in lymphocytes, RAG-deficient mice are unable to generate peripheral B cells, NKT cells as well as αβ or γδ T cells[43]. Follow up studies subsequently identified that αβ, γδ T cells[44,45], NKT, as well as NK cells[42] do all exert critical antitumor functions. While NK cells can detect tumor cells by a lack of MHC molecules and/or expression of stress-associated NKG2D ligands[46-48], NKT cells recognize glycolipid antigens presented by CD1d and mainly act by producing cytokines to promote differentiation and activation of surrounding immune cells[49]. In contrast, tumor cell recognition by γδ T cells has been attributed to NKG2D receptor as well as γδ T cell receptor (TCR) engagement, the latter of which is known to bind phospho-antigens[50]. The most investigated cell type, however, are αβ T cells, which recognize tumor antigen-

derived peptides, presented in the context of MHC. Initial human T cell responses against tumor cells could be observed *in vitro* by co-culturing patient-derived melanoma cell lines with autologous lymphocytes[51]. A few years later, the first human tumor antigen recognized by T cells could be identified in melanoma: MAGE-A1 (Melanoma associated antigen A1, aka MZ2-E)[52].

However, as cancers still arise, the process of immunosurveillance is not 100% efficient. The failure of this safeguard mechanism derives from immunological tolerance as a result of an initial lack of immunogenic antigens and the proper pro-inflammatory conditions. For instance, the emergence of so-called driver mutations in oncogenes (e.g. K-Ras) and tumor suppressor genes (e.g. p53) often comprise point mutations that suffice to initiate cellular transformation[9,53-55], while providing few possibilities for immunogenicity. In addition, an inflammatory response will only be initiated upon tumor growth when tumor necrosis and tissue invasion accompanied by destruction of the basement membrane promote the release of danger signals. For instance, released intracellular molecules, such as adenosine triphosphate (ATP), high mobility group box 1 (HMGB1), S100 or heat shock proteins serve as danger-associated molecular patterns (DAMPs) to activate pattern recognition receptors (PRRs) on resident immune cells, in turn initiating the inflammatory response[56]. Nevertheless, the lack of potent inflammatory stimuli, such as pathogen-associated molecular patterns (PAMPs) has led to the term “sterile inflammation” in this context and explains why a productive anti-tumor response may still not arise.

As mentioned, the antigen repertoire of cancer cells has also major implications for immune tolerance. Recent advances in the development of sophisticated screening technologies, such as mass-spectrometry, whole exome or RNA sequencing as well as bioinformatical epitope prediction and peptide-MHC binding algorithms have allowed the investigation of antigen epitopes presented by cancer cells and those specifically recognized by tumor infiltrating lymphocytes (TILs)[57,58]. Application of these technologies has revealed that primarily mutation-derived neo-epitopes trigger T cell-mediated cancer eradication and that these neo-antigen-specific T cells are exploited by cancer immunotherapies that rely on the endogenous T cell pool[59,60]. However, a high frequency of non-synonymous mutations and T cell neo-epitopes does not necessarily imply a productive T cell response. As evidenced in a recent study by Stronen et al. only 2 out of 126 predicted epitopes were recognized by TILs in melanoma patients[61]. Nevertheless, the authors showed that the naïve T cell

repertoire from healthy blood donors could mount an antigen-specific response against several of these epitopes, suggesting ineffective priming and/or tolerization of these T cells in the patient. Hence, there are several aspects of immune tolerance that counteract immune effector responses. While central tolerance relies on the absence of antigen-specific T cells due to thymic deletion of self-reactivity, peripheral tolerance results from a lack of co-stimulatory signals and tumor-mediated immunosuppression as explained further below.

5.3. The anti-cancer immune response, immunoediting and immune escape

The current understanding of anti-cancer immune responses involves virtually all cell types of the human immune system. In detail, an effective tumoricidal response is initiated by innate immune cells, which are activated by ligands in the tumor micro-environment, including type I IFNs, DAMPs like ATP or HMGB1, as well as stress-associated molecules like NKG2D ligands[62,63]. Activated macrophages or NK cells subsequently release pro-inflammatory cytokines and chemokines, which attract and favor the development of other immune cells, such as dendritic cells (DCs). After antigen uptake in the tumor DCs migrate to the lymph node, where they present processed antigens to $CD4^+$ T helper (Th) cells[64]. Upon engagement of their cognate TCRs and co-stimulation by DC-expressed CD80 and CD86 molecules $CD4^+$ T cells proliferate and differentiate into Th1 cells under the influence of DC-derived cytokines, such as Interleukin-12 (IL-12) and type I IFNs. Following activation, $CD4^+$ T cells upregulate CD40 ligand (CD40L) expression[65], in turn stimulating surrounding antigen-presenting cells (APCs) and promoting DC cross-presentation of internalized antigens on MHC class I molecules[66,67]. Interaction of $CD8^+$ T cells with their cognate MHC class I-peptide complex subsequently triggers the development and expansion of $CD8^+$ cytotoxic T lymphocytes (CTLs), which migrate to the tumor and exert their cytotoxic functions when encountering their target antigen.

Clinical evidence for an ongoing anti-cancer immune response in established tumors initially came from observations that the abundance of TILs correlates with good prognosis in melanoma patients[68,69]. Up to date numerous studies have attributed a prognostic value to TILs in a variety of cancers, including colorectal[70], ovarian[71] and hepatocellular carcinoma[72]. Detailed, systemical analysis further revealed that the cellular composition of the lymphocytic immune infiltrate decisively determines the outcome, as reviewed by Fridman and colleagues[73]. For instance, the presence of

Th1 cells or antigen-experienced ($CD45RO^+$) $CD8^+$ T cells is favorable[74,75], while the abundance of regulatory T cells (Tregs)[76,77] correlates with bad prognosis. The impact of Th2 and Th17 cells even depends on the cancer type[73,78].

The potential of the human immune system to combat cancer has further been highlighted by clinical epidemiology data. In detail, transplant recipients receiving immune-suppressive drugs exhibited higher tumor incidences in a variety of studies[79-82]. As evidenced in recent years, immunosuppressed individuals especially reveal higher susceptibility to cancers that exhibit a high number of somatic mutations (such as melanoma)[83] and hence are likely to be recognized by an intact immune system.

In contrast to its protective role in eliminating transformed cells, the immune system can also foster the generation of cancer cells with low immunogenicity. When the immune system continuously deletes nascent tumor cells, only those acquiring immunoevasive mechanisms can survive. First hints for this process came from tumor transplantation studies in immunocompetent versus immuno-compromised mice. While tumors from wild type (wt) mice grew equally well in immunocompetent or -compromised animals, tumors derived from RAG-$2^{-/-}$ or Perforin$^{-/-}$ animals only exhibited comparable growth kinetics in their syngeneic immunocompromised counterparts, while most of the tumors were rejected upon transplantation into wt mice[36,37]. From these experiments the authors concluded that tumors of wt mice had escaped immune recognition during the elimination phase and hence could not be recognized by the immune system of the syngeneic recipient. In contrast, tumors from immunodeficient mice did not experience shaping by the immune system due to the absence of immunological selection pressure and thus were unable to trigger tumor formation after transplantation into immunocompetent animals. This phenomenon of the immune system favoring the selection and outgrowth of escape variants with reduced immunogenicity has been called cancer immunoediting and has been extensively described and reviewed by Schreiber and colleagues[30,31,84,85].

5.4. Mechanisms of cancer immune escape

The emergence of immune escape variants in the process of cancer immunoediting can be considered an evolution-based scenario with a Darwinian-like selection process for poorly immunogenic tumor cells. Due to the huge heterogeneity of tumors and even the cellular heterogeneity within tumors, the mechanisms of

immune escape are very divers and success is determined by the accumulation of multiple immunoevasive features.

As mentioned, reducing immunogenicity represents a potent strategy to prevent an effector immune response. In this regard, several mechanisms have been explored. These include inhibiting antigen presentation (e.g. by downregulation of MHC molecules)[86], preventing antigen generation (e.g. by functional loss of proteins implicated in the antigen processing pathway, such as proteasome subunits LMP2/7 or the peptide transporter TAP)[87,88], or simply deletion of immunogenic antigens[89].

On the other hand, immune recognition does not necessary imply tumor cell killing, as tumor cells have also evolved mechanisms to prevent immune-mediated cell death. By upregulating anti-apoptotic proteins, such as cFLIP, XIAP or BCL-2, cancer cells directly interfere with the apoptosis-inducing effector mechanisms of immune cells, triggered by CD95 (aka FAS) or TRAIL receptor engagement[90-92].

While the above-mentioned strategies imply a rather passive form of immune escape, tumor cells can also directly inhibit the action of immune cells. Along this line surface expression of ligands, such as programmed death-ligand 1 (PD-L1)[93], HLA-G[94] or HLA-E[95] as well as CD95 ligand (CD95L)[96], interacts with T cell-associated receptors in order to counteract activation or induce apoptosis. Besides, metabolic enzymes in tumor cells such as indolamine-2,3-dioxygenase (IDO)[97,98], arginase[99,100] or inducible nitric oxide synthetase (iNOS)[101] can exert a variety of T cell suppressive functions[102]. Specifically, by catabolizing it into kyurenine IDO deprives tryptophan, which leads to downregulation of the CD3 zeta chain[103] as well as T cell apoptosis and impaired effector T cell differentiation[104]. Nitric oxide (NO) produced by iNOS, in turn can nitrate T cell receptors thereby blocking signal transduction[105]. In addition, tumor cells do also inhibit innate immune functions. For instance, shedding of soluble NKG2D ligands MICA or MICB impairs NK cell function[106], while sterol metabolites can block DC migration to the lymph nodes by suppressing chemokine receptor 7 (CCR7) expression[107].

Alternatively, tumor cells may promote the generation of an immunosuppressive microenvironment, as initially suggested by a study showing that mice bearing late-stage tumors which are not eliminated by the immune system exhibit functional systemic T cell responses[108]. The emergence of such an environment is fostered by the release of immunosuppressive factors which – besides directly inhibiting immune cells – trigger the differentiation of immunosuppressive cell types. As an example,

TGFβ induces the conversion of effector T cells into Tregs, which in turn inhibit effector T cell function by various mechanisms including IL-2 deprivation, production of the immunosuppressive cytokine IL-10[109] or the expression of PD-L1 or cytotoxic T lymphocyte-associated protein-4 (CTLA-4) molecules[110]. PD-L1 interacts with its receptor PD1 that is upregulated on T cells upon activation and IFNγ encounter. PD1 co-localizes with TCR microclusters and following ligand engagement recruits phosphatases such as SHP2 that dephosphorylate downstream signaling molecules like CD3-zeta or Zap70, thereby inhibiting T cell activation[111]. On the other hand, CTLA-4 is though to primarily exert its suppressive function by competing with CD28 for CD80 and CD86 binding, hence preventing their interaction and dampening co-stimulatory signaling[112]. Initially, CTLA-4 was thought to additionally downregulate CD80/CD86 expression on DCs[113,114], although recent work suggests no implication in this respect[115]. While Tregs utilize these two molecules to prevent autoimmunity under physiological conditions[116], they hamper antigen-specific $CD8^+$ T cell responses in the tumor microenvironment, thereby preventing tumor rejection[117-119].
Besides Tregs, the production and elaboration of factors such as granulocyte-macrophage colony-stimulating factor (GM-CSF), vascular endothelial growth factor (VEGF), IL-1β and prostaglandin E2 (PGE2) induces the differentiation and expansion of so-called myeloid-derived suppressor cells (MDSCs), which also hamper anti-tumor immunity. Initially, these and other factors like platelet-derived growth factor (PDGF) or epidermal growth factor (EGF) derive from M2 macrophages, which are implicated in wound healing and hence the first to migrate to the inflammatory tumor microenvironment[120]. These tumor-associated macrophages (TAMs) have been shown to support tumor progression by promoting angiogenesis, invasion as well as metastasis[121,122]. During the following phase of the anti-cancer immune response, myeloid precursor cells enter the tumor, in order to advance the local immune response. Nevertheless, chronic inflammation, hypoxia as well as tumor-derived factors within the microenvironment perturb the differentiation and maturation process, in turn producing highly immunosuppressive MDSCs[123]. As seen for many cancer-associated cells, MDSCs closely interact with TAMs by generating positive feedback loops, which – in turn – enhance immunosuppression: MDSC-derived IL-10 blocks IL-12 production in TAMs. Resulting high IL-10 and low IL-12 levels promote differentiation of type-2 T helper (Th2) cells, which secrete IL-4 that again triggers M2 polarization of macrophages.

Clinical reports have revealed that elevated MDSC levels correlate with cancer malignancy, owing to the multiple mechanisms MDSCs employ to manipulate tumor, endothelial as well as immune cells[124]. For example TAM- or MDSC-derived VEGF and IL-10 induce CD95L in tumor endothelial cells to trigger apoptosis of $CD8^+$ effector T cells[125]. In addition, MDSCs secrete CCR5 ligands and TGFβ/IL-10 to recruit and stimulate differentiation of Tregs, respectively[126,127]. As explained, Tregs express CTLA-4, which interferes with CD80 and CD86 availability on DCs[113,114]. As a consequence, tumor antigen-specific T cells experience a lack in co-stimulatory signals required for CD28 engagement, resulting in anergy. In addition, interaction with Tregs can prompt DCs to exert tolerogenic effects through CTLA-4-dependent production of IL-10 and IDO[128,129]. Besides, MDSCs also produce high levels of iNOS and IDO on their own, the action of which has already been explained above. Nitrating or nitrosylating amino acids within TCRs renders T cells unresponsive to antigenic stimulation[130]. In general, it seems that reactive oxygen species (ROS) have a pivotal role in the suppressive activity of MDSCs, as inhibition of ROS generation in MDSCs isolated from murine and human tumors completely abrogated the inhibitory effects *in vitro*[131,132]. Though, recent data suggest that physiologic concentrations of macrophage-derived NO promotes T cell infiltration into the tumor[133].

Thus tumors exert and induce a plethora of immunosuppressive mechanisms, including the generation of an intensely cooperating, highly complicated network of immunosuppressive immune cells that blocks immune recognition and allows cancer formation as well as progression.

5.5. Recent approaches in cancer immunotherapy

The potential of exploiting immune cells for cancer therapy has been decisively strengthened during the last decade. In particular, the exploration and advanced understanding of the numerous mechanisms of cancer immunosurveillance, immunoediting and immunosuppression has allowed and inspired the development of innovative therapeutics. Along this line, cytokine therapy including the administration of IL-2[134] or IFNα[135] were administered partially successfully. Promising results were also achieved with small molecule inhibitors trying to block IDO or iNOS function[102,136,137]. Yet, these approaches lacked cancer-specific targeting. Enhanced cancer-specificity was achieved by the use of monoclonal

antibodies targeting tumor antigens, such as CD20 (rituximab) in leukemia[138,139]. Besides blocking receptor signaling, these antibodies exploit the function of immune cells such as NK cells or neutrophils by triggering Fc-mediated antibody-dependent cellular cytotoxicity (ADCC) or by initiating complement-dependent cellular cytotoxicity (CDC).

Due to its huge diversity and capacity to specifically respond to arising mutations, the T cell repertoire represents a powerful natural defense mechanism against cancer formation and its heterogeneity. As a result of co-evolution, many immunoevasive mechanisms of tumors ultimately aim at interfering with tumor antigen-specific T cell responses and hence restoring, boosting or initiating their functionality seems desirable. In this context, the detection of graft-versus-leukemia effects after allogeneic hematopoietic stem cell transplantation can be considered one of the first successful approaches of exploiting T cells for cancer treatment[140]. Further on, the discovery of spontaneous T cell responses against tumor antigens in human patients has created the basis for T cell-based cancer immunotherapies[141,142]. Up to date, different approaches have already successfully attempted to amplify or induce the anti-cancer immune response, e.g. by adoptive transfer of *ex vivo* expanded TILs or by tumor vaccination therapy[59]. For instance, Carreno and colleagues have recently generated a dendritic cell vaccine by loading DCs with neo-antigen peptides, which efficiently broadened the repertoire of tumor antigen-specific T cells in melanoma[143].

In recent years, it has become clear that that especially cancers with high mutational load (such as melanoma) are immunogenic and counteract immune destruction by the generation of an immunosuppressive microenvironment[83,144]. In this respect, targeting of immune checkpoint pathways has emerged as a potent approach to revert immunosuppression and to restore the tumor-specific T cell response. Immune checkpoints exert either co-stimulatory or co-inhibitory functions and serve to regulate the amplitude and duration of immune responses[145]. Under physiological conditions these molecules hence function to restrain immune responses and maintain self-tolerance, e.g. by preventing excess pro-inflammatory damage to the host[146]. As already explained, tumors exploit co-inhibitory molecules, such as PD-L1 or CTLA-4 expressed either on tumor or immunosuppressive immune cells. As can be inferred from the above-mentioned functions, CTLA-4 primarily dampens the priming of naïve and memory T cells upon APC interaction[147], while PD1 engagement counteracts TCR signaling, thereby preventing proliferation as well as

cytotoxic function and ultimately resulting in T cell exhaustion and apoptosis[148-150]. In addition, stimulation of PD1 on macrophages has been shown to inhibit T cell responses by promoting IL-10 release in HIV-infected patients[151]. In recent years, several clinical studies have proven the therapeutic efficacy of checkpoint blockade for cancer immunotherapy[60]. Along this line, CTLA-4-blocking antibody ipilimumab was the first checkpoint inhibitor demonstrating survival benefit in a randomized trial of advanced melanoma[152]. Besides blocking intermolecular interactions of the CTLA-4 molecule, ipilimumab additionally triggers ADCC-mediated clearance of CTLA-4$^+$ cells, such as Tregs[153,154]. Similarly, antibodies blocking PD1 (nivolumab, pembrolizumab,) or PD-L1 (atezolizumab) have shown striking efficacy in clinical studies and have recently been approved by the Food and Drug Administration (FDA) as first line treatment for melanoma, bladder cancer, non-small-cell lung cancer (NSCLC) and Hodgkin lymphoma[155-157]. Although PD1 and CTLA-4 antagonists have been most intensively investigated to date, further inhibitory receptors such as TIM3 and LAG3 are being evaluated[146,158]. In addition, agonistic antibodies and fusion molecules targeting co-stimulatory T cell checkpoint receptors of the tumor necrosis factor (TNF) superfamily (e.g. OX40, CD40L, 4-1BB, GITR) are currently being assessed in clinical trials[145]. Promising data was achieved with an OX40 agonistic antibody, which induced regression of metastatic lesions in 12 out of 30 melanoma patients[159]. Moreover, 4-1BB agonistic treatment resulted in partial responses and stable disease in patients with renal cell carcinoma, ovarian cancer, prostate cancer and melanoma[160,161]. Based on these promising data and the known interplay between multiple immunosuppressive pathways within the tumor microenvironment, combinatorial targeting of different co-stimulatory and/or -inhibitory immune checkpoints seems reasonable. In this respect, combination therapy of ipilimumab and nivolumab exhibited 53% increased efficacy compared to monotherapy in a phase I trial of advanced melanoma[162]. Besides, pre-clinical mouse studies confirmed that combining PD1 blockade with either 4-1BB or OX40 antagonists results in an improved anti-cancer immune response[163,164].

Accumulating data suggests that targeting immune checkpoints is favorable in tumors, where a tumoricidal T cell response is prevented by an immunosuppressive microenvironment[165,166]. Besides melanoma, these particularly include cancers of the lung and bladder, which carry a high number of somatic mutations and hence provide a basis for the production of immunogenic antigens[83]. This hypothesis was

further strengthened by a genome-wide neo-epitope analysis in melanoma patients, where responsiveness to ipilimumab therapy could be correlated to mutational load[167]. Therefore, other immunotherapeutic strategies have been applied for the treatment of cancers with a low to moderate mutational background. Along this line, bispecific T cell engagers (BiTEs) and chimeric antigen receptor T cells (CAR-Ts) aim at triggering *de novo* T cell responses against cancer. BiTEs are bispecific antibody molecules carrying two different target moieties: one targets a tumor specific antigen and the other binds the CD3 part of the TCR in an agonistic manner. Hence, BiTEs function by redirecting T cells against tumor cells independently from their specificity. BiTEs have already revealed profound efficacy in hematological malignancies, whereas exhibiting limited potency in solid tumors. So far, an epithelial cell adhesion molecule (EpCAM)-targeting (catumaxomab), as well as a CD19-targeting BiTE (blinatomumab) have shown efficacy in several cancer types and have been approved by the FDA for therapy of malignant ascites and refractory B cell acute lymphoblastic leukemia (B-ALL), respectively[168-173]. Besides, a BiTE against the carcinoembryonic antigen (CEA) expressed in various solid tumors is being evaluated in phase I clinical trials[174].

On the other hand, CAR-Ts represent T cells that have been genetically engineered to express a chimeric antigen receptor, which consists of an extracellular single-chain variable fragment (scFv) binding the target and intracellular signaling domains of the TCR. Binding of the scFv to the tumor antigen induces TCR downstream signaling, in turn triggering T cell activation and cytotoxic activity. Recently, next generation CAR-Ts have been generated by including intracellular signaling domains from molecules implicated in co-stimulation, such as CD28, OX40 or 4-1BB[175]. CAR-Ts have proven striking efficacies in hematological cancers and adoptive transfer of the FDA-approved CART19 targeting the CD19 receptor has achieved 90% complete remission rates in patients with refractory B-ALL[176,177]. In addition, targeting the NY-ESO-1 antigen generated durable responses in multiple myeloma and synovial cell sarcoma patients[178,179]. In pre-clinical models, a mesothelin-targeting CAR-T was applied to eradicate human mesothelioma lesions[180].

Nevertheless, despite remarkable efficacy and sophisticated engineering technologies, immunotherapies have always entailed risks for immune-related side effects. While both BiTEs and CAR-Ts have been struggling with unexpected cytokine storm or tumor lysis syndrome, major concerns about CAR-T therapy

additionally derive from the possibility of insertional mutagenesis leading to T cell lymphoma[176,181-184].

5.6. Aim of the study

In order to overcome existing immune tolerance against endogenous tumor antigens, we employed a novel strategy of cancer immunotherapy by targeting virus-derived peptides to tumor cells, thereby exploiting the high affinity T cell repertoire. Our approach uses antibody-targeted pathogen-derived peptides (ATPPs) that deliver virus-derived, mature MHC class I peptides, which are bound via a disulfide bond to a tumor antigen-specific antibody.

In this study we primarily focused on CUB domain-containing protein 1 (CDCP1, aka Trask, CD318) as proof of concept target. The integral membrane protein CDCP1 negatively regulates cell adhesion upon Src-mediated phosphorylation by interacting with β1-integrin and signaling via PI3K/Akt pathway[185]. CDCP1 is highly expressed in various cancer types (including breast, kidney, lung, pancreas) and its upregulation correlates with increased relapse rate, metastasis and poor prognosis[186-189]. Although it is also low to moderately expressed in various healthy tissues, thereby probably not representing the antigen of choice for clinical translation of the ATPP concept, choosing CDCP1 as target allowed testing of the ATPP approach in multiple cancer cell lines. Moreover, a previous study has already proven CDCP1 internalization upon binding of the utilized antibody[190], which represents a prerequisite for ATPP functionality.

The postulated mode of action of ATPP immunoconjugates is depicted in Figure 5.1. After binding of ATPPs to the target antigen, the antigen-conjugate complex is internalized into the endocytic compartment. Given the findings from Yang et al.[191] that disulfide reduction efficiently occurs in endosomes, the peptides are subsequently released from the antibody. In general, external antigens enter the MHC class II processing and presentation pathway, while MHC-I molecules are loaded with endogenous peptides[192]. Nevertheless, ATPPs deliver mature 9-mers that can readily bind to the MHC-I molecule. By additionally exploiting the fact that recycling of MHC molecules to the cell surface – despite being dominant in DCs – also occurs under normal conditions[193,194], the ATPP approach aims at generating class I MHC-peptide complexes on the cell surface. Accordingly, peptide-specific T cells encounter a viral antigen, which prevents the possibility of autoimmune side

effects and additionally suggests higher immunogenicity than targeting a tumor antigen. By choosing immunodominant peptides binding to high frequency HLA allotypes (such as HLA-A1 or HLA-A2) and deriving from viruses that have high seroprevalence (e.g. Epstein-Barr virus or Influenza) this approach is supposed to ensure treatment of the vast majority if not the entire patient population.

The present study aimed at investigating the functionality and putative efficacy of ATPP conjugates both *in vitro* and *in vivo,* as well as to clarify the underlying mode of action.

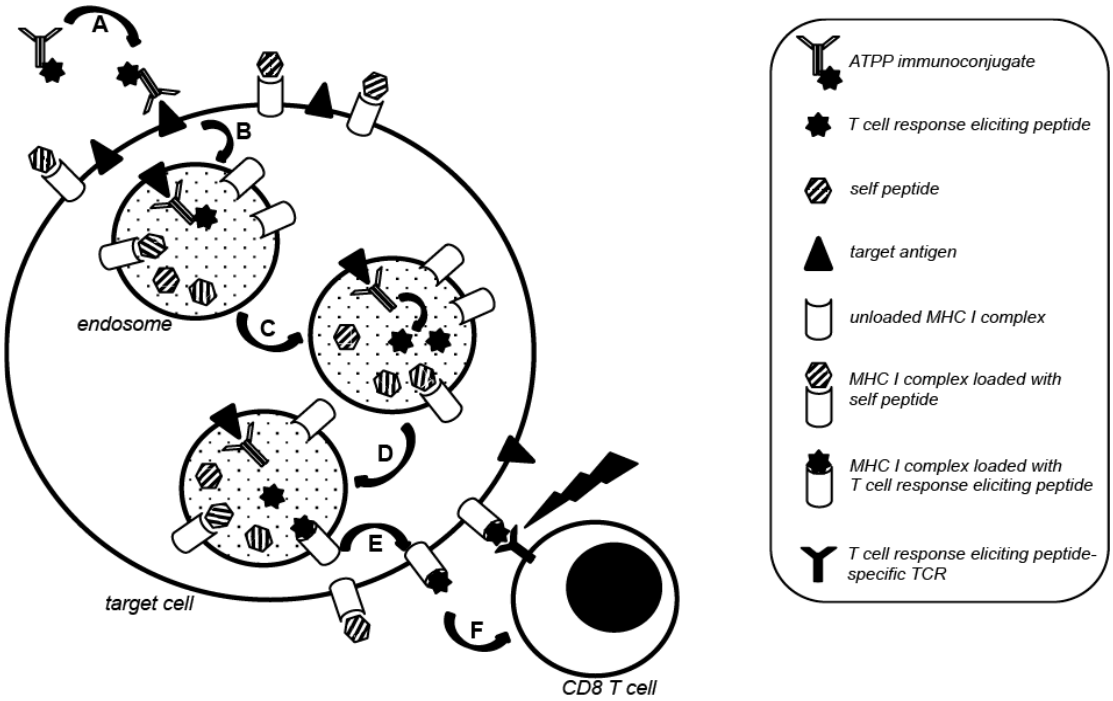

Figure 5.1 Proposed model for the mode of action of ATPP immunoconjugates.
A: Binding of ATPP immunoconjugates to target antigen. B: Internalization of ATPP into endosomal compartment. C: Release of T cell response eliciting peptide from the immunoconjugate in the endosomal compartment. D: Release of self-peptides and loading of recycling MHC class I molecules with delivered virus-derived peptides. E: Routing of viral peptide-loaded MHC class I complexes to target cell surface. F: Recognition of viral peptide-loaded MHC class I complexes on target cell surface by peptide-specific $CD8^+$ T cells, in turn inducing T cell activation and target cell lysis (death).

6. Materials and Methods

6.1. Materials

6.1.1. Laboratory Devices

Incubator BBD6220	Thermo Scientific Heraeus
Vi-Cell XR Cell Viability Analyzer	Beckman Coulter Biomedical
Centrifuge Multifuge 4 KR	Thermo Scientific Heraeus
Centrifuge Multifuge 3SR+	Thermo Scientific Heraeus
Centrifuge Rotanta 460 R	Hettich Lab Technology
Herasafe KS12 cabinet	Thermo Scientific
Laboratory scale	Sartorius
FACS Canto II analyzer	BD Biosciences
xCELLigence RTCA SP	ACEA Biosciences
Pipetboy acu 2	INTEGRA Biosciences
2.5, 10, 100, 200, 1000, 5000 µL pipettes	Eppendorf
300, 1000µL electric multi-channel pipettes	BioHit
Irradiation device GSR CI	GSM GmbH
Plate Reader Infinite 200Pro	TECAN Group Ltd.
ELISA plate washer MicroTek AWS	BioTek Instruments GmbH
Water bath Julabo 5M	Julabo
Leica SP8 microscope	Leica Instruments GmbH
ImmunoSpot S5 Analyzer	Cellular Technology Ltd.
RM5 roller mixer	CAT

6.1.2. Consumables

Cell culture flasks (T25, T75, T175)	Greiner
Low adherence cell culture flasks	Greiner
G-Rex10	Wilson Wolf
G-Rex100	Wilson Wolf
6 / 12 / 24 / 48 / 96-well plates, flat bottom	Greiner
96-well plates, u-bottom	Greiner
96-well plates, v-bottom (PE)	Greiner
E-Plates 96-well	ACEA Biosciences
0.5 / 1.5 / 2.0 mL Eppendorf tubes	Eppendorf
50 / 15 mL Falcon tubes	Greiner
250mL centrifugation tubes	Corning
2 / 5 / 10 / 25 / 50 mL pipet boy tips	Greiner
FACS tubes 5mL	BD Biosciences
Pipette tips	Eppendorf
Cryo tubes, 2mL	Greiner

6.1.3. Cell culture media and reagents

RPMI 1640	Gibco by Life technologies
CTS AIM-V medium	Gibco by Life technologies
DMEM	PAN Biotech
McCoy´s 5A medium	PAN Biotech
L-Glutamine, 100x, 200mM	Gibco by Life technologies
NEAAs, 100x (non-essential amino acids)	Gibco by Life technologies

Sodium pyruvate, 100mM	Gibco by Life technologies
FBS (fetal bovine serum) heat-inactivated	Gibco by Life technologies
Human serum (from human male AB plasma)	Sigma Aldrich
2-mercaptoethanol, 50mM	Gibco by Life technologies
DPBS	PAN Biotech
Accutase solution	Sigma Aldrich
Penicillin-Streptomycin, 500x	Roche Diagnostics GmbH
DMSO (Dimethyl sulfoxide)	Sigma Aldrich
HEPES (2-[4-(2-hydroxyethyl)piperazin-1- yl]ethanesulfonic acid)	Gibco by Life technologies
IL-15, human recombinant	R&D Systems
sIL-15Ra	R&D Systems

6.1.4. Antibodies for flow cytometry

6.1.4.1. Primary antibodies (against human antigens)

Target	Clone	Conjugate	Source	Isotype	Manufacturer
CD3	SK7	PE-Cy7	Mouse	IgG1, κ	BioLegend
CD3	SK7	FITC	Mouse	IgG1, κ	BioLegend
CD4	OKT4	PE	Mouse	IgG2b, κ	BioLegend
CD8	HIT8a	FITC	Mouse	IgG1, κ	BioLegend
CD8	HIT8a	APC-Cy7	Mouse	IgG1, κ	BioLegend
CD45	HI30	PerCP-Cy5.5	Mouse	IgG1, κ	BioLegend
CD45	HI30	PE	Mouse	IgG1, κ	BioLegend
CD45RO	UCHL1	PE	Mouse	IgG2a, κ	BioLegend
CD138	DL101	APC	Mouse	IgG1, κ	BioLegend
CD138	MI15	APC	Mouse	IgG1, κ	BioLegend
CD197 (CCR7)	G043H7	PE-Cy7	Mouse	IgG2a, κ	BioLegend

CD274 (PD-L1)	29E.2A3	APC	Mouse	IgG2b, κ	BioLegend
CD279 (PD1)	EH12.2H7	PE	Mouse	IgG1, κ	BioLegend
CD318 (CDCP1)	CUB1	PE	Mouse	IgG2b, κ	BioLegend
HLA-A1/36	8.L.104	Biotin	Mouse	IgM	Abcam
HLA-A1/11/26	8.L.101	-	Mouse	IgM	Abcam
HLA-A2	BB7.2	APC	Mouse	IgG2b, κ	BioLegend

6.1.4.2. Isotype control antibodies

Isotype	Clone	Conjugate	Source	Manufacturer
IgG2b, κ	MPC-11	PE	Mouse	BioLegend
IgG2b, κ	MPC-11	APC	Mouse	BioLegend
IgG1, κ	MOPC-21	FITC	Mouse	BioLegend
IgG1, κ	MOPC-21	APC	Mouse	BioLegend
IgM	MM-30	-	Mouse	BioLegend
IgG	# I2154	-	Human	Sigma Aldrich

6.1.4.3. Secondary antibodies

Target	Isotype	Conjugate	Source	Manufacturer
Mouse IgM	F(ab')2	FITC	goat	Life technologies
Biotin (Streptavidin)	-	PE	-	BioLegend
Human IgG (H+L)	polyclonal	Alexa 488	goat	Life technologies
Human IgG	IgG2a, κ	APC	mouse	BioLegend

6.1.4.4. Peptide-MHC pentamers (all from ProImmune)

Peptide sequence	Epitope origin	HLA allele	Conjugate	Order #
CLGGLLTMV	EBV, LMP-2 426-434	A*02:01	APC	F042
GLCTLVAML	EBV, BMLF1 259-276	A*02:01	APC	F001
CTELKLSDY	Influenza A, NP 44-52	A*01:01	APC	F076

6.1.5. Reagents for FACS and microscopic imaging

DAPI (4',6-diamidin-2-phenylindol)	Roche Diagnostics GmbH
TruStain fcX™, human	BioLegend
TruStain fcX™ (anti-mouse CD16/32 Ab)	BioLegend
EDTA, 0.5M	Gibco by Life technologies
PKH26	Sigma Aldrich
CMFDA	Life technologies
Culture-Insert 2 Well in µ-Dish 35 mm (# 81176)	Ibidi
Collagen type I	Sigma Aldrich
Alexa Fluor 647 conjugated αIgG (H+L) antibody	Life technologies
Paraformaldehyde (PFA)	Sigma Aldrich

6.1.6. Reagents for ELISA, ELSPOT and LDH assay

96-well MaxiSorp® plates	Nunc
Tween®20	Merck Millipore
10x PBS, premixed buffer	Roche Diagnostics GmbH
Bovine serum albumin (BSA), 7.5%	Sigma Aldrich
Normal goat serum (NGS)	R&D Systems
αHLA-ABC antibody (clone W6/32)	BioLegend
BM Blue POD Substrate solution	Roche Diagnostics GmbH
Sulfuric acid (H_2SO_4)	Merck
Triton X-100	Sigma Aldrich

6.1.7. Ready to use kits

Leucosep tubes	Greiner
RosetteSep RosetteSep™ Human CD8⁺ T Cell Enrichment Cocktail	Stem Cell technologies
Human IFN-γ ELISpot PRO kit (#3420-2APT)	Mabtech
Human IFN-gamma DuoSet ELISA kit (#DY285)	R&D Systems
Cytotoxicity Detection Kit (LDH)	Roche Diagnostics GmbH

6.1.8. Animals and in vivo equipment

NOG CIEA mice	Taconic Biosciences
Cages	Tecniplast
Drink Bottle	Tecniplast
Bedding	Ssniff
Pelleted standard diet	ProvimiKliba AG
Electric shaver	Harotec
Caliper	Mitutoyo Messgeräte
Surgical instruments	B. Braun Melsungen
Isoflurane Vaporizer	Eickenmeyer Medizintechnik
Isofluran CP (Isoflurane)	CP-Pharma
27G needles STERICAN	B. Braun Melsungen
1mL syringes	B. Braun Melsungen

6.1.9. Reagents and consumables for processing of tissue samples

DNase I	Roche Diagnostics GmbH
Collagenase IV	Sigma Aldrich
Dispase II	Roche Diagnostics GmbH
BD Pharm Lyse buffer	BD Biosciences
40µm cell strainer	Greiner
70µm cell strainer	Greiner

6.1.10. Software

Excel	Microsoft
Word	Microsoft
Prism	GraphPad
RTCA software	ACEA Biosciences
Tecan i-control	TECAN Group Ltd.
BD FACS Diva	BD Biosciences
Flow Jo X	TreeStar
CTL Immunospot 5.0 software	Cellular Technology Ltd.

6.2. Methods

6.2.1. Generation and analysis of ATPP and FRET conjugates

6.2.1.1. Antibodies used for ATPP generation

Anti-CD22 and anti-CD79b antibodies were kindly provided by Eike Hoffmann (Large Molecule Research, Roche Diagnostics GmbH, Penzberg). Anti-CD138 antibody was received from Martin Kuen (Discovery Oncology, Roche Diagnostics GmbH, Penzberg). The anti-CDCP1 (CD318, RG-7287) antibody was generated as described[190]. Anti-CD22, anti-CD79b and anti-CDCP1 antibodies carried the P329G LALA mutation for abolished binding to Fc-gamma receptors (FcRγ). Antibodies were stored in 0.1M potassium phosphate buffer containing 150 mM NaCl, pH 7.5 at -20°C for short or -80°C for long term, respectively.

Table 6.1 – Peptides used for ATPP generation

Abbreviation	Peptide sequence	Species	Gene	HLA class I binding*
pEBV_CLG	CLGGLLTMV	EBV	LMP-2	HLA-A02:01
pEBV_GLC	GLCTLVAML	EBV	BMLF-1	HLA-A02:01
pEBV_YGP	YGPVFMCLGGLLTMV	EBV	LMP-2	-
pINF_CTEL	CTELKLSDY	Influenza A	NP	HLA-A01:01

* only HLA genes relevant to performed experiments are considered.

6.2.1.2. Generation of peptides and ATPP conjugates

Utilized peptides are summarized in Table 6.1 and were synthesized using standard Fluorenylmethyloxycarbonyl (Fmoc)-chemistry. Both peptides and ATPPs were generated in the laboratory of Lars Hillringhaus (Peptide Chemistry, Roche Diagnostics GmbH, Penzberg). All generated ATPP conjugates are summarized in Supplemental Figure 9.1. Antibodies were mixed with 8 equivalents of N-Succinimidyl 3-(2-pyridyldithio)-propionate (SPDP, Pierce) for two hours of reaction time. Hereafter, 0.1 M potassium phosphate buffer containing 150 mM NaCl and 10

mM EDTA (pH 7.0) was used for dialysis of the derivatized antibody. Next, 6 equivalents of the respective peptide were added and incubated overnight. The final product was dialyzed against storage buffer (20mM Histidine, 150mM NaCl) and stored at -20°C.
ATPP conjugates containing a non-cleavable thioether linker were generated according to the mentioned protocol using succinimidyl iodoacetate (SIA, Pierce) instead of SPDP.

6.2.1.3. Mass spectrometric analysis of ATPP peptide labeling rates
ATPP conjugates were analyzed by mass spectrometry in the laboratory of Gloria Tabares (Protein Chemistry, Roche Diagnostics GmbH, Penzberg), in order to determine the average peptide labeling rates. ATPPs and unlabeled reference antibodies were deglycosylated using N-glycosidase F and analyzed by means of liquid chromatography electrospray ionisation mass spectrometry (LC-ESI-MS) using a high pressure liquid chromatography (HPLC) System (Waters) in combination with a reverse-phase column containing a water-acetonitrile gradient and subsequent electrospray ionisation time of flight mass spectrometry (ESI-TOF-MS) measurement and detection. Data analysis was performed using the MassLynx Software (Waters).

6.2.1.4. Synthesis of the anti-CDCP1-FRET construct
Generation of the FRET construct was adapted from Yang et al.[191] and performed in the laboratory of Lars Hillringhaus (Peptide Chemistry, Roche Diagnostics GmbH, Penzberg). Fmoc-chemistry was applied to generate the following linker peptide: Acetyl-Cys-Lys-Ala-Glu-ßAla-Glu-ßAla-Glu-Aha. After peptide cleavage from the TentaGel R RAM resin, the peptide was purified by preparative HPLC. Next, cysteamine dithiopyridyl (1 equivalent) and trimethylamine (4 equivalents) were dissolved in dimethylformamide (DMF) and reacted with a solution of sulforhodamine B acid chloride (1 equivalent). 2 equivalents of the resulting rhodamine dithiopyridine were incubated with the linker peptide (1 equivalent) in phosphate buffer at pH7.5. After 90 minutes, 4,4-difluoro-5,7-dimethyl-4-bora-3α,4α-diaza-s-indacene-3-propionic acid (BODIPY) FL N-hydroxy-succinimide (NHS) ester (2 equivalents) was added and incubated for 90 minutes. The resulting FRET peptide was purified by preparative HPLC.

The αCPDP1 antibody was incubated with 5 equivalents of cyclooctyne NHS ester (SX-A1028, Synaffix) in phosphate buffer at pH 8.3 and subsequently purified by gel filtration. The resulting αCPDP1-cyclooctyne conjugate was incubated with 30 equivalents of FRET peptide in phosphate buffer at pH 7.0 for 3 hours and the final αCPDP1-FRET conjugate was purified by gel filtration and stored in 20mM histidine, 150mM NaCl at -20°C.

6.2.2. Cell culture

6.2.2.1. Cell lines and culture conditions

Utilized cancer cell lines were originally purchased from the American Type Culture Collection (ATCC) and were provided by Roche cell bank, where they were verified as pathogen-free and identity was confirmed by means of single nucleotide polymorphism (SNP)-PCR or short tandem repeat (STR) analysis. Cell lines were grown in a humidified incubator at 37°C supplied with 5% CO_2 in dedicated media as specified in Table 6.2. U266B1 cells were grown in low-adherence flasks. Before *in vivo* inoculation the absence of murine pathogens was additionally confirmed by PCR analysis.

Table 6.2 – Utilized cancer cell lines

Cell line	Cancer type	Cell culture medium
MDA-MB231	breast	RPMI1640, 10%FBS, 2mM L-Glutamine
HCT-116	colon	McCoy´s 5A, 10%FBS, 2mM L-Glutamine
A375	skin (melanoma)	DMEM, 10% FBS, 2mM L-Glutamine
PC-3	prostate	RPMI1640, 10% FBS, 2mM, L-Glutamine, 1mM Sodium Pyruvate, 10mM HEPES
BxPC-3	pancreas (adenocarcinoma)	RPMI1640, 10% FBS, 2mM, L-Glutamine, 1mM Sodium Pyruvate, 10mM HEPES
U266B1	blood (multiple myeloma)	RPMI1640, 15% FBS, 2mM, L-Glutamine, 1mM Sodium Pyruvate, 10mM HEPES

6.2.2.2. Passaging and counting of cells

Cancer cell lines were grown to 70-100% confluency, subsequently passaged for a maximum of 5 times and freshly thawed thereafter. Cells were detached by means of accutase, resuspended in FBS-containing medium and collected by means of centrifugation (300g, 3min). Cell numbers were determined by means of the Vi-Cell XR Cell Viability Analyzer.

6.2.2.3. Freezing and thawing of cells

Cells were frozen in FBS containing 10% DMSO. Cryo tubes were placed in CoolCell (Biocision) freezing containers and incubated at -80°C. After 2 days tubes were transferred to liquid nitrogen and stored until required.

Thawing of cells was performed by placing cryo tubes in a 37°C water bath for approximately 30 seconds. Next, cell suspension was mixed with equivalent volume of pre-warmed media and subsequently transferred to falcon tubes containing the same medium. Cells were pelleted by centrifugation (300g, 3min) to remove DMSO. The cell pellet was resuspended in cell culture medium and transferred to culture flasks.

6.2.3. Isolation of PBMCs from human blood and *in vitro* expansion of peptide-specific T cells

6.2.3.1. Isolation of PBMCs from human blood

Peripheral blood mononuclear cells (PBMCs) were isolated by Ficoll gradient centrifugation from EDTA-blood of healthy donors (employees of Roche Diagnostics GmbH, Medical Services Department, Penzberg). For this purpose, equal volumes of blood and PBS were mixed and 35mL were transferred to 50mL Leucosep tubes (Greiner). After 20min centrifugation (800g, w/o break) at room temperature (RT), the PBMC containing interphase was transferred to 50mL falcon tubes and mixed 1:1 with PBS. To remove platelets, PBMCs were washed 3 times with PBS (250g, 10min). PBMCs were frozen as described in section 6.2.2.3.

6.2.3.2. $CD8^+$ T cell isolation from human blood

The RosetteSep™ Human $CD8^+$ T Cell Enrichment Cocktail (StemCell) was used according to the manufacturer´s instructions, in order to isolate $CD8^+$ T cells from human blood. This cocktail isolates $CD8^+$ T cells by negative selection using bispecific antibodies, which pellet the unwanted cells along with the erythrocytes during Ficoll gradient centrifugation. Hence, the interphase is supposed to only contain $CD8^+$ T cells. The enrichment quality was subsequently investigated using flow cytometry.

6.2.3.3. Expansion of peptide-specific T cells from human PBMCs

$2x10^5$ freshly isolated PBMCs were cultured per u-bottomed 96-well in 200µL RPMI+ medium (RPMI1640, 8% heat-inactivated human AB serum, 1mM Sodium Pyruvate, 1mM non-essential amino acids, 2mM L-Glutamine, 50µM β-mercaptoethanol and PenStrep) containing 1µM of the respective peptide (Table 6.1). After 3 days and again on day 10, 150µL of medium were exchanged and fresh peptide and 20ng/mL Interleukin 15 (IL-15) and 500ng/mL soluble, Fc-fused IL15-Receptor alpha (sIL15Ra-Fc, R&D Systems) were added. Until day 20, similar medium exchange without peptide addition was performed if required. On day 20, $5\text{-}10x10^7$ T cells were transferred to G-Rex10 cell culture containers in 10mL old medium and restimulated with peptide-pulsed, irradiated, autologous PBMCs (1:1). PBMCs were thawed as described in section 6.2.2.3 and incubated with 0.1mg/mL DNase I and 5µM peptide for 1 hour at 37°C, 5%CO_2. After irradiation with 40Gy, PBMCs were washed twice in RPMI1640/10%FBS (300g, 10min) and subsequently added to T cells. G-Rex10 containers were filled up to 40mL with RPMI+ and 20ng/mL IL-15 and 500ng/mL sIL15Ra-Fc were added. Cells were restimulated every two weeks with irradiated (80Gy), peptide-pulsed lymphoblastoid cells (LCLs) and expanded every 4-5 days with fresh medium supplemented with IL-15 and sIL15Ra-Fc as indicated above. Peptide-specific expansion of T cells was monitored on a regular basis by flow cytometric analysis using MHC-peptide pentamers. Cultures used for functional assays were >70% $CD8^+$, >80% peptide-specific and 10-13 days after last restimulation.

6.2.3.4. ATPP-mediated expansion of peptide-specific T cells

$2x10^5$ freshly isolated PBMCs were cultured per u-bottomed 96-well in 200µL RPMI+ medium (RPMI1640, 8% heat-inactivated human AB serum, 1mM Sodium Pyruvate, 1mM non-essential amino acids, 2mM L-Glutamine, 50µM β-mercaptoethanol and PenStrep) containing 13, 1.3 or 0.13nM of the EBV_CLG peptide or the respective CD22- or CD79b-targeting ATPP. After 3 days and again on day 10, 150µL of medium were exchanged and fresh peptide or ATPPs and 20ng/mL Interleukin 15 (IL-15) and 500ng/mL soluble, Fc-fused IL15-Receptor alpha (sIL15Ra-Fc, R&D Systems) were added. Cells were expanded every 4-5 days with fresh medium supplemented with IL-15 and sIL15Ra-Fc as indicated above. Peptide-specific expansion of T cells was monitored by flow cytometric analysis using MHC-peptide pentamers on day 13, 20 and 26.

6.2.4. Flow cytometric analyses

6.2.4.1. Target, HLA expression and ATPP binding on tumor cell lines

Cancer cells were detached by means of accutase and washed in FBS-containing medium (300g, 3min). $2x10^5$ cells were transferred per v-bottomed 96-well, washed and stained in 100µL of FACS buffer (PBS, 3% FBS, 2mM EDTA) containing respective primary antibodies, isotype control antibodies or ATPPs for 20min at 4°C. Cells were washed three times in FACS buffer and – in case required – incubated with secondary antibodies in FACS buffer for 20min at 4°C. 1µg/mL DAPI was added either to primary or secondary antibodies, in order to stain dead cells. While primary, secondary and isotype control antibodies were used according to the manufacturers instructions, ATPPs or respective uncoupled antibodies were used at 10µg/mL. Following three additional washing steps in FACS buffer, Flow cytometry was performed using the BD Biosciences Canto II and data was analyzed by means of the FlowJo (Treestar) software.

6.2.4.2. ATPP internalization on tumor cells

Cancer cells were harvested by means of accutase and washed in FBS-containing medium (300g, 3min). $2x10^5$ cells were transferred per v-bottomed 96-well and

stained in 100µL of cell culture medium containing 10µg/mL of ATPPs, the respective uncoupled antibody or the corresponding human IgG isotype control antibody (Sigma) for 30min at 4°C. Cells were washed three times and subsequently incubated in cell culture medium at 4°C and 37°C. After t=0, 0.5, 1, 2, 4 and 23hours, cells were stained with secondary antibody for 30min on ice (polyclonal goat anti-human IgG-Alexa488, Life technologies) to detect non-internalized ATPPs at the cell surface. 1µg/mL DAPI was added to stain dead cells. Cells were washed three times in FACS buffer (PBS, 3% FBS, 2mM EDTA), samples were run at the BD FACS Canto II and data was analyzed by means of the FlowJo (TreeStar) software. Percent internalization for each time-point was calculated as follows: (MFI at 37°C / MFI at 4°C) x 100.

6.2.4.3. Analysis of peptide-specific T cells

5-10x10^5 PBMCs or T cells were transferred per v-bottomed 96-well, washed (300g, 2min) and stained in 100µL FACS buffer (PBS, 3% FBS, 2mM EDTA) containing respective peptide-MHC pentamers (1:10, ProImmune) for 1 hour at 4°C. Having washed three times in FASC buffer, cells were incubated in 50µL FACS buffer containing 5µL human TruStain fcX™ (BioLegend) for 15min at 4°C, in order to block human Fc receptors. For analysis of isolated tumor xenografts, cells were additionally incubated with TruStain fcX™ (anti-mouse CD16/32 Ab, BioLegend). Next, 50µL FACS buffer containing primary antibodies and 1µg/mL DAPI were added and incubated for 20min at 4°C. Finally, cells were washed three times in FACS buffer and subjected to flow cytometric analysis at the BD FACS Canto II. Data were analyzed by means of the FlowJo (TreeStar) software.

6.2.5. T cell activation and cytotoxicity assays

6.2.5.1. Interferon-γ ELISPOT

The Human IFN-γ ELISpot PRO kit (Mabtech, #3420-2APT) was used according to the manufacturer´s instructions, in order to investigate ATPP-mediated T cell activation. The kit uses alkaline phosphatase (ALP)-conjugated antibodies for one-step visualization of released Interferon-γ (IFNγ) by means of BCIP/NBT-plus substrate.

Pre-coated 96-well plates were washed 4 times with PBS, tumor cells were harvested by means of accutase and $1x10^4$ tumor cells were plated per well in 200µL of respective cell culture media. Tumor cells were treated with ATPPs, peptides or control antibodies and placed in the incubator for 20-24 hours, if not stated otherwise. Plates were wrapped in aluminum foil during the incubation period. Next, adherent tumor cells were washed once with 150µL AIM-V medium and 200 *in vitro* expanded, peptide-specific $CD8^+$ T cells were added in 200µL AIM-V medium. After 24 hours incubation at 37°C, 5%CO_2, ELISPOT plates were developed and – after drying – analyzed by means of the ImmunoSpot S5 Analyzer (CTL) using the ImmunoSpot 5.0 software.

6.2.5.2. Interferon-γ ELISA

The Human IFN-gamma DuoSet ELISA kit (R&D Systems, #DY285) was used according to the manufacturer´s instructions, in order to investigate ATPP-mediated T cell activation. The kit uses the sandwich ELISA setup and streptavidin-conjugated horseradish peroxidase (HRP) for visualization of released interferon-γ (IFNγ) in the supernatant.

Tumor cells were harvested by means of accutase and $1.5x10^4$ tumor cells were plated per well of a flat-bottomed 96-well plate in 200µL of respective cell culture media. Tumor cells were treated with ATPPs, peptides or control antibodies and placed in the incubator for 20-24 hours. Next, adherent tumor cells were washed once with 150µL AIM-V medium and $4.5x10^4$ *in vitro* expanded, peptide-specific $CD8^+$ T cells or $3x10^5$ $CD8^+$ T cell-enriched PBMCs were added in 200µL AIM-V medium. U266B1 cells were transferred to v-bottomed 96-well plates and centrifuged (2min, 300g) for washing. For MHC blocking experiments, αHLA-ABC antibody (clone W6/32, BioLegend) was added to tumor cells 10min before T cell addition. After 24 hours incubation at 37°C, 5%CO_2, samples were transferred to v-bottomed 96-well plates, supernatants were collected after centrifugation (2min, 300g) and directly used or frozen at -20°C.

Flat-bottomed 96-well MaxiSorp® plates (Nunc) were coated with 50µL of the diluted IFNγ capturing antibody (1:120 in PBS) over night at RT. After blocking for at least 2 hours in blocking buffer (PBS, 1%BSA), 50µL of assay supernatants were transferred per well and incubated for 2 hours at RT. After washing, 50µL of the diluted detection antibody (1:60 in PBS, 0.1% BSA, 0.05% Tween®20, 2%NGS)

were added and incubated for 2 hours at RT. Having washed again, 50µL of diluted Streptavidin-HRP (1:40 in PBS, 0.1% BSA, 0.05% Tween®20) were added and incubated for 20min at RT. After washing, ELISA plates were developed using 50µL of the BM Blue POD Substrate solution (Roche Diagnostics GmbH). Development was stopped by adding 50µL of 1M H_2SO_4. Washing between different steps was performed by means of the MicroTek ELISA plate washer applying four wash steps with 200µL of washing buffer (PBS, 0.05% Tween®20 was used for washing of plates. Tween 20 (Roche Diagnostics GmbH), bovine serum albumin (BSA, Sigma Aldrich) and normal goat serum (NGS, R&D Systems) were used for buffers. ELISA plates were analyzed by measuring absorbance at 450nm and 620nm (reference wavelength) by means of the Infinite 200Pro plate reader (TECAN Group Ltd.) using the Tecan i-control software. Reference values were subtracted from the absorbance and final IFNγ concentrations were calculated based on a calibration curve.

6.2.5.3. LDH release assay

Tumor cells were harvested by means of accutase and $1.5x10^4$ tumor cells were plated per well of a flat-bottomed 96-well plate in 200µL of respective cell culture media. Tumor cells were treated with ATPPs, peptides or control antibodies and placed in the incubator for 20-24 hours. Next, adherent tumor cells were washed once with 150µL AIM-V medium and *in vitro* expanded, peptide-specific $CD8^+$ T cells or $CD8^+$ T cell-enriched PBMCs were added at different effector-to-target ratios in 200µL AIM-V medium. After 24 hours incubation at 37°C, 5%CO_2, samples were transferred to v-bottomed 96-well plates, supernatants were collected after centrifugation (2min, 300g) and directly used or frozen at -20°C.

100µL of assay supernatant were transferred per well of flat-bottomed 96-well plates. The Cytotoxicity Detection Kit (Roche Diagnostics GmbH) was used according to the manufacturer´s instructions in order to measure LDH activity. 100µL of freshly prepared reaction mixture were added per well and after 5-15min absorbance was detected at 492nm (reference: 620nm) using the Infinite 200Pro plate reader (TECAN Group Ltd.) in combination with the Tecan i-control software. Maximum LDH release was determined by lysing target cells with 1% Triton X-100 (Sigma-Aldrich). Percentage of lysis was calculated as [(LDH release during treatment – LDH release of target cells)/(maximum LDH release – LDH release of target cells) x 100].

6.2.5.4. Real-time cytotoxicity detection by xCELLigence

For real-time analysis of target cell killing the xCELLigence analyzer (ACEA Biosciences) was used, where the impedance is regularly measured at the bottom of a well and serves as a correlate for cell attachment and viability.

50µL of cell culture medium were added per well of a 96-well E-plate (ACEA Biosciences) and background measurement was performed at the xCELLigence RTCA instrument. Tumor cells were harvested by means of accutase and $1.5x10^4$ tumor cells were added in 150µL of cell culture media. Tumor cells were treated with ATPPs, peptides or control antibodies and placed in the incubator for approximately 24 hours. When cell indices >1.0 were reached, adherent tumor cells were washed once with 150µL AIM-V medium and $4.5x10^4$ *in vitro* expanded, peptide-specific $CD8^+$ T cells were added in 200µL AIM-V medium. Cell indices were monitored and normalized to the time point of T cell addition. Target cell killing in % was calculated as [(cell index of target cells – cell index treatment)/(cell index of target cells] x 100.

6.2.6. Confocal microscopy

6.2.6.1. Time-lapse imaging of ATPP-mediated tumor cell killing by T cells

Time-lapse imaging was established and performed in the laboratory of Olaf Mundigl (Large Molecule Research, Roche Diagnostics GmbH, Penzberg). Ibidi µ-dish chambers (Culture-Insert 2 Well in µ-Dish 35 mm, Ibidi, # 81176) were coated with Collagen type I (Sigma) at 10µg/cm^2 for 3-4 hours at RT and washed twice with PBS afterwards. $3x10^3$ HCT-116 tumor cells were plated per well in 100µL cell culture medium. After 2 days, medium was exchanged and tumor cells were treated with 0.132nM αCDCP1-CLG or control αCD22-CLG ATPP over night. After 20 hours tumor cells were stained for 15min with 2µM 5-Chlormethylfluorescein-diacetat (CMFDA, Life technologies) in cell culture medium at 37°C, 5%CO_2 and *in vitro* expanded, peptide-specific $CD8^+$ T cells were labeled for 3min with 2µM PKH26 (Sigma Aldrich) in supplied buffer. Cells were washed twice with PBS and T cells were added in phenol red-free RPMI1640 supplemented with 2%FBS at an effector-target ratio of 2:1. Time-lapse fluorescence imaging was performed in a 37°C, 5%CO_2, 95% humidity chamber on a Leica SP8 microscope using hybrid detectors

(HyD) and a 63x/1.20 water immersion lens with sequential acquisition for each channel. CMFDA signals were acquired using white light laser excitation at 488nm and emission at 492-553nm while PKH26 was excited at 561nm and detected at 567-670nm.

6.2.6.2. FRET Imaging

FRET imaging was established and performed in the laboratory of Olaf Mundigl (Large Molecule Research, Roche Diagnostics GmbH, Penzberg). $1x10^5$ MDA-MB231 cells were grown on cover slips for 24 hours and pulsed with 10µg/mL of αCDCP1-FRET conjugate for 30min on ice. Cells were washed twice with PBS, incubated in cell culture medium for t=0, 2 or 18 hours at 37°C, 5%CO_2 and subsequently fixed with 4% PFA. To investigate donor (BODIPY) and antibody co-localization Alexa Fluor 647 conjugated αIgG (H+L) antibody (Life technologies) was used. Confocal microscopy was performed on a Leica SP8 microscope using hybrid detectors (HyD) and a 100x/1.46 N.A. oil immersion lens with sequential acquisition for each channel. BODIPY signals were acquired using white light laser excitation at 488nm and emission at 492-553nm, while Rhodamine was detected at 567-670nm. Alexa Fluor 647 was excited at 647nm and detected at 653-700nm.

6.2.7. In vivo experiments and harvest of sample material

6.2.7.1. Animal facility

Animals were housed under specified pathogen free (SPF) conditions in the animal facility of Roche Diagnostics GmbH in Penzberg in compliance with national and international regulations. The facility is accredited by the Association for Assessment and Accreditation of Laboratory Animal Care (AAALAC), hence demonstrating its commitment to responsible and humane animal care. Mice were tested for defined pathogens on a regular basis according to the guidelines of the Federation of Laboratory Animal Science Associations (FELASA). Mice were kept in a 12-hour dark/light-rhythm and fed with autoclaved standard diet. Hemp pads were used for environmental enrichment. Cages, food pellets, water bottles and bedding were exchanged by animal caretakers on a weekly basis and animals were monitored

daily for general health conditions. All experiments were approved by the Government of Upper Bavaria.

6.2.7.2. Animals used for experiments

Female CIEA NOG mice® were purchased from Taconic Biosciences and used for experiments at the age of 5-7 weeks, but not before an adaption period of at least one week after arrival.

The CIEA NOG mouse® was developed by Mamoru Ito at the Central Institute for Experimental Animals (CIEA, Japan). Besides hampered innate immune components derived from the NOD inbred strain, such as macrophage and complement dysfunctions, NOG mice exhibit two major mutations leading to its immunodeficiency and thus enabling engraftment of human immune cells. These include the so-called severe combined immunodeficiency (SCID) mutation, which is an autosomal recessive mutation of the Prkdc gene ($Prkdc^{scid}$; protein kinase, DNA activated, catalytic polypeptide), an enzyme involved in DNA repair. As a result, VDJ recombination is impaired leading to the inability to generate mature B and T lymphocytes. In addition, the animals are homozygous for a loss-of-function mutation in the interleukin-2 receptor (IL-2R) gene, also known as the common cytokine receptor gamma chain, which is encoded on the X-chromosome. As the common gamma chain (γ_c) is an important component of the high-affinity receptors for various cytokines including IL-2, IL-4, IL-7, IL-9, IL-15 and IL-21, the γ_c^{null} mutation – besides impairing T and B cell development – results in lack of NK cells and dendritic cell dysfunctions.

6.2.7.3. Tumor inoculation, measurements and calculation of tumor volumes

For in vivo experiments tumor cells were expanded in cell culture medium without antibiotics and tested for the absence of murine pathogens. Cells were detached by means of accutase, washed once in FBS containing medium, once in PBS and finally resuspended at $5x10^7$ cells/mL in PBS.

The right flank of mice was carefully shaved and mice were anesthetized by means of isoflurane. $5x10^6$ tumor cells were injected subcutaneously in 100µL PBS per mouse.

Tumor growth as well as body weight were measured 2-3 times per week by means of a caliper or a laboratory scale, respectively. Ellipsoid tumor volumes were

calculated as follows: Tumor volume [mm^3] = length of tumor [mm] * (width of tumor [mm])^2 / 2.

6.2.7.4. Adoptive transfer of human T cells

Human blood donors were tested for absence of HIV and Hepatitis B/C infections. *In vitro* expanded, human, EBV_CLG peptide-specific $CD8^+$ T cells were collected by centrifugation for 5min at 300g. T cells were washed once in PBS and subsequently resuspended in PBS containing 15µg/mL IL-15 and 70µg/mL sIL15Ra-Fc (R&D Systems). Depending on the experiment, 5 or $10x10^6$ T cells were injected intravenously into the tail vein per mouse in 100µL PBS containing 1.5µg IL-15 and 7µg sIL15Ra-Fc.

6.2.7.5. Necropsy and harvest of sample material

Mice were sacrificed by cervical dislocation. Tumors were excised with a scalpel and tumor weight was determined by means of a laboratory scale. Harvested spleens and tumors were collected in RPMI1640 medium and stored on ice until further processing.

6.2.7.6. Treatment with ATPPs and antibodies

After randomization and assignment to treatment and control groups animals were injected intraperitonally with ATPPs or unconjugated control antibodies. Depending on the experiment, mice were injected (1q/3d) with 10mg/kg per week of the IgG4-based constructs or with 20mg/kg per week of the conjugates with IgG1 backbone carrying the P329G LALA mutation for abolished FcRγ binding. ATPPs or control antibodies were diluted in PBS and administered in a final volume of 100µL. Anti-human PD1 monoclonal antibody (αPD1 Ab) was kindly provided by Stefan Seeber (Large Molecule Research, Roche Diagnostics GmbH, Penzberg). αPD1 Ab was also administered in 100µL after dilution in PBS (5mg/kg/week, 1q/7d). Tested compounds exhibited endotoxin levels <0.16 EU/mL.

6.2.7.7. Processing of tumors for flow cytometry

Harvested tumors were transferred to 6-well plates and sliced into small pieces by means of a scalpel. Tumor pieces were transferred into 50mL falcon tubes and digested in 5mL RMPI1640 medium containing 1mg/mL Dispase II (Roche

Diagnostics GmbH), 1mg/mL Collagenase IV (Sigma Aldrich) and 0.1mg/mL DNase I (Roche Diagnostics GmbH). After digestion for 15min at 37°C under slow rotation (12-15rpm), the digest was transferred through a 70µm cell strainer by gently pressing the tumor through the sieve with the plunger of a syringe. The mesh was washed with 20mL FACS buffer (PBS, 3% FBS, 2mM EDTA) and the tumor cell suspension was collected by centrifugation (300g, 5min, RT). All following steps were performed at 4°C or on ice. The cell suspension was strained through a 40µm cell strainer, collected by centrifugation and finally transferred into v-bottomed 96-well plates for subsequent staining and analysis by flow cytometry.

6.2.7.8. Processing of spleens for flow cytometry

Harvested spleens were cleaned from contaminating tissue and transferred through a 70µm cell strainer by gently pressing the tissue through the sieve with the plunger of a syringe. The mesh was washed with 30mL RPMI1640 medium and the tumor cell suspension was collected by centrifugation (300g, 5min, RT) in 15mL falcon tubes. For lysis of red blood cells 5mL of BD Pharm lyse buffer (BD Biosciences) were added per tube and cells were resuspended with a 1mL pipet. After incubation for 5min at RT under slow rotation, lysis was stopped by adding 30mL of cold FACS buffer (PBS, 3% FBS, 2mM EDTA). All following steps were performed at 4°C or on ice. The cell suspension was strained through a 40µm cell strainer, collected by centrifugation and finally transferred into v-bottomed 96-well plates for subsequent staining and analysis by flow cytometry.

6.2.8. Statistics and data analysis

6.2.8.1. Analysis of in vitro data

In vitro data was analyzed and graphs were generated by means of the Microsoft Excel software. Experiments were performed at least twice with a minimum of 3 replicates.

6.2.8.2. Analysis of in vivo data

In vivo data was analyzed and graphs were generated by means of the GraphPad Prism software. Statistical analysis of experimental data was performed using one-

way ANOVA followed by Turkey´s multiple comparison test comparing the mean of each data set with every other mean with a 95% confidence interval. Results were considered statistically significant if $p < 0.05$. Tumor growth inhibition in % was calculated as $[[(Vc_{end}-Vc_{start}) – (Vt_{end}-Vt_{start})] / (Vc_{end}-Vc_{start})]*100$, where Vc, Vt are the mean tumor volumes of control and treated groups at the start (staging of tumors) or end of the study.

7. Results

7.1. Generation of ATPP immunoconjugates

We generated a panel of antibody immunoconjugates called antibody-targeted pathogen-derived peptides (ATPPs) by conjugating virus-derived, cysteine-containing peptides to free amino groups of lysine residues on tumor antigen-specific antibodies via N-Succinimidyl 3-(2-pyridyldithio)-propionate (SPDP) linkers (Figure 7.1). Peptides were covalently bound to SPDP linkers via their cysteines, generating a disulfide bond. Average peptide labeling rates were determined by mass spectrometry and can be found in Supplemental Figure 9.1d. Immunodominant 9-mers from Epstein-Barr virus (EBV) or Influenza A (INF) were selected for conjugation, which can readily bind to HLA-A02:01 or -A01:01 molecules, respectively. The peptides and their corresponding sequences are summarized in Table 6.1.

Choosing the integral membrane protein CUB-domain-containing-protein-1 (CDCP1) as primary proof of concept target allowed testing of the ATPP approach in multiple cancer cell lines, as CDCP1 is highly expressed in various cancer types. Moreover, the target efficiently internalizes upon binding of the receptor-specific antibody[190].

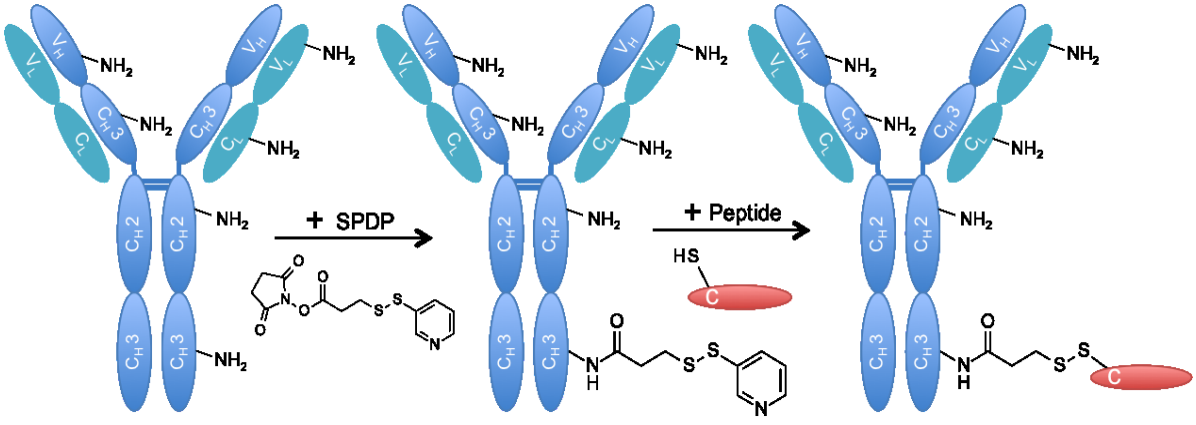

Figure 7.1 Generation of ATPP immunoconjugates.
ATPP conjugates were generated by covalently binding N-Succinimidyl 3-(2-pyridyldithio)-propionate (SPDP) linkers to the free amino group of lysine residues on utilized antibodies. Subsequently, cysteine-containing peptides (red) were linked via their thiols, generating a disulfide bond between the peptide and the linker. In the illustration, one peptide was randomly coupled to the antibody, while in theory any lysine residue offers a possibility for linker and subsequent peptide attachment. C_H: constant and V_H: variable domains of antibody heavy chains (dark blue). C_L: constant and V_L: variable domains of antibody light chains (light blue). C on peptide indicates cysteine. ATPP conjugates were generated in the laboratory of Lars Hillringhaus (Peptide Chemistry, Roche Diagnostics GmbH, Penzberg).

Importantly, utilized antibodies had a human IgG1 backbone and carried the P329G LALA mutation for abolished binding to Fc-gamma receptors (FcγR)[195]. Hence, the antibodies did not bind to FcγRI, FcγRII and FcγRIII, whereas FcRn (neonatal Fc-receptor) binding was unchanged, leading to IgG-like half-life and pharmacokinetics. As the mutations also prevent interactions with components of the complement system, antibodies do neither exhibit antibody-dependent cellular cytotoxicity (ADCC) nor complement-dependent cytotoxicity (CDC).

7.2. Phenotypic characterization and selection of target cells

In order to investigate the functionality of generated ATPP conjugates, we had to choose cancer cell lines expressing both the target as well as the respective HLA molecules that allow peptide binding. Along this line, CDCP1-positive ($CDCP1^+$) cell lines were pre-selected by mRNA expression and further analyzed by flow cytometry for CDCP1 and HLA-A1 and -A2 expression (Figure 7.2). As there is no commercially available HLA-A1 targeting antibody, we had to apply combined analysis for HLA-A1/11/26 and HLA-A1/36 (Figure 7.2d, g). Based on these data we selected 5 cell lines, which exhibited differing expression levels of CDCP1 and HLA molecules. These included a breast cancer (MDA-MB231), a colorectal cancer (HCT-116), a prostate cancer (PC-3), a pancreatic cancer (BxPC-3), as well as a melanoma (A-375) cell line. The corresponding CDCP1 and HLA expressions, including relevant HLA genotypes are summarized in Table 7.1.

Table 7.1 – CDCP1 and HLA expression on utilized cancer cell lines

Cancer cell lines	CDCP1	HLA-A2	HLA-A1/A11/A26	HLA-A1/A36
MDA-MB-231	36,366	147,187 *(A2*01, A2*17)*	-	-
HCT-116	47,678	7,990 *(A2*01)*	24,679 *(A1*01)*	1,747 *(A1*01)*
A-375	1,736	8,629 *(A2*01)*	21,758 *(A1*01)*	710 *(A1*01)*
PC-3	43,488	-	24,452 *(A1*01)*	1,336 *(A1*01)*
BxPC-3	16,632	-	35,430 *(A1*01)*	2,069 *(A1*01)*

Values represent mean fluorescence intensity (flow cytometry). Brackets indicate relevant HLA genotypes, as determined by PCR-based genotyping (ProImmune Ltd.).

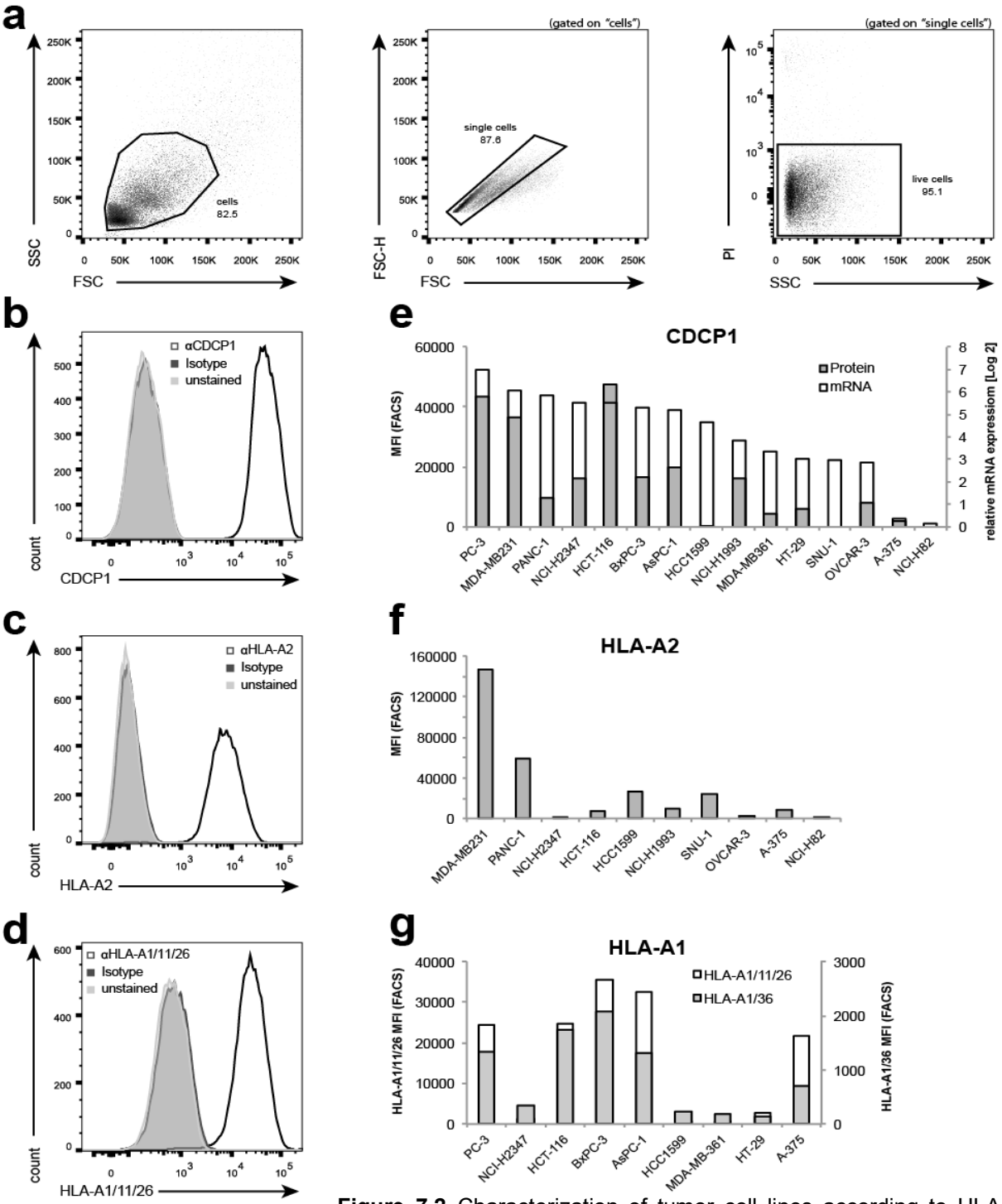

Figure 7.2 Characterization of tumor cell lines according to HLA and target expression.
(**a**) Representative gating strategy and (**b**) flow cytometric analysis of CDCP1, (**c**) HLA-A2 and (**d**) HLA-A1 expression, shown for HCT-116 cells. (**e**) mRNA as well as flow cytometry-derived CDCP1, (**f**) HLA-A2 and (**g**) HLA-A1 protein expression. MFI: mean fluorescence intensity. mRNA data were provided by Fabian Birzele (Roche Pharmaceutical Sciences) and derived from the Roche CELLO database. FACS data were partially generated in collaboration with Dominique Ostler (Discovery Oncology, Roche Diagnostics GmbH, Penzberg).

7.3. Generation of peptide-specific CD8⁺ T lymphocytes as effector cells

Having selected the appropriate target cells, we next sought to expand peptide-specific CD8⁺ T lymphocytes from human blood, which could be used as effector cells in the following experiments. For this purpose we screened a variety of human donors for HLA-A1/-A2 positivity and the abundance of peptide-specific CD8⁺ T cells (Figure 7.3). In this respect, peripheral blood mononuclear cells (PBMCs) were isolated by Ficoll gradient centrifugation and subjected to flow cytometric analysis using peptide-MHC pentamers. A representative analysis for the abundance of EBV_CLG peptide-specific T cells is depicted in Figure 7.3a. After establishing a method for *in vitro* generation of peptide-specific CD8⁺ T cell cultures by bi-weekly stimulation with peptide-loaded, autologous PBMCs or lymphoblastoid cells (LCLs), expansion was monitored by flow cytometric analysis using peptide-MHC pentamers (Figure 7.4). Cultured T cells were used as effector cells, when they exhibited 80-100% peptide-specificity. Importantly, the expansion protocol generated CD8⁺ effector memory T cells as revealed by CD45RO⁺ CCR7⁻ expression (Figure 7.5b),

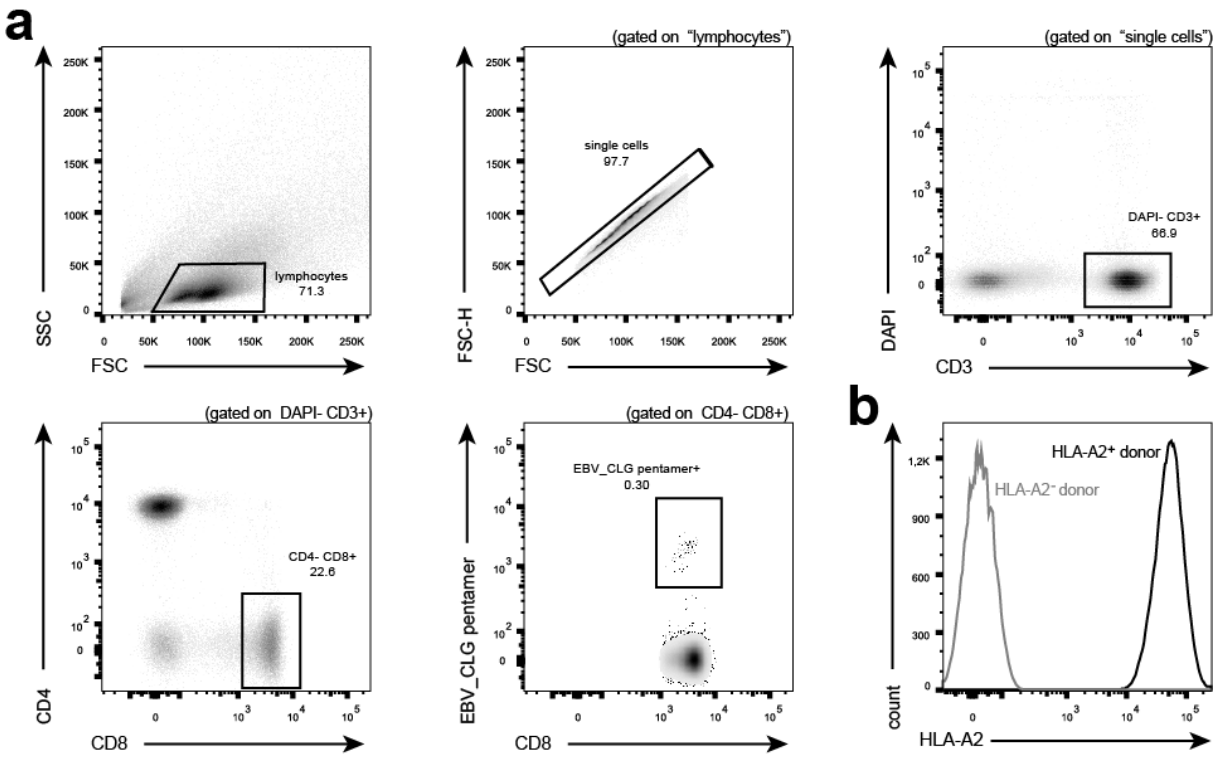

Figure 7.3 Characterization of blood donors according to HLA status and abundance of peptide-specific T cells.

PBMCs from healthy blood donors were subjected to flow cytometric analysis. (**a**) Representative gating strategy to screen for peptide-specific CD8⁺ T cells. Here, the abundance of EBV_CLG peptide-specific CD8⁺ T cells was analyzed after gating on $CD3^+CD4^-CD8^+$ cells. (**b**) Flow cytometric analysis of HLA-A2 expression on donor-derived PBMCs. A comparison between an HLA-A2⁻ (grey) and an HLA-A2⁺ donor (black) is shown.

while 75% of peptide-specific CD8$^+$ T cells in peripheral blood of donors exhibited a CD45RO$^+$ CCR7$^+$ central memory phenotype (Figure 7.5a).

In order to prove the functionality and specificity of expanded T cells, we investigated their capacity to secrete interferon-gamma (IFNγ) in response to antigenic stimulation by tumor cells loaded with the respective HLA-A02:01-binding EBV_CLG peptide. Expectedly, T cells only secreted IFNγ when encountering peptide-pulsed MDA-MB231 cells, but not when applying untreated tumor cells, as determined by IFNγ-ELISPOT (Figure 7.6a). When comparing all screened tumor cell lines, HLA-A2$^+$ MDA-MB231, HCT-116 and A-375 cells mediated strong T cell activation after peptide-loading (Figure 7.6b), again highlighting their usability to investigate ATPP functionality. As expected, HLA-A2$^-$ cell lines did not trigger T cell stimulation, when pulsed with the HLA-A2 restricted EBV_CLG peptide.

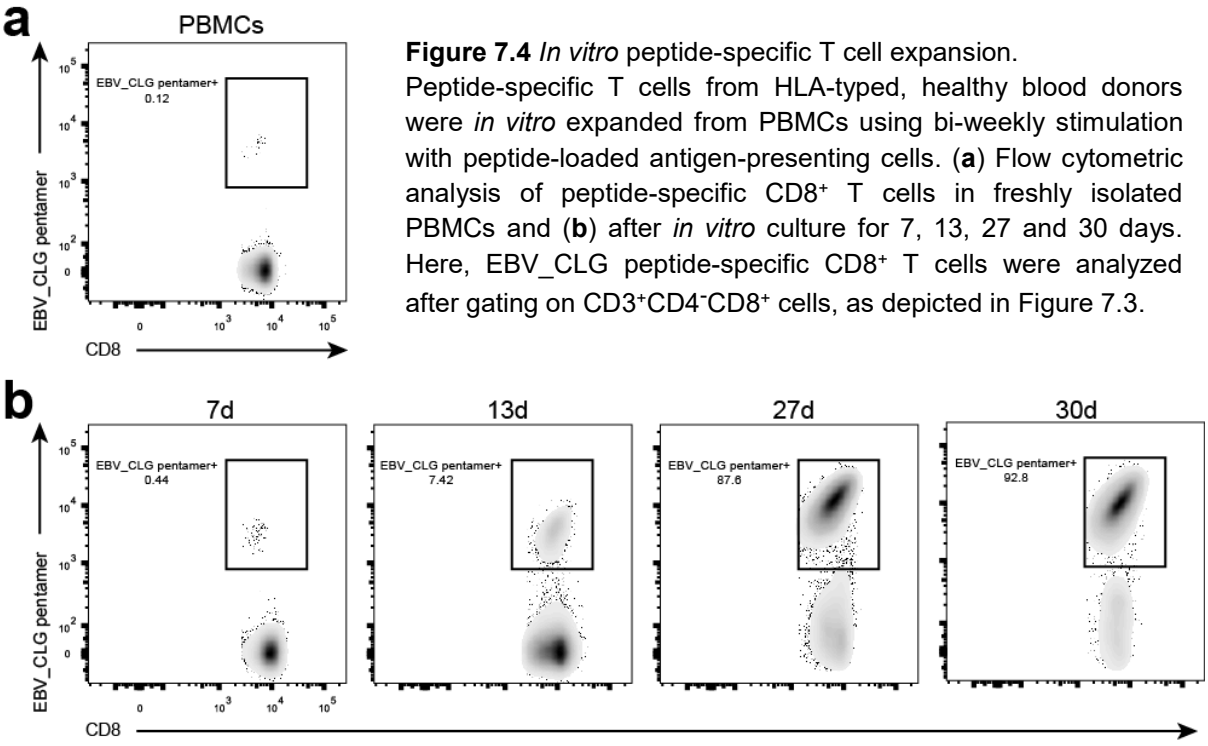

Figure 7.4 *In vitro* peptide-specific T cell expansion.
Peptide-specific T cells from HLA-typed, healthy blood donors were *in vitro* expanded from PBMCs using bi-weekly stimulation with peptide-loaded antigen-presenting cells. (**a**) Flow cytometric analysis of peptide-specific CD8$^+$ T cells in freshly isolated PBMCs and (**b**) after *in vitro* culture for 7, 13, 27 and 30 days. Here, EBV_CLG peptide-specific CD8$^+$ T cells were analyzed after gating on CD3$^+$CD4$^-$CD8$^+$ cells, as depicted in Figure 7.3.

7.4. ATPPs bind to the target and become internalized

As depicted in Figure 5.1, the ATPP concept requires binding of antibodies to the target on the cell surface and subsequent internalization of ATPP-receptor complexes into the endosomal compartment, where peptide release is supposed to occur. Since SPDP-linked peptides were randomly conjugated to lysines on the antibody and hence could theoretically affect antibody binding to the antigen and

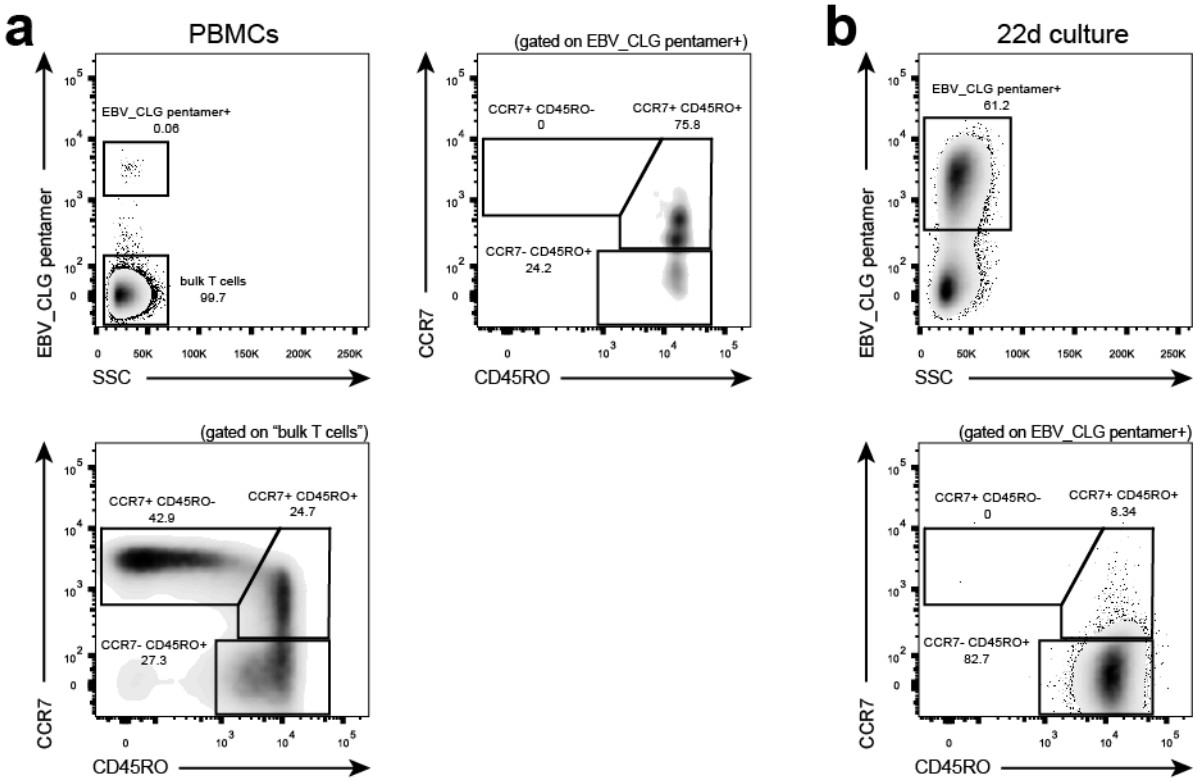

Figure 7.5 Phenotypic characterization of *in vitro* expanded, peptide-specific T cells.
(**a**) Flow cytometric analysis of freshly isolated PBMCs or (**b**) 22 days *in vitro* expanded T cells for CCR7 and CD45RO expression after gating on bulk or EBV_CLG peptide-specific T cells.

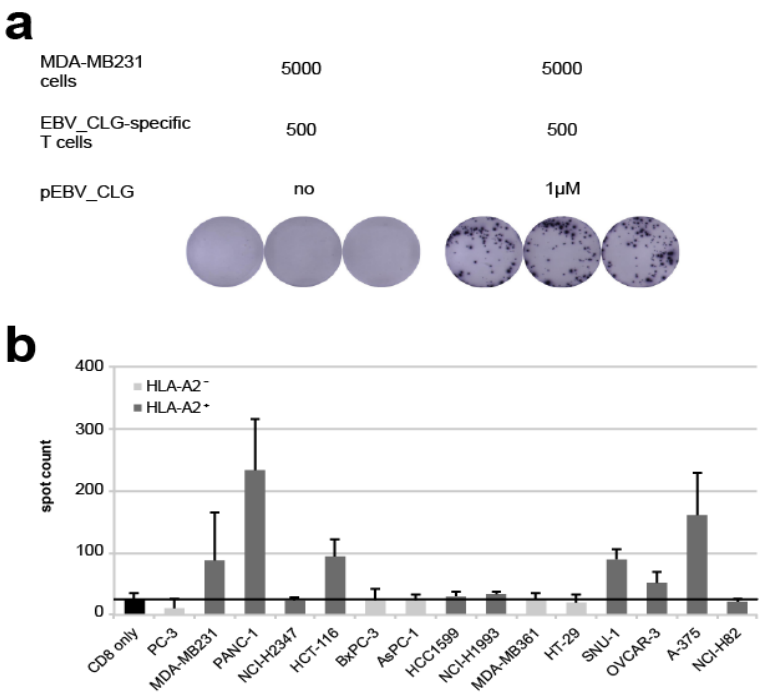

Figure 7.6 Functional characterization of *in vitro* expanded, peptide-specific CD8⁺ T cells.
(**a**) IFNγ ELISPOT assay using 5x10³ MDA-MB231 tumor cells as targets and 500 *in vitro* expanded, EBV_CLG-specific CD8⁺ T cells as responders. Cells were either treated with 1µM EBV_CLG peptide (pEBV_CLG) or left untreated. (**b**) Analysis of IFNγ ELISPOT assays with the same setup as in (a), but using different HLA-A2⁻ (light grey) or HLA-A2⁺ tumor cell lines (dark grey) as targets. All graphs represent mean of replicates (n=3) and error bars indicate standard deviation.

internalization of complexes, ATPPs were tested in FACS to confirm target specificity and to compare the kinetic of the internalization process to the parental antibodies. Along this line, we pulsed CDCP1-expressing MDA-MB231 tumor cells with the EBV_CLG peptide-conjugated αCDCP1-CLG ATPP or the corresponding unconjugated αCDCP1 antibody (Ab), which were subsequently stained with fluorescently labeled αIgG Abs. Flow cytometric analysis revealed no difference in antigen binding (Figure 7.7a). In line with these results, we also detected comparable internalization rates between ATPP conjugate and parental antibody (Figure 7.7b, c). In detail, both compounds exhibited rapid internalization reaching 50% after 2 hours and approximately 90% after 23 hours (Figure 7.7d).

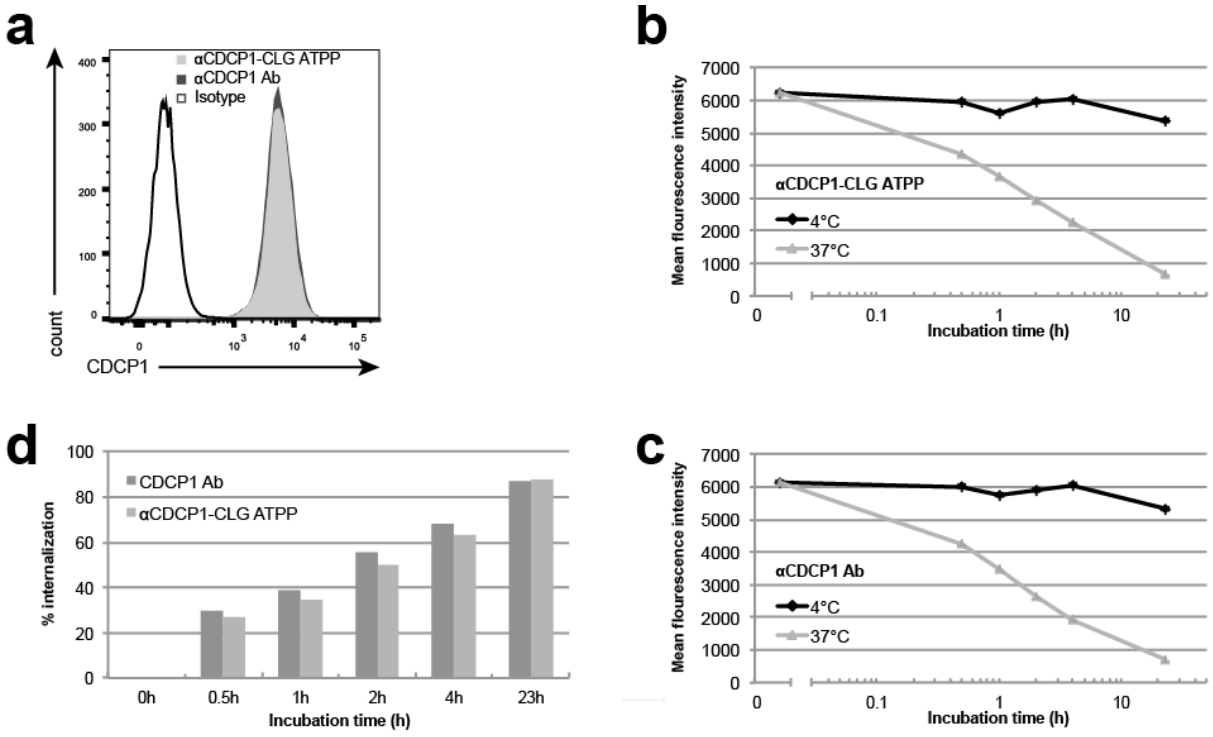

Figure 7.7 ATPP binding to the target and internalization.
(**a**) Flow cytometric analysis of αCDCP1 antibody (Ab) and ATPP binding to the target on MDA-MB231 cells using a FITC-labeled secondary antibody. (**b**) Internalization of the αCDCP1-CLG ATPP or (**c**) the αCDCP1 Ab. MDA-MB231 cells were pulsed with Ab or ATPP and incubated for indicated time points at 4°C (black) or 37°C (grey). Non-internalized antibodies were subsequently detected by means of a FITC-labeled secondary antibody. (**d**) Percentage of internalization of αCDCP1 Ab (dark grey) and ATPP (light grey) as calculated from (b) and (c).

7.5. ATPP treated tumor cells mediate efficient T cell activation in a TCR and target-dependent manner

In the following we investigated whether ATPP loaded tumor cells could trigger activation of previously expanded, peptide-specific $CD8^+$ T cells *in vitro*. For this

purpose, MDA-MB231 cells were loaded with ATPP or control compounds for 6 or 24 hours, challenged with T cells and monitored for IFNγ release. While the native αCDCP1 Ab did not exhibit any effect, the αCDCP1-CLG ATPP triggered significant T cell activation at 13.2 and 1.32nM, corresponding to 2 and 0.2µg/mL (Figure 7.8a, b). Similarly to the unconjugated control Ab, a non-cleavable ATPP construct, where the peptide was conjugated via a thioether instead of a disulfide bond, showed no

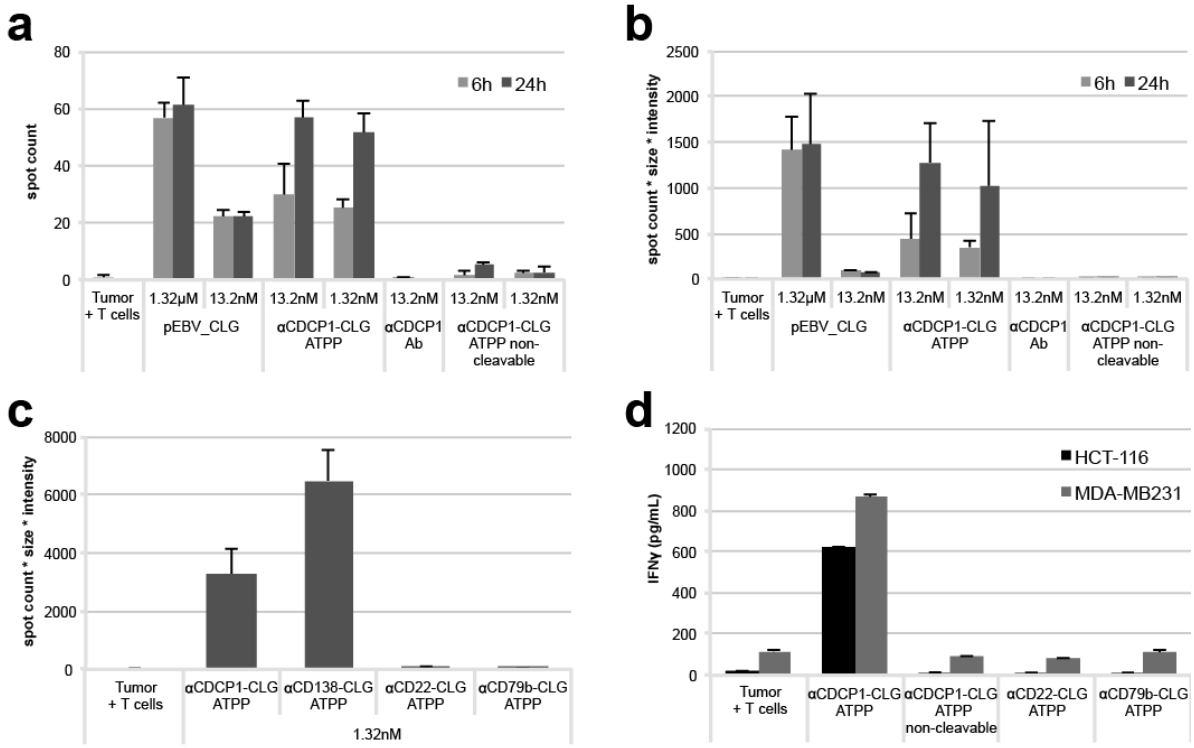

Figure 7.8 ATPP-mediated T cell activation in a target-dependent manner.
(**a**-**c**) IFNγ ELISPOT assay using $5x10^3$ MDA-MB231 tumor cells as targets and 200 *in vitro* expanded, EBV_CLG-specific $CD8^+$ T cells as responders. Cells were treated for 6 (light grey) or 24 hours (dark grey) with indicated substances prior to T cell addition. In addition to the CDCP1-targeting ATPP carrying the EBV_CLG peptide (αCDCP1-CLG ATPP), tumor cells were treated with a non-cleavable thioether construct or ATPPs targeting CD138, CD22 or CD79b proteins. Free peptide (pEBV_CLG) served as reference and αCDCP1 antibody (Ab) carrying no peptides as control. (**b**, **c**) Indicated values were generated by multiplying spot count, mean spot size and mean spot intensity per well. (**d**) IFNγ ELISA using $1.5x10^4$ HCT-116 (black) or MDA-MB231 (grey) tumor cells as targets and $4.5x10^4$ EBV_CLG-specific $CD8^+$ T cells as responders. Cells were pre-treated for 24 hours with indicated substances and IFNγ was quantified 24 hours after T cell addition. All graphs represent mean of replicates (n=3) and error bars indicate standard deviation.

effect, in turn highlighting that disulfide-dependent peptide release is important for ATPP functionality. Interestingly, free peptide mediated strikingly lower T cell activation, requiring 1.32µM to achieve comparable signals. Though, while free peptide generated similar responses regardless of incubation time, the ATPP effect increased remarkably when incubating tumor cells with the conjugates for 24

compared to 6 hours. These data suggest that, although transfer of introduced peptides onto MHC molecules seems to occur more efficiently in endosomes, the entire ATPP-mediated loading process requires more time than external loading of MHC molecules with free peptides. This effect is however reasonable, as the supposed action of ATPPs involves binding to the target, target internalization, endosomal peptide release and transfer onto MHC molecules, as well as recycling of MHC-peptide complexes to the cell surface.

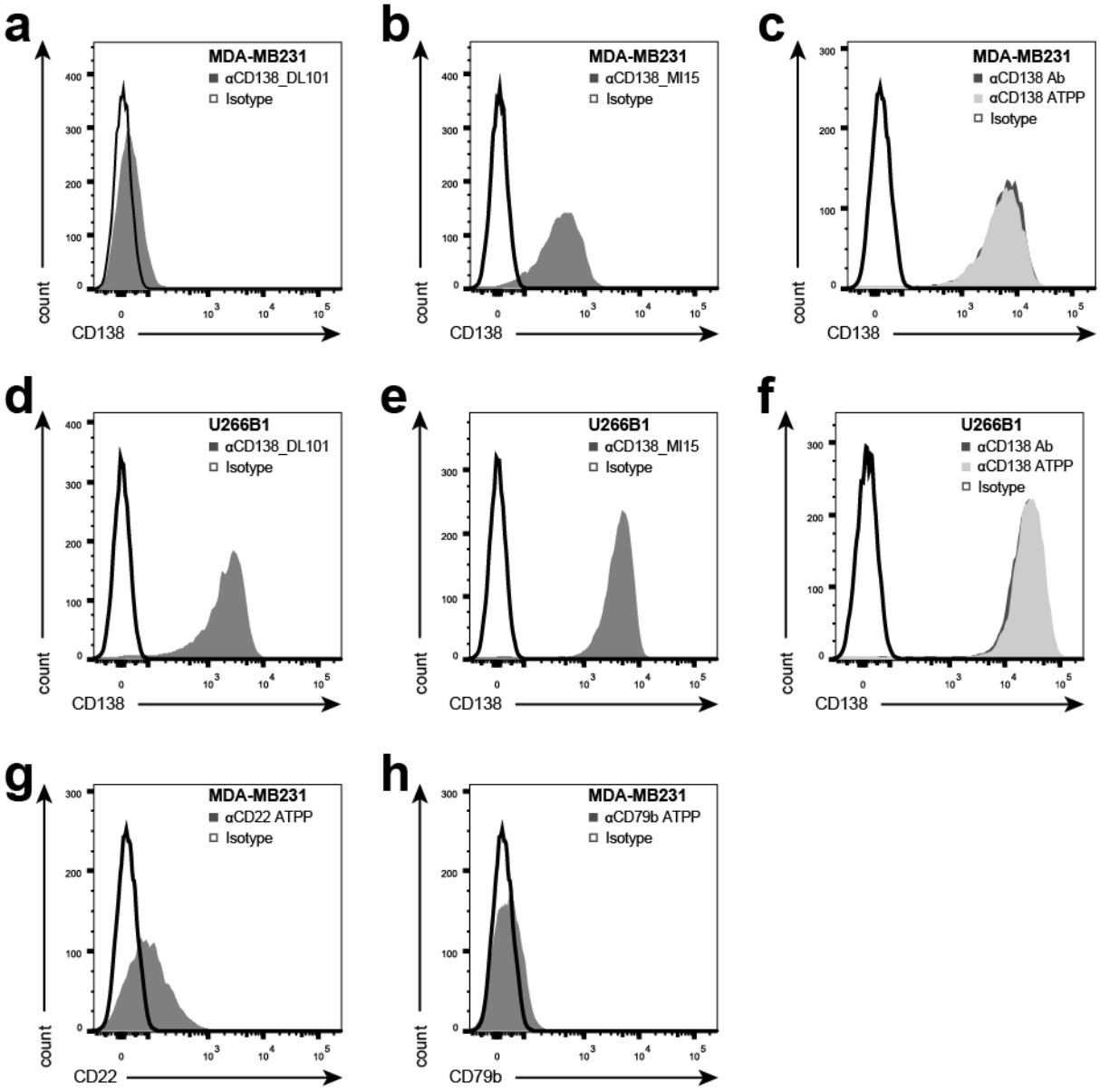

Figure 7.9 Expression of targets and control targets.
(**a**-**c**) Flow cytometric analysis of CD138 expression on MDA-MB231 or (**d**-**f**) U266B1 cells using the antibody clone DL101, the clone MI15, the αCD138-CLG ATPP or the respective cold αCD138 antibody (Ab). (**g**) Binding of the αCD22- or (**h**) the αCD79b-CLG ATPP on MDA-MB231 cells. Binding of ATPPs or respective cold Abs was visualized by means of a FITC-labeled αIgG secondary antibody. Isotype-matched control antibodies were used to compensate for Fc-mediated antibody binding.

Next, we sought to investigate target specificity of the ATPP approach. Hence, we generated pEBV_CLG-conjugated ATPPs against hematological targets that are supposed to be not expressed on MDA-MB231 breast cancer cells. Expectedly, both αCD22-CLG as well as αCD79b-CLG ATPPs did not trigger T cell activation (Figure 7.8c). However, surprisingly the CD138-targeting conjugate exhibited even stronger effects than the αCDCP1-CLG ATPP. Thus, we analyzed target expression by flow cytometry. Interestingly, we could not detect CD138 expression on MDA-MB231 cells (Figure 7.9a), while the U266B1 multiple myeloma cell line serving as positive control showed obvious staining for the antibody clone DL101 (Figure 7.9d). Nevertheless, when using the MI15 clone, we observed substantial expression in both cell lines (Figure 7.9b, e). Therefore, we analyzed target expression with the respective ATPP antibodies and subsequent detection by means of fluorescently labeled αIgG Abs in the following. In this setting, we detected clear binding of the αCD138-CLG ATPP on MDA-MB231 and U266B1 cells (Figure 7.9c, f), while both the αCD22-CLG as well as the αCD79b-CLG ATPP showed no considerable staining on MDA-MB231 cells (Figure 7.9g, h), in turn explaining the ELISPOT results. The ELISPOT data could be readily reproduced by IFNγ ELISA using MDA-MB231 and HCT-116 cells (Figure 7.8d).

As we could barely detect a reduction in the ATPP effect upon dilution from 13.2 to 1.3nM in the former assays, we next performed a titration of all generated ATPP constructs in previously selected cell lines. When using αCDCP1 ATPPs carrying the HLA-A2 restricted pEBV_CLG or pEBV_GLC peptides, we consistently detected a very low if any effect dilution from 13.2 to 0.132nM with HLA-A2$^+$ MDA-MB231, HCT-116 and A-375 cells (Figure 7.10a-c, e-g). Intriguingly, A-375 melanoma cells, which exhibit very low CDCP1 expression (Figure 7.2, Table 7.1), showed comparable results. Though, the effect completely disappeared in all cell lines upon dilution to 0.0132nM, suggesting saturation of the system until a certain concentration between 0.132 and 0.0132nM. When using the HLA-A1 restricted pINF_CTEL peptide, we observed similar results despite a small effect remaining at 0.0132nM with investigated HLA-A1$^+$ HCT-116, A-375, BxPC-3 and PC-3 cells (Figure 7.11). However, αCDCP1-CTEL ATPPs exhibited higher peptide-loading rates, carrying 5.35 peptides per Ab, while αCDCP1-CLG and αCDCP1-GLC ATPPs had 1.38 and 1.83 peptides bound, respectively (Supplemental Figure 9.1d). As suggested in previous experiments, free peptide exhibited similar effects at 1,320nM compared to

13.2 - 0.132nM ATPP. Considering the average peptide labeling rate of e.g. 1.38 peptides per Ab for the αCDCP1-CLG conjugate, the lowest concentration corresponds to a >7200-fold difference in the amount of peptide required to elicit a

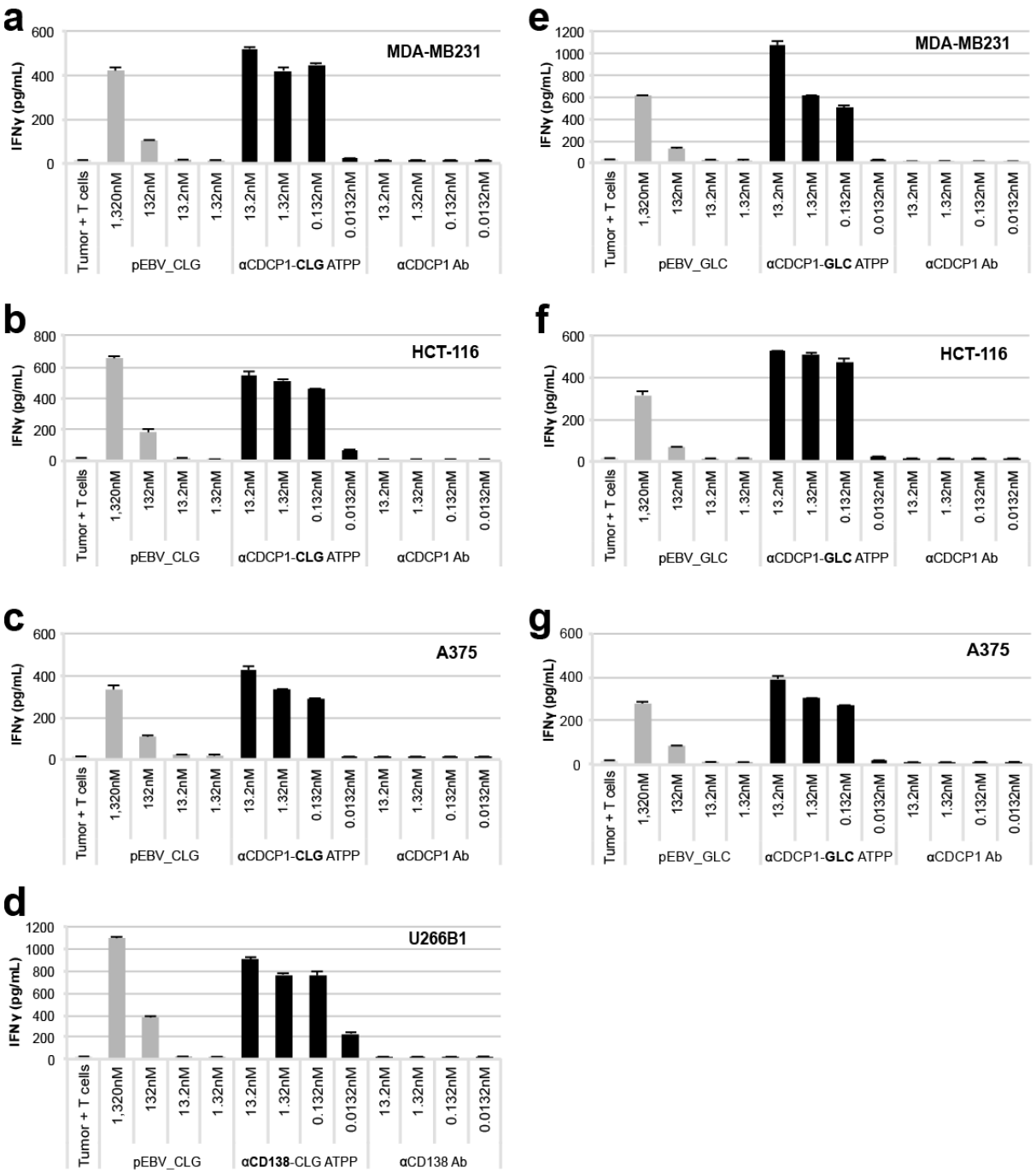

Figure 7.10 Dose-dependency of the ATPP approach using HLA-A2 restricted EBV-derived peptides. IFNγ ELISA using $1.5x10^4$ HLA-A2$^+$ tumor cells as targets and $4.5x10^4$ *in vitro* expanded, peptide-specific CD8$^+$ T cells as responders. (**a**-**c**) MDA-MB231, HCT-116 or A375 cells were treated with the HLA-A02:01-binding EBV_CLG peptide (pEBV_CLG), the control αCDCP1 antibody (Ab) or the αCDCP1-CLG ATPP. (**d**) CD138 was chosen as target in U266B1 cells. (**e**-**g**) The HLA-A02:01-binding EBV_GLC peptide was used instead of the EBV_CLG peptide. Cells were pre-treated for 24 hours with indicated substances and IFNγ was quantified 24 hours after T cell addition. All graphs represent mean of replicates (n=3) and error bars indicate standard deviation.

similar T cell response by free peptide versus ATPP. As already proven for MDA-MB231 cells, targeting the cell surface proteoglycan CD138 (Syndecan-1) on U266B1 cells exhibited comparable efficacy (Figure 7.10d), thus proving transferability of the ATPP approach to other cancer targets.

In order to ensure that the ATPP-mediated IFNγ release derives from T cell activation upon TCR interaction with the cognate MHC-peptide complex, we next tried to block the MHC accessibility by means of an HLA binding antibody. Expectedly, adding the antibody clone W6/32, which binds to conserved residues on α1 and α2 domains of HLA-A, B and C molecules, abolished T cell activation in a concentration-dependent manner for both MDA-MB231 and A375 cells (Figure 7.12).

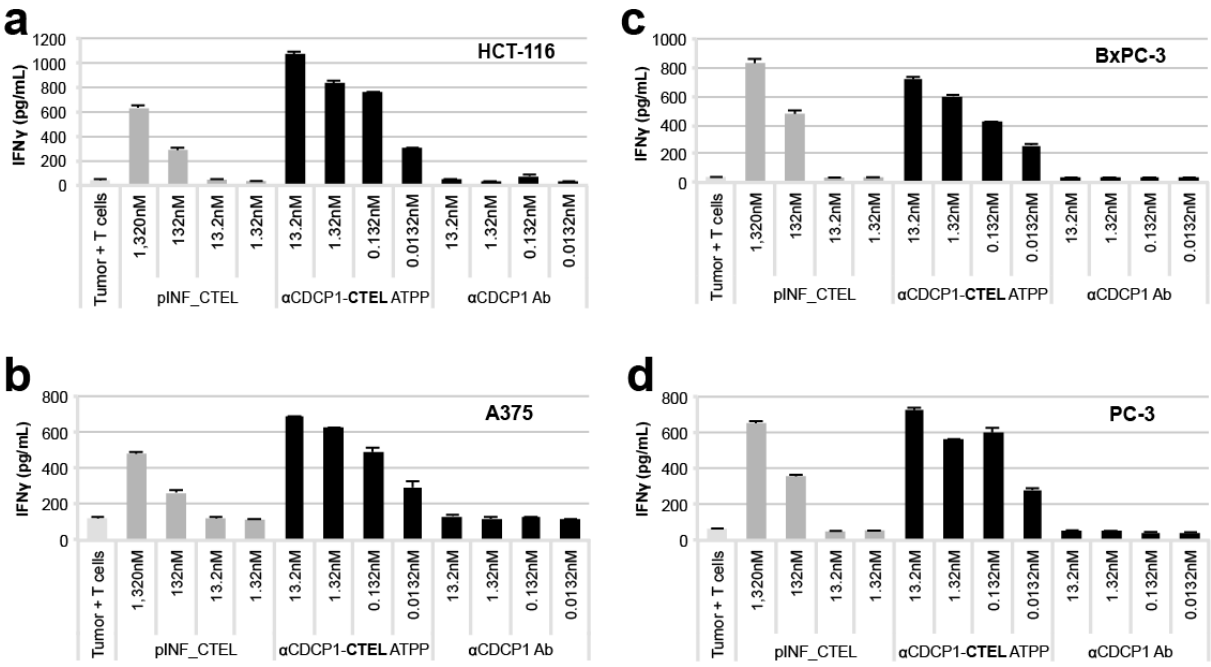

Figure 7.11 Dose-dependency of the ATPP approach using an HLA-A1 restricted influenza-derived peptide.

IFNγ ELISA using 1.5x10^4 HLA-A1$^+$ tumor cells as targets and 4.5x10^4 *in vitro* expanded, peptide-specific CD8$^+$ T cells as responders. (**a**) HCT-116, (**b**) A375, (**c**) BxPC-3 or (**d**) PC-3 cells were treated with the HLA-A01:01-binding INF_CTEL peptide (pINF_CTEL), the control αCDCP1 antibody (Ab) or the αCDCP1-CTEL ATPP. Cells were pre-treated for 24 hours with indicated substances and IFNγ was quantified 24 hours after T cell addition. All graphs represent mean of replicates (n=3) and error bars indicate standard deviation.

7.6. Virus-specific CD8$^+$ T cells efficiently kill ATPP treated tumor cells *in vitro*

After demonstrating that ATPP loaded tumor cells potently trigger activation of peptide-specific CD8$^+$ T cells, we aimed at determining whether this activation also mediates lysis of target cells. As ATPP conjugates did not exhibit a titration-

dependent efficacy reduction from 13.2 to 0.132nM in the previous experiments, we primarily focused on the 0.132nM concentration as the minimum effective dose (MED) in the following. Along this line, treatment of both MDA-MB231 and HCT-116 cells with the αCDCP1-CLG ATPP resulted in efficient killing of tumor cells starting at an effector-to-target (ET) ratio of 1:1, as detected by lactate dehydrogenase (LDH) release in the supernatant (Figure 7.13a). Importantly, an ET-ratio of 3:1 was sufficient to trigger 60-70% target cell killing, while both cell lines were almost com-

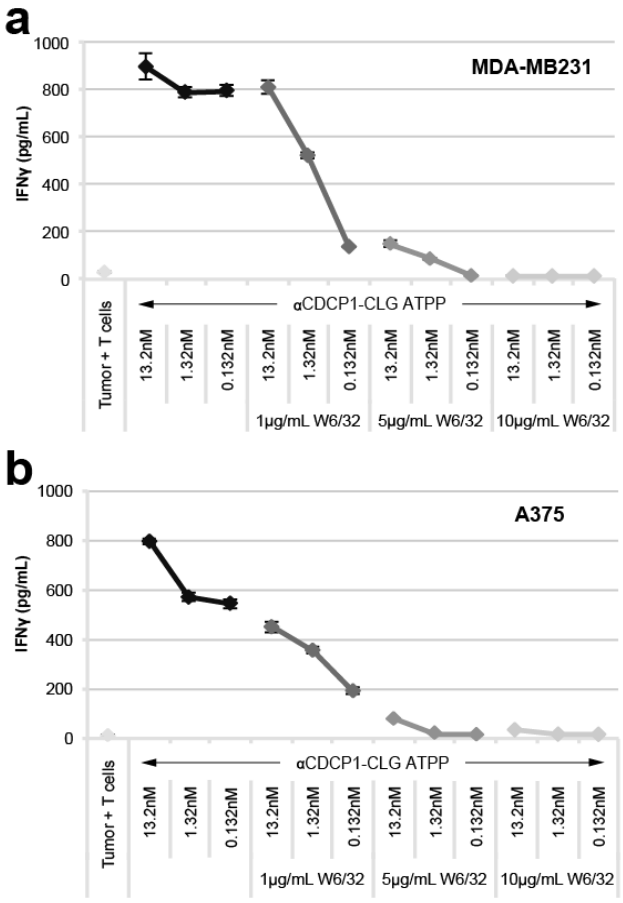

Figure 7.12 Dependency on MHC-TCR interaction of the ATPP approach.
IFNγ ELISA using 1.5x10^4 HLA-A2$^+$ tumor cells as targets and 4.5x10^4 *in vitro* expanded, EBV_CLG-specific CD8$^+$ T cells as responders. (**a**) MDA-MB231 or (**b**) A375 cells were treated with indicated concentrations of the CDCP1-targeting ATPP carrying the EBV_CLG peptide. After 24 hours different concentrations of the HLA-binding antibody clone W6/32 were added prior to T cells. IFNγ was quantified 24 hours after T cell addition. All graphs represent mean of replicates (n=3) and error bars indicate standard deviation.

pletely lysed when using 12 T cells per tumor cell. In line with previous results, a 1000-fold higher concentration of free peptide was less efficient and the non-targeting αCD22-CLG ATPP showed no effect.

In order to investigate the kinetic of the killing process, we made use of the xCELLigence system, which allows continuous monitoring of target cell lysis via impedance measurement of adherent tumor cells. As MDA-MB231 cells generated too low cell indices, we concentrated on the HCT-116 cell line in this respect. Using an ET-ratio of 3:1, the αCDCP1-CLG ATPP triggered rapid lysis of tumor cells after T cell addition, leading to >60% of killing within the first 6 hours, while the residual

killing took place during the following 18 hours (Figure 7.13b, c). As before, a 1000-fold higher concentration of free peptide showed inferior efficacy and non-targeting as well as non-cleavable controls exhibited no effects. These results were additionally confirmed by applying time-lapse live-cell imaging. In this context, addition of the αCDCP1-CLG ATPP induced serial killing of HCT-116 cells by peptide-specific CD8⁺ T cells, while T cells did not attack tumor cells treated with the CD22-targeting ATPP (Figure 7.14).

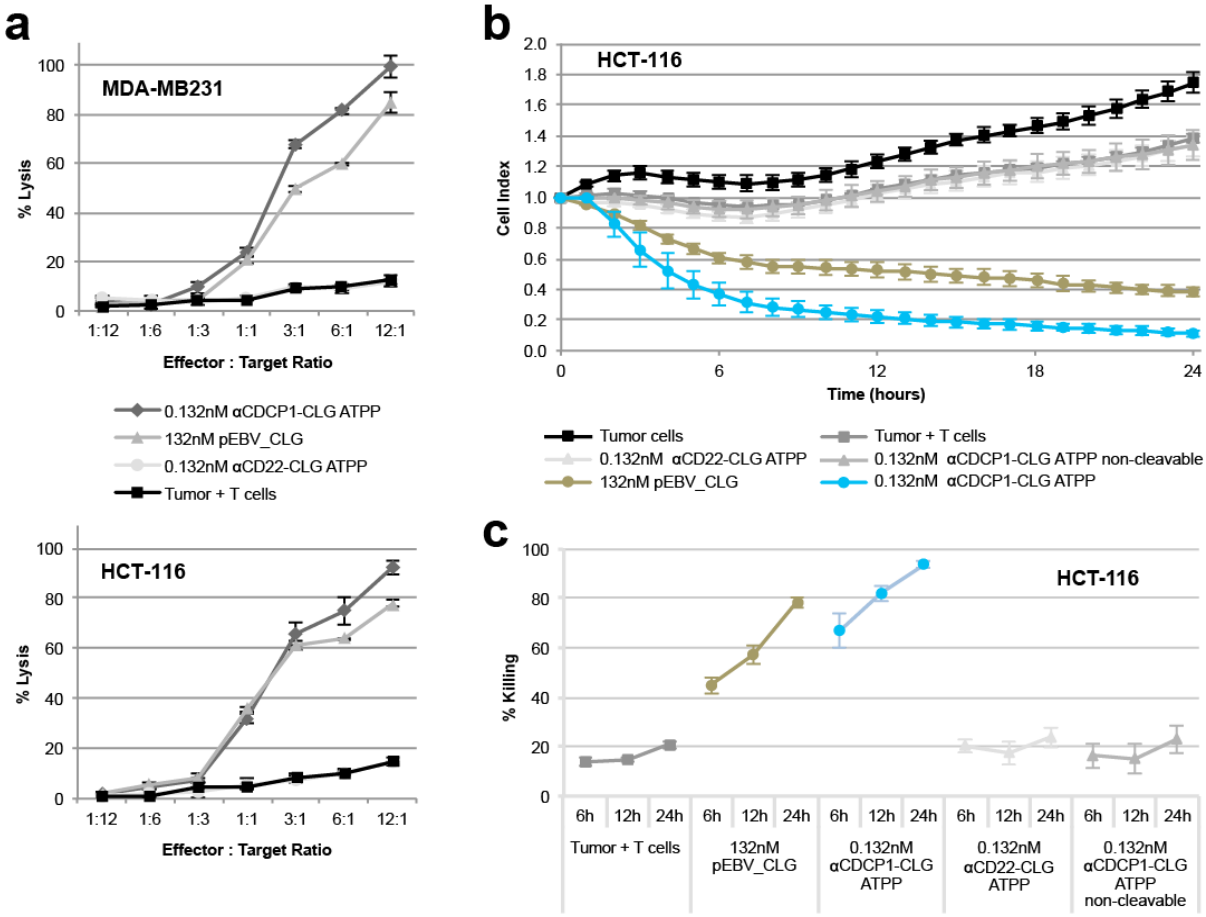

Figure 7.13 ATPP-mediated tumor cell killing by peptide-specific CD8⁺ T cells.
(**a**) LDH release assay using 1.5x10⁴ MDA-MB231 (top) or HCT-116 cells (bottom) as targets and *in vitro* expanded, EBV_CLG peptide-specific CD8⁺ T cells as effectors. Tumor cells were pre-treated for 24 hours with substances and T cells were added at indicated effector-to-target ratios. LDH was quantified after 24 hours in the supernatant and used to calculate tumor cell lysis. (**b**) Real-time analysis of target cell killing by the xCELLigence system using HCT-116 cells, which were previously incubated 24 hours with indicated substances. EBV_CLG-specific CD8⁺ T cells (E-T ratio 3:1) were added at t=0. (**c**) Percentage of tumor cell killing was calculated with data received from (b) at indicated time points. In addition to the CDCP1-targeting ATPP carrying the EBV_CLG peptide, tumor cells were treated with free peptide (pEBV_CLG), a non-cleavable thioether construct or the CD22-targeting ATPP as control. All graphs represent mean of replicates (n=3) and error bars indicate standard deviation.

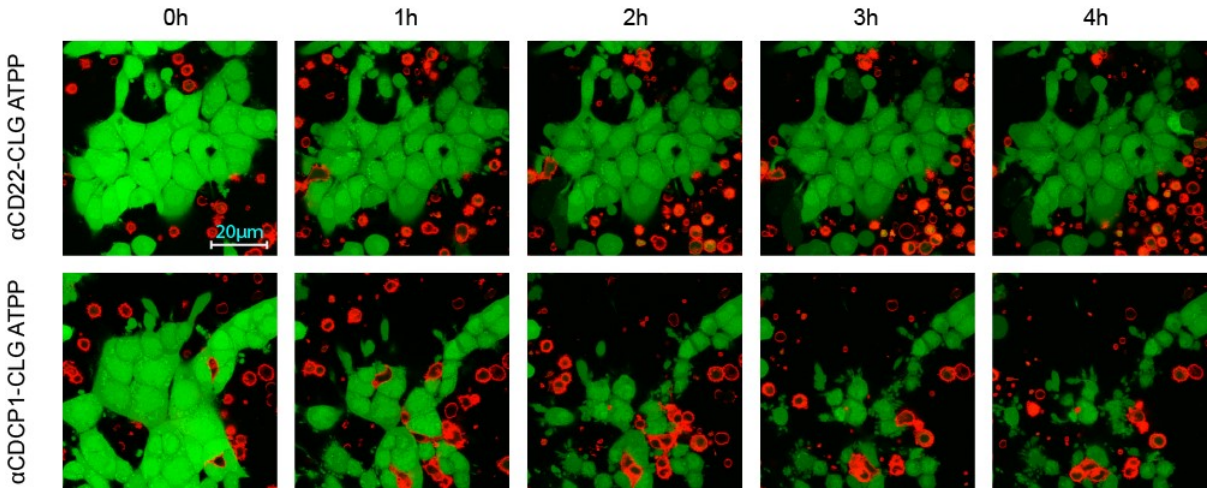

Figure 7.14 Time-lapse imaging of ATPP-mediated tumor cell killing.
Time-lapse confocal microscopy of HCT-116 cells (green, CMFDA) being killed by *in vitro* expanded, EBV_CLG peptide-specific $CD8^+$ T cells (red, PKH-26) upon ATPP treatment. Tumor cells were pre-treated for 24 hours with 0.132nM αCDCP1-CLG ATPP or the control αCD22-CLG ATPP, stained and after T cell addition subjected to optical imaging for indicated time points. Scale bar: 20µm. Data were generated in collaboration with Heike Seul (Large Molecule Research, Roche Diagnostics GmbH, Penzberg).

7.7. ATPP delivered peptides are released in endosomes and do not enter the classical MHC class I antigen processing pathway

Having proven the functionality of generated ATPP immunoconjugates, we aimed at clarifying the underlying mode of action in the following. First, we wanted to determine where exactly peptide release does occur. Based on the technique used by Yang and colleagues[191] we generated an ATPP reporter construct, which allows visualization of disulfide bond cleavage by fluorescence resonance energy transfer (FRET) technology. As depicted in Figure 7.15a, the reporter molecule consisted of a linker peptide, which was covalently bound to the αCDCP1 Ab and served as a backbone for fluorophore attachment. The FRET donor BODIPY was linked to the peptide via an amide bond, while the acceptor rhodamine was conjugated via a reducible disulfide bond, in turn serving as a mimic for the releasable peptide in ATPP immunoconjugates. When the disulfide bond is intact, excitation of BODIPY at 488nm results in intramolecular energy transfer to rhodamine and emission of red light (Figure 7.15a). Upon disulfide reduction, rhodamine is released from the conjugate, resulting in the loss of FRET, in turn generating a green (BODIPY) signal (Figure 7.15b). Using this construct we monitored the spatiotemporal peptide release by live-cell imaging (Figure 7.16). As shown in Figure 7.16a, peptide release occurred in endosomes as revealed by green BODIPY signals at t = 2 hours, while

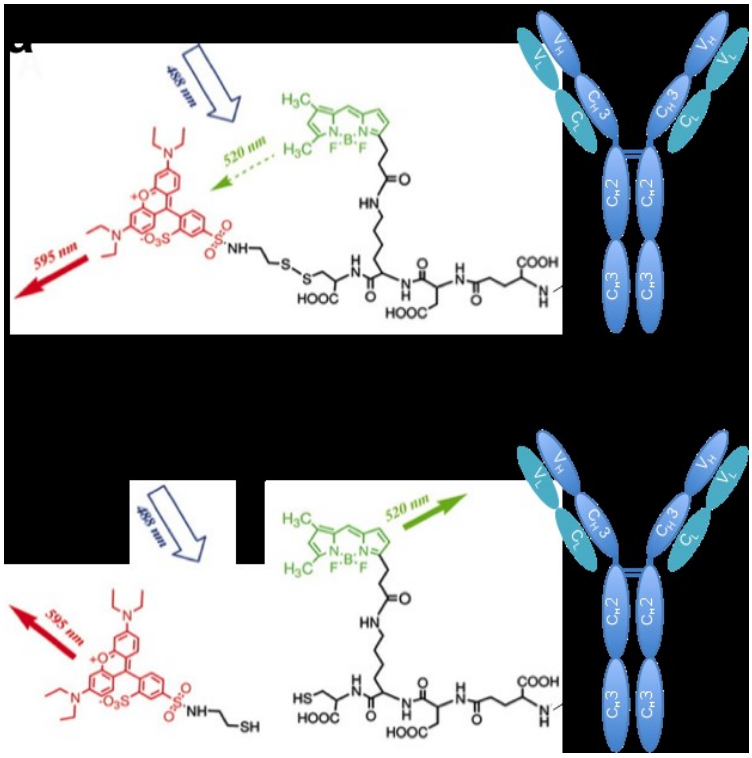

Figure 7.15 Schematic and functional illustration of the CDCP1-FRET reporter molecule.
The CDCP1-FRET reporter was generated by conjugating a BODIPY (green) linked peptide sequence to the C-terminus of the αCDCP1 antibody, while a Rhodamine fluorophore (red) was linked via a disulfide bond to a cysteine on the same peptide. (**a**) Excitation of the BODIPY fluorophore results in FRET from BODIPY to rhodamine and subsequent rhodamine (red, 595nm) emission. (**b**) Upon disulfide reduction, rhodamine is released from the conjugate, in turn allowing BODIPY (green, 520nm) emission. The CDCP1-FRET molecule was generated in the laboratory of Lars Hillringhaus (Peptide Chemistry, Roche Diagnostics GmbH, Penzberg). The figure was modified after adaption from Yang et al.[191]

only red FRET signals could be detected at the cell surface at t = 0. Green background signals may derive from incomplete FRET efficacy, which was about 90% (data not shown). Green fluorescence increased upon proceeding incubation time, suggesting accumulation of cleaved constructs. Importantly, separate excitation of the acceptor rhodamine revealed its release into the endosomal lumen, while the BODIPY donor remained membrane bound (Figure 7.16b). This finding confirmed that separation of the donor and the acceptor did not derive from proteolytic digestion, but from disulfide-dependent release of the acceptor from the conjugate. Co-localization of the donor and the antibody backbone (Figure 7.16c) additionally confirmed this finding and showed that the backbone was still intact.

In order to prove the postulated mode of action of ATPPs comprising the exchange of self-peptides on MHC class I complexes for delivered viral peptides in the endosomal compartment, we generated an extended EBV_CLG peptide by N-terminally elongating the peptide by the natural 6 amino acids of the LMP2 protein, in turn generating the EBV_YGP peptide (Table 6.1). In order to be presented on MHC class I, this peptide would require classical antigen processing, e.g. trimming by endoplasmic reticulum (ER)-associated aminopeptidases 1 and 2 (ERAP1/2) in the ER, in order to generate pEBV_CLG-MHC complexes. When performing IFNγ ELISA or LDH release assays with MDA-MB231 or HCT-116 cells, we realized that – in

contrast to the EBV_CLG peptide – neither free EBV_YGP peptide, nor the αCDCP1-YGP ATPP triggered T cell activation or lysis of tumor cells (Figure 7.17), in turn confirming that ATPP-delivered peptides do not enter the classical MHC class I antigen processing and presentation pathway.

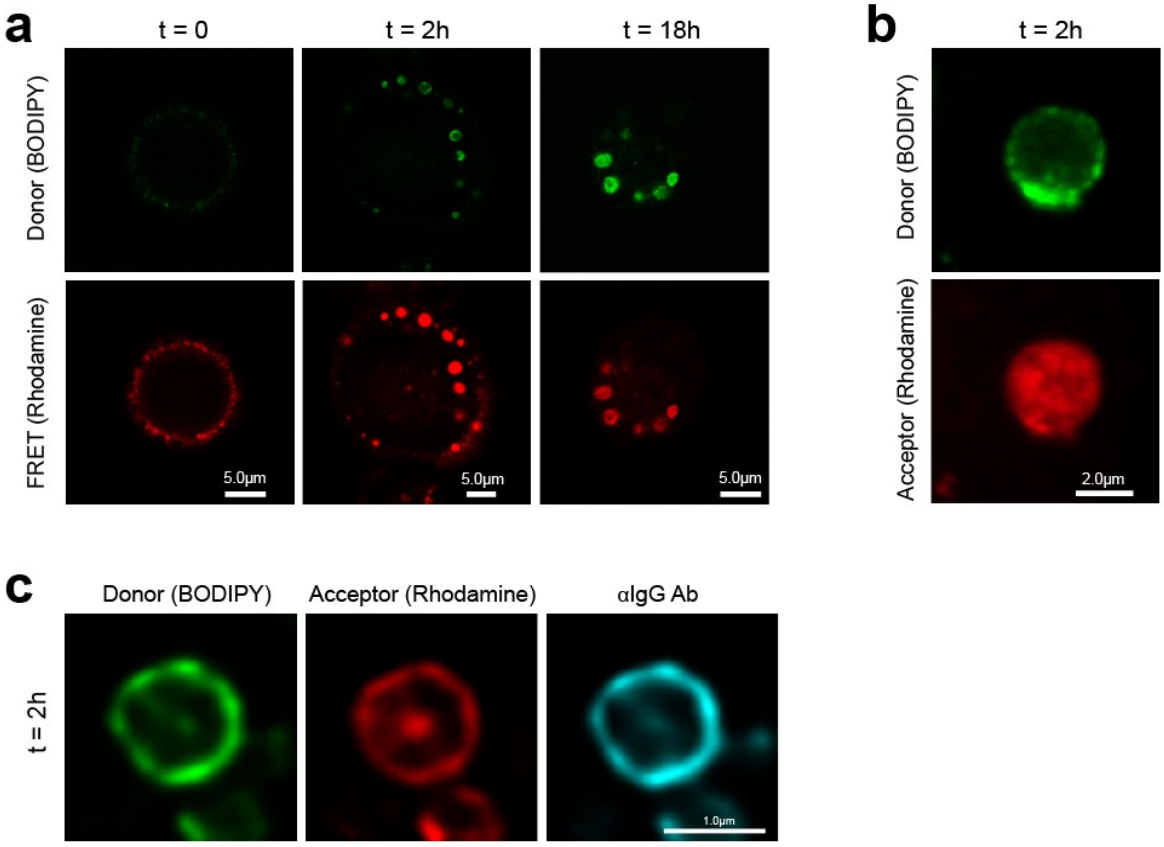

Figure 7.16 Endosomal disulfide reduction visualized by FRET.
FRET confocal microscopy using MDA-MB231 cells. (**a**) Tumor cells were pulsed with the αCDCP1-FRET construct and analyzed for BODIPY (upper channel) and rhodamine (FRET, lower channel) emission after BODIPY excitation at 488nm by confocal microscopy at t=0, 2, 18h. (**b**) Endosome of a tumor cell 2h after pulsing with the FRET construct. Excitation and emission of the donor (BODIPY, upper channel) as well as separate excitation and emission of the acceptor (rhodamine, lower channel) is shown. (**c**) Higher magnification of an endosome 2h after pulsing with the FRET construct. Detection of the αCDCP1 Ab by a secondary Ab (αIgG Ab) in addition to the donor and acceptor signals. Data were generated in collaboration with Doris Ziegler-Landesberger (Large Molecule Research, Roche Diagnostics GmbH, Penzberg).

7.8. Peripheral blood peptide-specific CD8$^+$ T cells respond to ATPP treatment and efficiently kill ATPP treated tumor cells *in vitro*

Previous data revealed the potential of ATPPs as efficient treatment against multiple cancer types, provided that the constructs do trigger activation of the corresponding peptide-specific memory T cells. In the former experiments we utilized T cell cultures that had been expanded *in vitro* to achieve higher frequency of peptide-specific cells.

In the following, we used freshly isolated PBMCs from human blood, in order to show ATPP induced activation of pre-existing circulating virus-specific T cells without culture-depended reactivation and propagation. PBMCs were simply enriched for $CD8^+$ T cells by negative selection, in order to reduce alloreaction-derived background signals. Analyzing the sort purity by flow cytometry revealed that 97.3% of the obtained $CD3^+$ T cell population were $CD8^+$, whereof 0.52% recognized the EBV_CLG peptide (Figure 7.18a). In line with previous results, ATPP loaded MDA-MB231 cells triggered activation of freshly isolated, non-expanded T cells, while controls showed no signals (Figure 7.18b). Remarkably, despite the low frequency of pEBV_CLG-specific T cells resulting in an ET-ratio of 1:10, >20% of target cells treated with 0.132nM αCDCP1-CLG ATPP were lysed after 24 hours (Figure 7.18c).

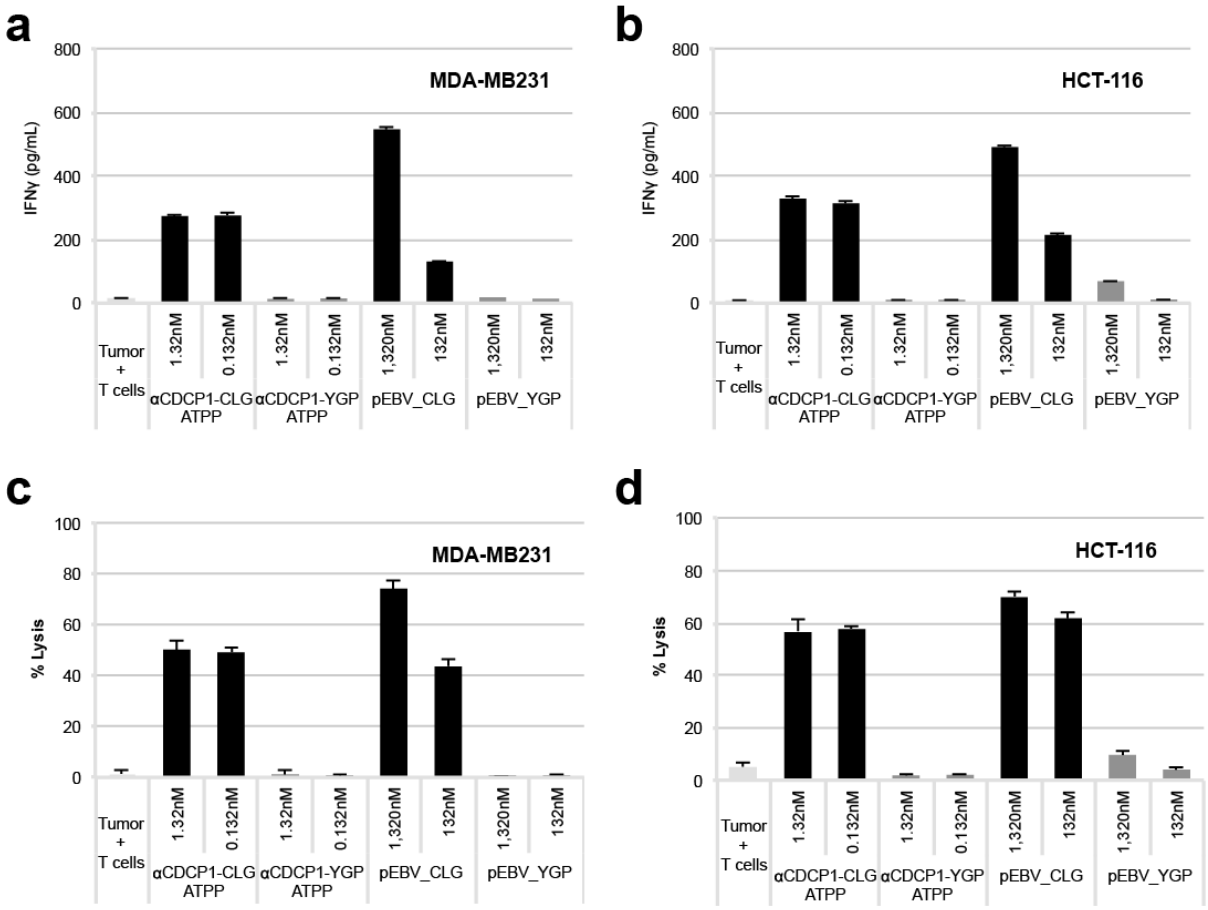

Figure 7.17 Investigation of intracellular processing of ATPP-delivered peptides.
(**a, b**) IFNγ ELISA or (**c,d**) LDH release assay using $1.5x10^4$ MDA-MB231 or HCT-116 tumor cells as targets and $4.5x10^4$ *in vitro* expanded, EBV_CLG peptide-specific $CD8^+$ T cells as responders. Tumor cells were pre-treated for 24 hours with indicated concentrations of free peptide or the αCDCP1 ATPP carrying either the EBV_CLG (pEBV_CLG) or the EBV_YGP peptide (pEBV_YGP). The latter represents the EBV_CLG peptide that is N-terminally extended by the naturally occurring 6 amino acids of the LMP-2 protein. IFNγ or LDH was quantified 24 hours after T cell addition. For peptide sequences see Table 6.1. All graphs represent mean of replicates (n=3) and error bars indicate standard deviation.

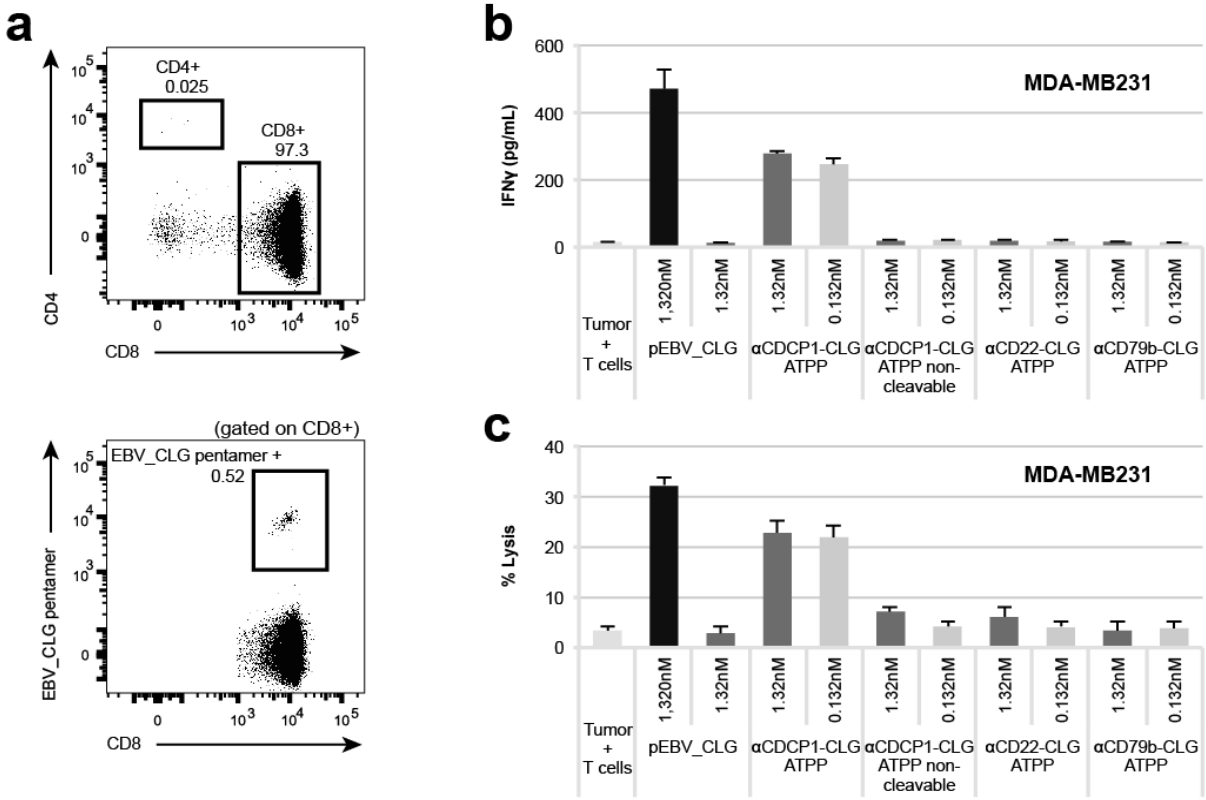

Figure 7.18 ATPP-mediated activation of freshly isolated, PBMC-derived CD8⁺ T cells.
(**a**) Flow cytometric analysis of sort purity and abundance of peptide-specific T cells after RosetteSep™-mediated sorting of CD8⁺ T cells from human blood. (**b**) IFNγ ELISA or (**c**) LDH release assay using $1.5x10^4$ MDA-MB231 tumor cells as targets and $3x10^5$ CD8⁺ T cell enriched PBMCs as responders. Tumor cells were pre-treated for 24 hours with indicated substances and IFNγ or LDH was quantified 24 hours after T cell addition. In addition to the CDCP1-targeting ATPP carrying the EBV_CLG peptide, tumor cells were treated with free peptide (pEBV_CLG), a non-cleavable thioether construct or a CD22-/CD79b targeting ATPP as control. All graphs represent mean of replicates (n=3) and error bars indicate standard deviation.

While these data show that peripheral peptide-specific memory T cells can kill ATPP loaded tumor cells, regression of an established tumor in patients would probably require expansion of the peptide-specific T cell pool. To address this question *in vitro*, we cultured PBMCs with varying concentrations of ATPPs targeting the B cell receptors CD22 or CD79b and monitored peptide-specific T cell expansion by flow cytometry using peptide-MHC pentamers. A representative analysis for the αCD22-CLG ATPP is depicted in Figure 7.19b. While the frequency of peptide-specific CD8⁺ T cells rather declined over time in untreated culture medium, treatment with αCD22- or αCD79b-CLG ATPPs resulted in significant expansion of peptide-specific cells (Figure 7.19a). Interestingly, both ATPPs exhibited strikingly higher potential to trigger T cell expansion compared to free peptide, which only showed an effect at the highest concentration. Although both ATPPs displayed comparable efficacy at 13nM, targeting CD22 receptors seemed to be more efficient at lower concentrations.

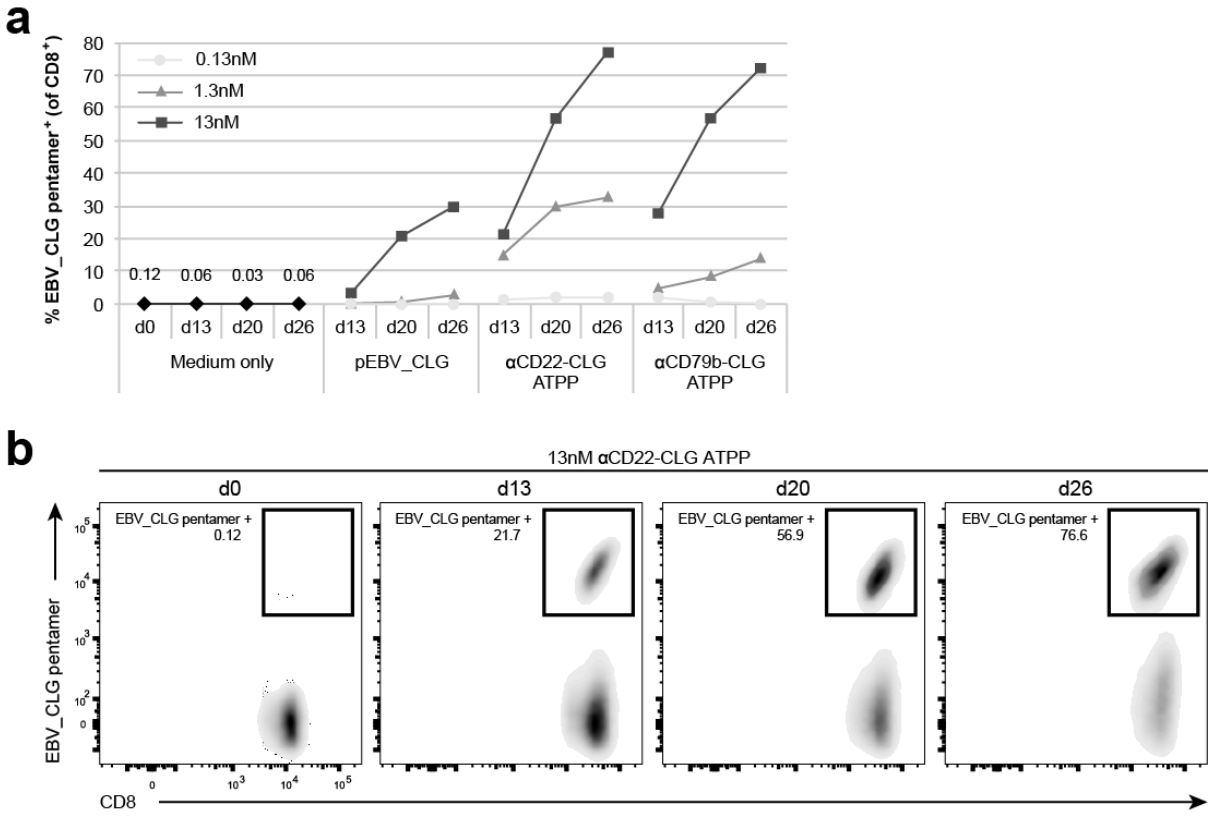

Figure 7.19 ATPP-mediated peptide-specific CD8⁺ T cell expansion by targeting B cell receptors. (**a**) EBV_CLG peptide-specific CD8⁺ T cell abundance as determined by flow cytometry, after culturing PBMCs with free EBV_CLG peptide (pEBV_CLG) or CD22- vs. CD79b-targeting ATPPs for indicated time. (**b**) Representative flow cytometric analysis of EBV_CLG peptide-specific CD8⁺ T cells in freshly isolated PBMCs (d0) and after *in vitro* culture for 13, 20 and 26 days with 13nM of the αCD22-CLG ATPP. EBV_CLG peptide-specific CD8⁺ T cells were analyzed after gating on $CD3^+CD4^-CD8^+$ cells, as depicted in Figure 7.3.

7.9. Peptide-specific CD8⁺ T cells accumulate in tumors in response to ATPP treatment and trigger tumor cell killing *in vivo*

In order to investigate the *in vivo* efficacy of ATPP treatment, we next performed a subcutaneous tumor xenograft study in NOG mice using the CDCP1⁺, HLA-A2⁺ MDA-MB231 breast cancer cell line. In the first experiment we decided to apply a preventive setting, where ATPP treatment was started at the day of tumor inoculation (Figure 7.20a). Of note, we used the αCDCP1-CLG ATPP with an IgG4 backbone, as IgG4 is known to not bind to FcγRs in humans. *In vitro* expanded, peptide-specific, human T cell cultures served as effector cells and were transferred intravenously per mouse on day 1 and again on day 16. As survival of human T cells is critical in mice, we had chosen cultures with lower peptide-specificity and higher CD4⁺ T cell frequency to possibly support effector T cell survival. Hence, cultures were 79.1 or 84.3% CD8⁺ and only 18.1 or 26.7% peptide- specific. When monitoring

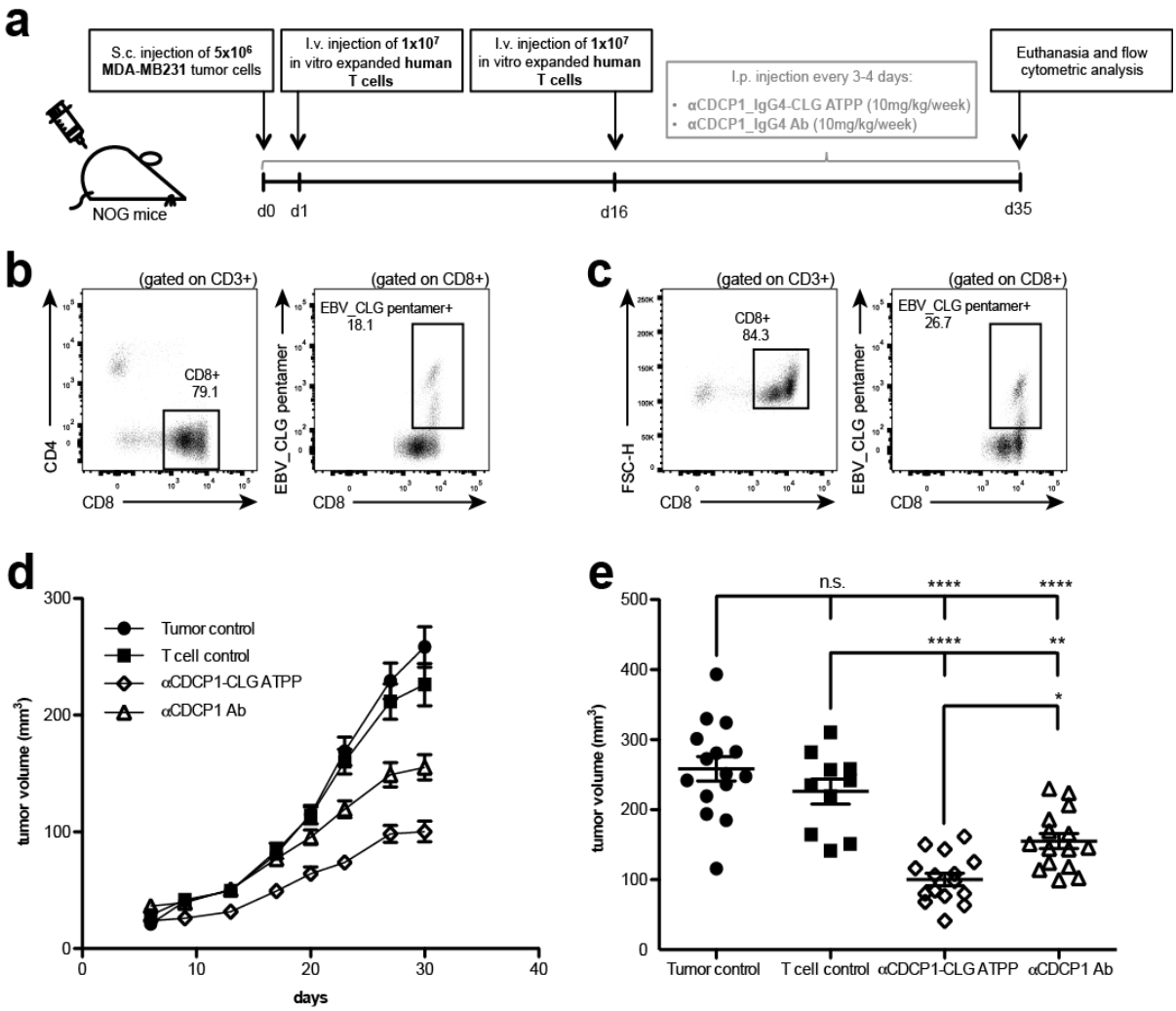

Figure 7.20 In vivo efficacy of the αCDCP1-CLG ATPP carrying an IgG4 backbone in a preventive xenograft tumor setting.
(**a**) Overview of the study setup, using the MDA-MB231 s.c. breast cancer xenograft model in NOG mice and adoptive transfer of *in vitro* expanded, human EBV_CLG peptide-specific $CD8^+$ T cells. $5x10^6$ MDA-MB231 cells were subcutaneously injected into the right flank of NOG mice. On day 1 and day 16 $1x10^7$ *in vitro* expanded, human T cells were adoptively transferred by intravenous injection into the tail vain. αCDCP1_IgG4-CLG ATPP and control αCDCP1_IgG4 Ab were administered intraperitonally, starting on d0. (**b**) Flow cytometric analysis of adoptively transferred T cells on d1 and (**c**) on day 16 prior to adoptive transfer. (**d**) Kinetic of MDA-MB231 tumor growth as determined by caliper measurement. Mice were either only injected s.c. with tumor cells (Tumor Control), additionally received i.v. T cells (T cell Control) and were additionally treated with αCDCP1_IgG4-CLG ATPP or the respective αCDCP1_IgG4 antibody (Ab) carrying no peptides as control. (**e**) Endpoint analysis of tumor volume on day 30. For each chart, data is shown as mean and error bars indicate standard error of mean (n=15, n=10 for T cell control). The *p* values represent comparisons between groups using one-way ANOVA followed by Turkey´s multiple comparison test. *$p < 0.05$, ** $p < 0.01$, ****$p < 0.0001$, n.s.: not significant.

tumor volume over time, we observed striking tumor growth inhibition for the αCDCP1_IgG4-CLG ATPP (Figure 7.20d), resulting in tumors with 94.5mm^3 in average after 30 days, while mice only receiving tumor cells exhibited tumors with

averaged 249.2mm^3 (Figure 7.20e). Adoptive transfer of T cells did not influence tumor growth (Tumor control vs. T cell control, not significant). Mice treated with the unconjugated αCDCP1_IgG4 Ab showed a prominent reduction in tumor volume, although still exhibiting significantly bigger tumors than ATPP treated animals (150.2 vs. 94.5mm^3, $p<0.05$). When monitoring the health status of the animals during the experiment, we realized a distinct reduction in body weight after day 30 in mice that had received T cell transfer (Figure 7.21a). Flow cytometric analysis of spleens (Figure 7.21b) and tumors (Figure 7.21c) on day 34 revealed massive infiltration of human T cells associated with a substantial expansion of the CD4$^+$ T cell population, suggesting an ongoing graft-versus-host disease (GvHD). In accordance with animal welfare guidelines the experiment was terminated and tumor volumes were only measured until day 30.

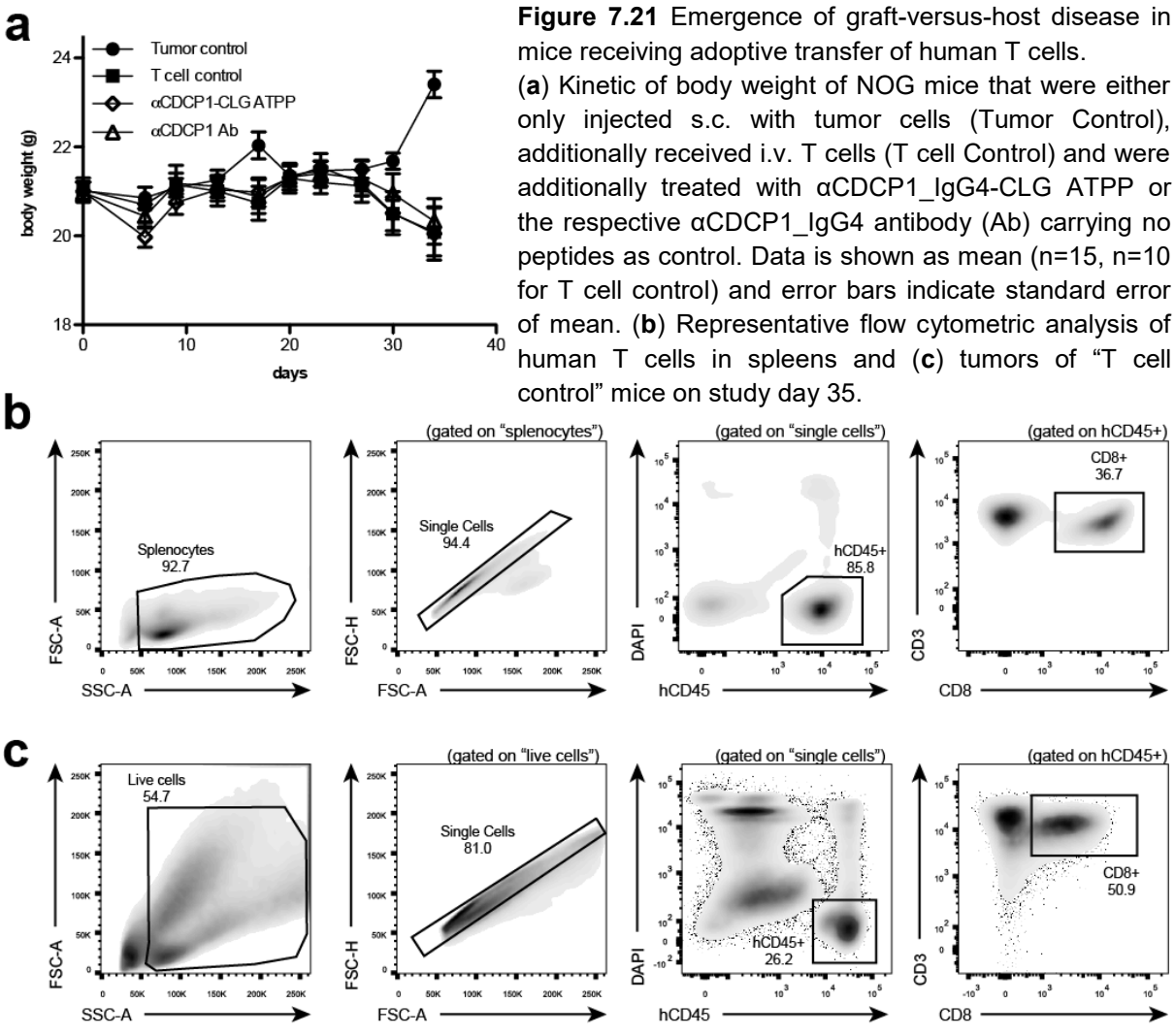

Figure 7.21 Emergence of graft-versus-host disease in mice receiving adoptive transfer of human T cells.
(**a**) Kinetic of body weight of NOG mice that were either only injected s.c. with tumor cells (Tumor Control), additionally received i.v. T cells (T cell Control) and were additionally treated with αCDCP1_IgG4-CLG ATPP or the respective αCDCP1_IgG4 antibody (Ab) carrying no peptides as control. Data is shown as mean (n=15, n=10 for T cell control) and error bars indicate standard error of mean. (**b**) Representative flow cytometric analysis of human T cells in spleens and (**c**) tumors of "T cell control" mice on study day 35.

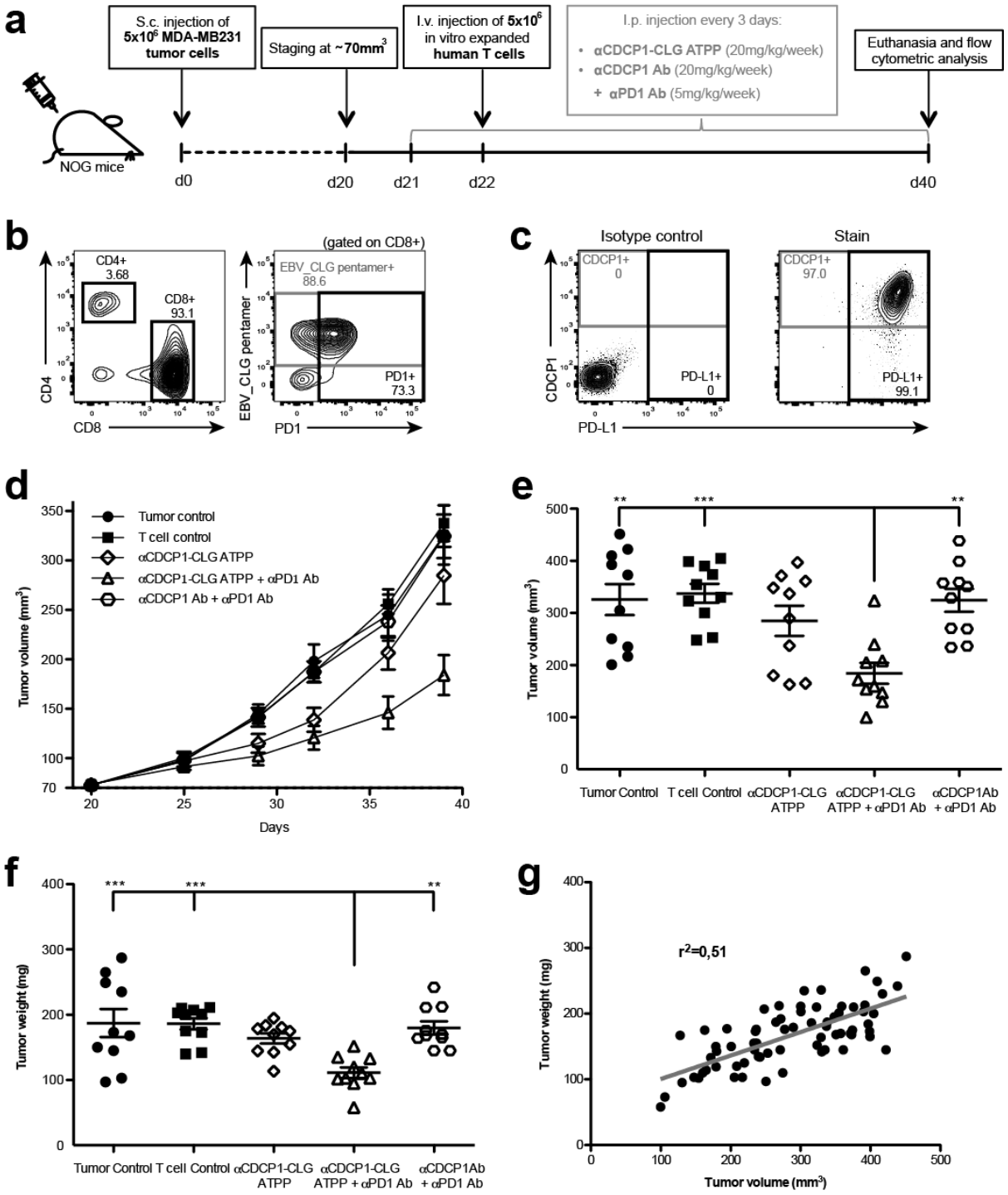

Figure 7.22 In vivo efficacy of the Fc-binding depleted αCDCP1-CLG ATPP in combination with αPD1 treatment using a therapeutic xenograft tumor setting.

(**a**) Overview of the study setup, using the MDA-MB231 s.c. breast cancer xenograft model in NOG mice and adoptive transfer of *in vitro* expanded, human EBV_CLG peptide-specific $CD8^+$ T cells. $5x10^6$ MDA-MB231 cells were subcutaneously injected into the right flank of NOG mice. When tumors reached approximately $70mm^3$, mice were i.p. injected with 20mg/kg/week of αCDCP1-CLG ATPP or the respective control αCDCP1 Ab, consisting of an IgG1 backbone with the P329G LALA mutation for abolished Fc-receptor binding. On day 22, $5x10^6$ *in vitro* expanded, human T cells were adoptively transferred by intravenous injection into the tail vain. (**b**) Flow cytometric phenotyping of adoptively transferred T cells prior to transfer according to peptide specificity and CD4, CD8 and PD1 expression. (**c**) Analysis of target (CDCP1) and PD-L1 expression in s.c. MDA-MB231 tumors by flow

cytometry. (**d**) Kinetic of MDA-MB231 tumor growth as determined by caliper measurement. Mice were either only injected s.c. with tumor cells (Tumor Control), additionally received i.v. T cells (T cell Control) and were treated with αCDCP1-CLG ATPP or αCDCP1 antibody (Ab) carrying no peptides as control, as well as with αPD1 Ab. (**e**) Endpoint analysis of tumor volume on day 39. (**f**) Analysis of tumor weight on day 40. (**g**) Correlation of tumor weight (d40) and tumor volume (d39). r^2: coefficient of determination. For charts d-f, data is shown as mean and error bars indicate standard error of mean (n=10). The *p* values represent comparisons between groups using one-way ANOVA followed by Turkey´s multiple comparison test. ** $p < 0.01$, ***$p < 0.001$.

As the observed effect of the αCDCP1 Ab possibly derived from the human IgG4 backbone, which – despite its inert phenotype in the human system – can bind to all murine FcγRs[196], we utilized the αCDCP1-CLG ATPPs with the P329G LALA-mutated IgG1 backbone, as previously used *in vitro*. Since the results from the initial animal study demonstrated first hints for anti-tumor efficacy of ATPPs *in vivo*, we next evaluated the therapeutic effect of ATPP treatment by using the same xenograft model but with established tumors (Figure 7.22a). For this purpose, mice were staged on day 20 according to tumor volume (70mm^3) and subsequently treated with the αCDCP1-CLG ATPP or the control Ab. Human, peptide-specific T cells were adoptively transferred on day 22. Due to the GvHD observed in the former study, were used cultures that were 93.1% $CD8^+$ and 88.6% peptide-specific (Figure 7.22b). Due to the extended expansion period and repeated antigenic stimulations required to achieve higher frequency of peptide-specific T cells, CTLs exhibited a $PD1^+$ phenotype. As MDA-MB231 tumor cells simultaneously expressed high levels of PD-L1 *in vivo* (Figure 7.22c), we additionally included αPD1 Ab treatment. When monitoring tumor volume over time, we observed substantial tumor growth inhibition in αCDCP1-CLG ATPP treated animals until day 32 (Figure 7.22d). However, tumors started to resume exponential growth after that time point. On day 39 there was no significant difference between tumor control (312.8mm^3), T cell control (333.1mm^3) and ATPP only-treated mice (270.2mm^3, Figure 7.22e). In contrast, animals receiving ATPP in combination with αPD1 treatment exhibited a striking and sustained delay in tumor growth until the end of the study (175.1mm^3), while the combination of αPD1 treatment with αCDCP1 Ab therapy did not show any effect (317.7mm^3, $p<0.01$). Based on these data, combined ATPP and αPD1 treatment accounted for 58.4% tumor growth inhibition at the end of the study. Analysis of tumor weights after necropsy revealed comparable results (Figure 7.22f), though showing imperfect correlation to tumor volumes (r^2=0.51, Figure 7.22g), which

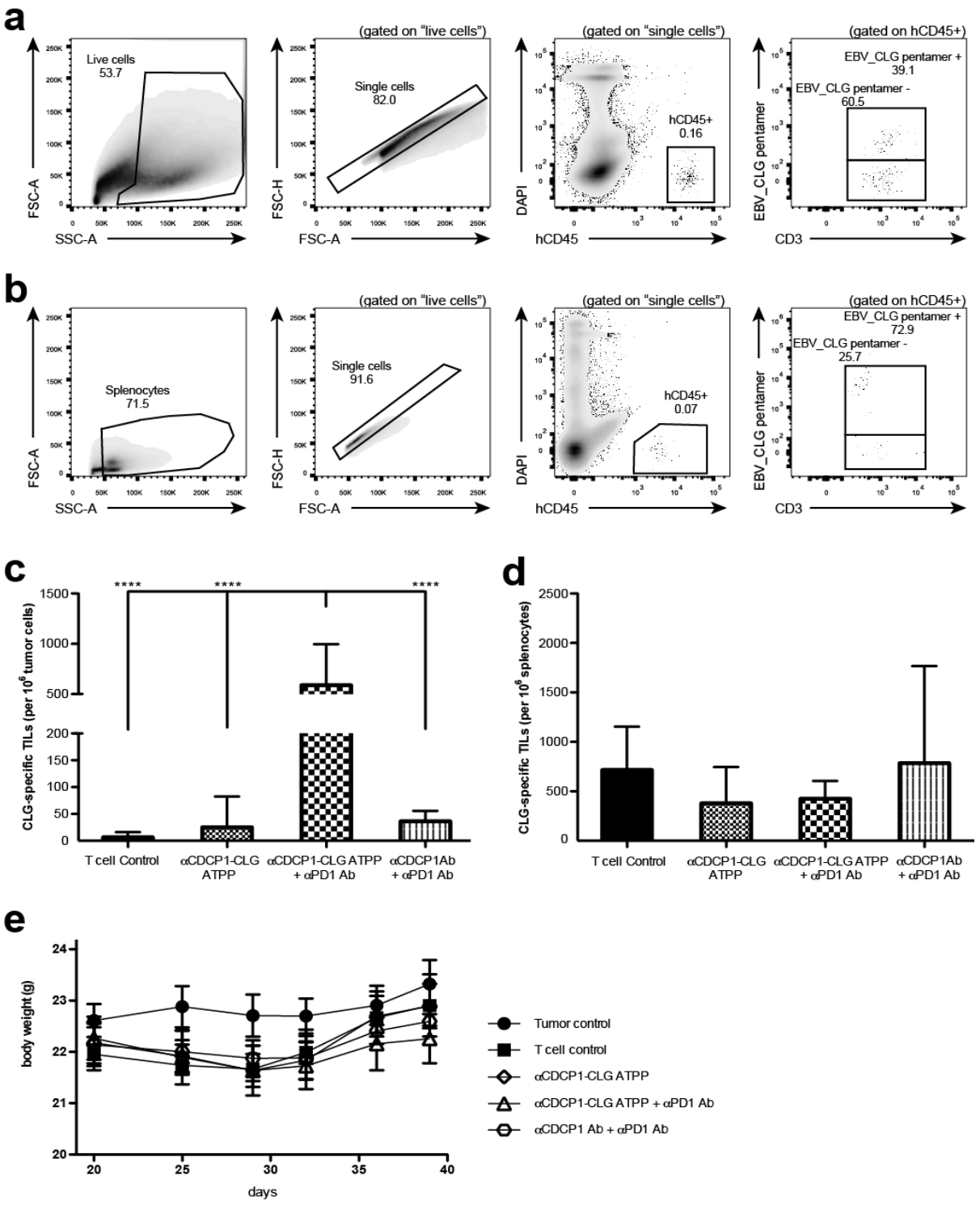

Figure 7.23 Analysis of adoptively transferred human T cells in tumors and spleens of mice.
(**a**) Representative flow cytometric analysis of adoptively transferred T cells in tumors and (**b**) spleens according to peptide-specificity using peptide-MHC pentamers. (**c**) Combined analysis of EBV_CLG peptide-specific CD8⁺ tumor infiltrating lymphocytes (TILs) in s.c. MDA-MB231 tumors on day 40 in mice either only injected with tumor and T cells (T cell Control) or additionally treated with αCDCP1-CLG ATPP or αCDCP1 antibody (Ab) carrying no peptides as control, as well as with αPD1 Ab. (**d**) Combined analysis of EBV_CLG peptide-specific CD8⁺ T cells in spleens on day 40. (**e**) Kinetic of body weight of NOG mice in the study. For each chart, data is shown as mean and error bars indicate standard error of mean (n=10). The *p* values represent comparisons between groups using one-way ANOVA followed by Turkey´s multiple comparison test. ****$p < 0.0001$.

possibly derived from the fact that MDA-MB231 tumors developed necrotic areas very early. When analyzing tumors (Figure 7.23a) and spleens (Figure 7.23b) by flow cytometry, we could not detect abnormal T cell expansion as observed in the previous study, suggesting no GvHD associated problems, as additionally confirmed by consistent body weight development in all treatment groups (Figure 7.23e). Though importantly, we detected a striking increase in EBV_CLG peptide-specific tumor infiltrating lymphocytes (TILs) in the group treated with ATPP and αPD1 Ab (Figure 7.23c), suggesting enhanced tumor infiltration, proliferation or survival of peptide-specific T cells in this setting, while there was no difference observed in the spleen (Figure 7.23d).

In summary, these results show that ATPP immunoconjugates can selectively deliver immunogenic peptides to tumor cells, in turn triggering activation of peptide-specific effector memory T cells, which are able to mediate tumor cell lysis *in vitro* and *in vivo*.

8. Discussion

The aim of this thesis was to generate immunoconjugates that selectively deliver virus-derived, immunogenic MHC-I peptide epitopes to cancer cells via a tumor antigen-specific antibody for the induction of tumoricidal, T cell-mediated cytotoxicity. Our results show that these antibody-targeted pathogen-derived peptides (ATPPs) efficiently release the peptides in endosomal compartments of tumor cells. Upon loading into cellular MHC complexes, these peptides triggered activation of peptide-specific CTLs and subsequent killing of various cancer cell lines *in vitro*. *In vivo*, therapeutic ATPP treatment generated significant anti-tumor effects in the subcutaneous MDA-MB231 breast cancer xenograft model with adoptive transfer of *in vitro* expanded, human, peptide-specific T cells, especially when combined with αPD1 Ab therapy. These findings may have substantial importance with respect to the development of novel immunotherapies.

8.1. Therapeutic implications of ATPP immunoconjugates and suggestions for further pre-clinical experimentation

Immune tolerance is a major reason for the ineffectiveness of the anti-cancer immune response as well as for the failure of cancer immunotherapies that exploit the endogenous T cell repertoire (e.g. checkpoint inhibition or adoptive transfer of TILs)[59,60]. The usefulness of T cells for recognition of self-peptides presented on self-MHCs is restricted by tolerance conferred during thymic development. As a result, antigen-specific T cell responses are limited to cancers with high numbers of non-synonymous mutations that generate immunogenic neo-epitopes. Hence, the therapeutic application of ATPPs seems particularly feasible for conferring immunogenicity to cancers with low mutational load, where checkpoint inhibitor therapy fails. Besides, targeting of cancer antigens (e.g. by cancer vaccination therapies) often requires simultaneous interference with peripheral tolerance mechanisms (such as depletion of Tregs) that additionally prevent effective immunity against tumor antigens[197,198]. Therefore, checkpoint inhibitor therapy may be applied after introduction of ATPP-delivered antigens, in order to counteract peripheral immune tolerance and immunosuppression that might prevent efficient T cell responses.

Importantly, immune tolerance mechanisms also play a decisive role in tumors with high numbers of non-synonymous somatic mutations. Although exhibiting higher immunogenicity, productive T cell responses are rarely observed in these patients[61]. Therefore, overcoming immune tolerance against already pre-existing antigens represents a major objective of cancer immunotherapy. Along this line, ATPPs exploit the endogenous, virus-specific high affinity T cell repertoire, in contrast to e.g. adoptive cellular therapies infusing *ex* vivo expanded tumor-reactive TILs. The potential of viral epitopes in mediating tumor rejection is well known[199] and additionally highlighted by the high abundance of virus-induced cancers in immunosuppressed patients[200]. As the tumoricidal T cells exploited by ATPP treatment target foreign, virus-derived antigens, there´s no potential for auto-reactivity. Hence, the endogenous T cell repertoire could additionally be boosted by vaccination prior to treatment. Furthermore, vaccination could be applied to replenish the effector T cell pool after a first round of therapy, e.g. when CTLs have become exhausted or tolerized in the tumor microenvironment.

ATPP therapy may especially qualify to avoid cancer progression after an initial response to checkpoint inhibition, that might result from the emergence of escape variants with reduced immunogenicity. In general, combined treatment with checkpoint inhibitors seems reasonable to support proper T cell function at the tumor site. Especially cancers with increased mutational burden are known to generate a highly immunosuppressive microenvironment that may hamper even high affinity T cell responses.

The beneficial potential of combining checkpoint inhibitors with ATPP treatment has been distinctly proven *in vivo*, resulting in 60% tumor growth inhibition. While the utilized model seems to perfectly qualify for investigating the possibility to combine ATPP with αPD1 treatment (high PD-L1 expression on MDA-MB231 and high PD1 expression on transferred T cells), it has several drawbacks in elucidating the achievable anti-tumor effect of ATPPs. Clearly, T cell function and/or survival are obviously hampered by PD1/PD-L1 interaction and it remains to be elucidated whether the applied αPD1 therapy can completely abolish this impediment. In addition, adoptively transferred T cells exhibited an exhausted phenotype due to repeated stimulation with antigen in culture, as evidenced by high PD1 expression and inferior cytolytic capacity *in vitro* compared to freshly isolated T cells. Furthermore, despite *in vitro* T cell expansion supported by IL-15 in the absence of

IL-2, which entails better survival and activity of human memory T cells in mice[201,202], survival, functionality and especially expansion of these cells are hampered in a xenogeneic host. These limitations may explain the lacking efficacy of ATPP monotherapy at the end of the study, whereas TILs were probably present and active at earlier time points, as suggested by the obvious effect of ATPP treatment in the beginning (Figure 7.22). Hence, the implementation of a syngeneic model with unimpaired T cell functionality seems reasonable. In such a setting we would expect more robust tumoricidal responses, as memory T cells typically undergo rapid population expansion upon antigen re-challenge. Moreover, it excludes the possibility of graft-versus-host reactions, in turn allowing extended therapy and monitoring. Importantly, the utilization of a syngeneic mouse model would additionally enable the investigation of vaccination as an approach to boost the T cell repertoire employed by ATPPs.

In general, the simplest model with respect to the generation of the antigen-specific T cell repertoire would involve the adoptive transfer of peptide-specific T cells from TCR-transgenic mice. In this respect, the use of OT-I mice in combination with the (OVA)-deduced SIINFEKL peptide as antigen seems most feasible, as this system would also allow investigation of ATPP-mediated peptide delivery via detection of MHC-peptide complexes on the cell surface of tumor cells by means of the 25-D1.16 antibody[203]. Nevertheless, this model would utilize naïve instead of effector memory cells. Hence, OVA-specific immunization may be applied in immunocompetent C57BL/6 mice to generate and also boost the effector T cell pool. The vaccination strategy would imply the generation of memory T cells in the course of an immune response and hence better recapitulate the clinical situation. To achieve the clinically most authentic situation, we suggest to utilize a syngeneic model based on acute or chronic viral infection such as the Lymphochoriomeningitis Virus (LCMV) model used by Cesson et al.[204]. This setup would probably generate the most physiologic T cell repertoire in terms of cell numbers and functionality and additionally allow assessing the impact of vaccination-based amplification of the antigen-specific T cell pool at any point of the treatment.

8.2. Comparison to similar formulations

Up to date, various efforts have been made to deliver viral antigens to tumor cells, in order to redirect virus-specific T cells against cancer, thereby exploiting their high

affinity TCRs. Along this line, several groups have generated targeted peptide-MHC tetramers by conjugating MHC molecules containing viral peptides to tumor antigen-specific antibodies by means of the biotin-streptavidin system[205-208]. Specific delivery to tumor-associated CD20, CEA or ErbB-2 surface antigens resulted in efficient target cell lysis by peptide-specific CTLs *in vitro*. Nevertheless, the large molecular mass (>400kDa) of these conjugates prevents effective tissue penetration, hence limiting their *in vivo* applicability. Besides, streptavidin is a highly immunogenic protein[209] that may favor the generation of anti-drug antibodies as well as the induction of immune-related adverse effects.

In order to overcome these limitations, targeted peptide-MHC fusions have been generated as fully recombinant molecules. These consist of a tumor antigen targeting binding moiety, either antibody or antibody-derived fragment, and a covalently linked MHC class I molecule containing the immunogenic peptide epitope. Various peptide-MHC fusions have already proven significant anti-tumor effects *in vitro*[210-214]. For instance, Schmittnaegel and colleagues have successfully generated a fusion molecule with a full length IgG1 backbone[214]. By using the immunodominant pp65 peptide epitope from the human Cytomegalovirus (CMV) they could efficiently induce lysis of various tumor cells *in vitro* by targeting differing surface antigens, including melanoma-associated chondroitin sulfate proteoglycan (MCSP). *In* vivo efficacy of those molecules could be shown when effector cells were co-engrafted with tumor cells and/or cancer cells were pre-loaded with the compound prior to implantation[213-215]. However, none of these molecules has yet advanced to clinical development. With respect to clinical applicability, the utility of peptide-MHC fusions is generally limited by their restriction to the patient population with corresponding HLA genotypes. In contrast, a major advantage of the ATPP concept represents the exploitation of cellular MHC complexes, hence not requiring sophisticated cloning and expression technologies. ATPPs are generated by biochemical conjugation, thereby allowing feasible production of multiple differing molecules.

All of the aforementioned formulations have tried to trigger tumoricidal T cell activity by delivering mature MHC-peptide complexes to the tumor site. As a result, these functional entities can also directly bind to TCRs before reaching the target cells, e.g. in the bloodstream. Due to their structural design, MHC tetramers provide four sites for TCR engagement and thus can efficiently trigger activation of circulating T cells without binding to the tumor antigen, in turn resulting in significant off-target

toxicity[216]. In contrast, binding of peptide-MHC fusions is unlikely to mediate T cell activation due to imperfect TCR clustering. Yet, sub-threshold stimulation and the lack of co-stimulatory ligands may lead to T cell anergy[150,217], in turn compromising the functionality of the T cell repertoire. On the other hand, delivery of full peptide-MHC complexes has also certain advantages. For instance, it will overcome one of the major immune escape mechanisms of cancer cells that relies on the loss or downregulation of HLA molecules. In contrast, ATPPs depend on cellular MHC molecules and hence will allow outgrowth of clones that have lost expression of the respective HLA allotypes required for presentation of the delivered epitopes.

In recent years, various technologies have emerged that – comparable to ATPPs – simply deliver immunogenic antigens to the target cell, where they require loading into cellular MHC complexes for eliciting a T cell response. In 2015, Yu and colleagues have generated antigen-armed antibodies by directly incorporating immunodominant T cell epitopes from EBV proteins into the antibody sequence[218]. By targeting the B cell surface receptors CD19-CD22 they efficiently delivered EBV antigens into lymphoma cells *in vitro*, thereby triggering activation of antigen-specific $CD4^+$ but not $CD8^+$ T cells. This represents an important difference to the ATPP approach that potently stimulates antigen-specific $CD8^+$ CTLs, which have strikingly higher cytotoxic potential than $CD4^+$ T cells. Since ATPPs release the delivered peptides within endosomes in a disulfide-dependent manner, they can be directly loaded into recycling MHC-I complexes without requiring further processing. This process is probably facilitated by endosomal acidification promoting the release of bound self-peptides[192]. As proven, ATPP-delivered peptides do not enter classical MHC-I antigen processing (Figure 7.17). In contrast, antigen-armed antibodies generated by Yu et al. depend on cellular antigen processing for the generation of mature peptides that can be loaded on MHC. However, endocytosed antigens are not accessible for the MHC-I antigen processing machinery that resides in the cytosol and ER, where it processes intracellular proteins[192]. Processing and presentation of exogenous antigen on MHC class I is restricted to cross-presenting DCs[219]. Therefore, these constructs disqualify for target cells only expressing MHC-I, hence excluding treatment of solid tumors. However, targeting of hematological malignancies allows processing along the MHC class II antigen presentation pathway and subsequent induction of $CD4^+$ T cell responses. Nevertheless, ATPP-mediated activation of $CD8^+$ CTLs would probably induce stronger cytotoxic effects

compared to $CD4^+$ T cell stimulation and ATPPs could presumably be employed to deliver MHC-II peptides, as well.

The strategy that most closely resembles the ATPP approach has been published by Kang and colleagues[220]. They have generated a fully recombinant chimeric antibody containing immunogenic MHC-I peptides (OVA or E7 protein of human papillomavirus 16) incorporated into the Fc part and flanked by cleavage sites for the endoprotease furin. Similar to ATPPs, these molecules simply release immunogenic peptides independently of the cellular antigen processing machinery. Nevertheless, this approach requires expression of furin for the liberation of the delivered peptide epitopes. By targeting the ovarian cancer-associated antigen mesothelin, the compounds induced efficient (80-90%) lysis of mesothelin-transfected cancer cells by peptide-specific T cell lines *in vitro* at 0.5 to 0.05µg/mL. Although *in* vitro efficacy depends on a variety of assay-specific factors, such as E-T ratio or the type of utilized cancer and effector cells, the concentrations are comparable to those required for ATPP efficacy *in vitro* (0.132nM ≈ 0.02µg/mL). *In vivo*, Kang et al. observed very prominent anti-tumor effects when applying the mesothelin-targeting construct containing the OVA peptide, which mediated even slight regression of established ID8 tumors transfected with human mesothelin. Yet, tumor implantation, adoptive transfer of OT-I cells as well as drug administration was all performed intraperitonally, thus resulting in intratumoral injection of effector cells and test compounds, in turn compromising clinical transferability. As discussed above, it remains to be investigated how ATPPs will perform in a syngeneic setting. The major difference to the ATPP concept, however, represents the obscurity about the spatial occurrence of furin-mediated peptide release. Although the authors did not specifically address this question, their data suggest that cleavage may at least partially take place outside the cell. Most importantly, even mesothelin-negative cell lines were lysed by 20-30%, demonstrating that the peptides may not only be liberated extracellularly but also in the absence of target antigen. Given that furin additionally becomes highly upregulated at sites of inflammation[221], these findings entail critical concerns in terms of off-target toxicity and suggest that furin-dependent peptide release might not be the mode of choice for the clinical translation of the concept.

8.3. Comparison to clinically advanced T cell-based cancer immunotherapies

While the aforementioned formulations have only experienced pre-clinical evaluation so far, advancement of the ATPP concept would eventually require comparison to clinical competitor technologies. Up to date, CAR-Ts and BiTEs represent the clinically most investigated and advanced therapeutic concepts.

BiTEs have already proven substantial clinical value especially for the treatment of hematological malignancies and two compounds have been approved by the FDA for the treatment of malignant ascites and refractory B cell acute lymphoblastic leukemia[168-173]. A major advantage of BiTEs is their great potency. As these molecules trigger TCR activation by agonistically binding to the CD3 part, they stimulate T cells independently of their specificity, thereby mediating activation of a considerable pool of polyclonal T lymphocytes. At the same time, however, this feature is responsible for the two major side effects associated with BiTE therapy: Tumor lysis and cytokine release syndrome. While the former refers to the release of a tremendous amount of DAMPs due to the rapid lysis of a multitude of cancer cells, the latter results from simultaneous cytokine production by the plethora of activated T cells. In contrast to BiTEs, ATPP therapy only activates the antigen-specific sub-population of the T cell repertoire, which possibly results in delayed tumoricidal effects. At the same time, however, the lower number of T cells activated in the first instance may simultaneously reduce cytokine release- and tumor lysis-associated side effects and thus allow better toxicity management in the beginning.

The stimulation of a distinct, antigen-specific endogenous T cell repertoire by ATPPs entails additional advantages in terms of monitoring, controlling and even vaccination-based enhancement of the effector pool, as previously discussed. Moreover, the selective delivery of immunogenic, virus-derived peptides stimulates pre-existing memory T cells, which have life-long persistence and activity. These lymphocytes represent an already differentiated cell population that requires low doses of antigen, exhibits effector functions with fast kinetics and is less dependent on co-stimulation signals[222-224], which are often absent in tumor microenvironments. Hence, the utilization of immunogenic MHC-I restricted peptides specifically stimulates a T cell repertoire with known effector memory phenotype, while circumventing the activation of potentially counterproductive T cell populations, such as Tregs or Th2 cells. This hypothesis is supported by recent findings from Schmittnaegel et al., who have compared cytokine release upon treatment with

BiTEs or peptide-MHC fusion molecules carrying the CMV-pp65 epitope. When using PBMCs as effectors, they could only detect Th2- and Treg-associated cytokines such as IL-4, IL-5 and IL-10 upon stimulation with BiTEs, but not when using their fusion molcules[214]. This scenario may especially be relevant in solid cancers that promote the generation and accumulation of immunosuppressive immune cells within the tumor microenvironment, putatively providing one reason for the compromised efficacy of BiTEs in solid versus hematological cancers.

Besides BiTEs, CAR-Ts represent another technology that has generated significant clinical responses in patients with hematological malignancies. Recently the CD19-targeting CART19 has been approved by the FDA for treatment of refractory B-ALL[176,177], highlighting the great therapeutic value of this approach. Similar to BiTEs, the major side effects of CAR-Ts are tumor lysis syndrome and cytokine storm due to the activation of large numbers of effector cells. As explained, CAR-Ts represent genetically engineered T cells expressing a chimeric antigen receptor, where target binding is mediated by an scFv-fragment. Thus, additional concerns about safety derive from insertional mutagenesis that might result from genetic manipulation and lead to T cell leukemia. Although the co-expression of so-called suicide genes has been proposed to selectively deplete the transferred CAR-T cell population[175], genetic mutations or gene silencing (e.g. by methylation) might eventually trigger escape and outgrowth of certain clones.

The generation of CAR-Ts requires collection of autologous T cells, sophisticated genetic engineering, *in vitro* expansion and infusion into the patient. This very time-consuming procedure that has to be performed separately for each patient represents a substantial technological drawback of the concept, in turn limiting its large-scale applicability. In this respect, ATPPs exhibit superior utility, as they exploit an already pre-existing endogenous T cell repertoire and can be easily designed in a flexible, combinatorial manner allowing treatment of a broad patient population (further described below). Nevertheless, as ATPPs simply deliver immunogenic antigen, they depend on cellular MHC molecules, which may entail possible problems in cancers that frequently downregulate/lose HLA expression. These escape variants could potentially be targeted with therapies that do not rely on cellular HLA proteins, such as CAR-Ts, BiTEs or peptide-MHC fusions.

All in all, every approach has specific assets and drawbacks and it remains to be elucidated which technology – also with regard to further sophistications – will

eventually exhibit the greatest therapeutic benefits for what type of malignancy. In general, reasoned combination of different immunotherapies may be beneficial and especially application of checkpoint inhibitors or co-stimulators (e.g. 4-1BB or OX40 agonistic Abs or fusion molecules) with direct T cell-engaging approaches represents the most feasible and promising strategy at the moment.

8.4. How to achieve tumor-specific delivery of immunogenic antigen

The delivery of conjugated drugs or immunogenic antigens via antibodies aims at specifically targeting cancer cells while sparing healthy tissue, thereby limiting drug-mediated toxicity and improving the therapeutic window. Therefore, the selection of a suitable target antigen is a crucial determinant of a drug´s efficacy and safety profile.

As the primary aim of this thesis was to generate proof of concept data, the experiments have been mainly performed with the test antigen CDCP1. However, despite being upregulated in various cancer types, low to moderate CDCP1 expression in several healthy tissues excludes its consideration as clinically relevant ATPP target[188,189,225,226]. Nevertheless, the presented data have revealed that the ATPP approach also works with other target antigens, as shown for CD22, CD79b and CD138 (Figure 7.10d, Figure 7.19). Moreover, cancer cell lines from different tissues could be efficiently lysed *in vitro*, in turn proving that intracellular peptide release and loading into MHC class I molecules is not limited to a specific cell type. These results prove the transferability of the therapeutic concept, hence raising the question for a suitable target antigen.

In general, ATPP therapy requires a target that exhibits sufficient tumor specificity, cell surface expression and good internalization after antibody binding. Of note, the latter requirement fundamentally differs from target selection for BiTEs or peptide-MHC fusions, as these rely on sustained, direct interaction with effector cells on the cell surface. Possibly, investigated CD22, CD79b or CD138 receptors may be promising ATPP targets. However, CAR-Ts and BiTEs have already proven significant clinical efficacy for the treatment of hematological malignancies.

In solid tumors, target antigens require more thorough selection as simultaneous expression on healthy cells can lead to severe tissue-related toxicities. Cancer testis antigens are considered favorable targets with good safety profiles due to their high tumor-specificity. Yet, their utility for ATPP therapy is limited by the requirement of surface expression. Hence, an ideal, tumor-exclusive target might be difficult to find

or be not even available at the moment. However, even if target antigens are not tumor-restricted, additional specificity and safety may be achieved, when antibodies have limited access to the target on healthy versus malignant tissues. For instance, while being upregulated on several carcinomas, polarized expression of carcinoembryonic antigen (CEA, aka carcinoembryonic antigen-related cell adhesion molecule 5) only on the apical surface of glandular epithelial cells in the gastrointestinal system results in strikingly reduced accessibility by systemically administered antibodies[227,228]. These characteristics have already led to the development of a CEA-targeting BiTE that has proven pre-clinical efficacy and is being investigated in phase I clinical trials[174].

Nonetheless, the unique mode of action of ATPP conjugates might also allow targeting of other cancer-associated antigens, which exhibit low expression on healthy tissues (such as HER2[5,229], EGFR[230,231] or mesothelin[232-234]). Especially the selection of growth receptors may result in enhanced tumor specificity due to cancer-related aberrations in endocytic circuits. In normal cells, growth receptor engagement triggers internalization and subsequent sorting to lysosomal degradation as part of negative feedback mechanisms. In cancer cells, however, derailed endocytic pathways favor the recycling of these complexes to the cell surface to promote enhanced pro-tumorigenic signaling[235,236]. As ATPPs require and trigger receptor internalization, healthy cells will downregulate target expression upon treatment, whereas tumor cells will exhibit continuously high surface levels. This temporal aspect of target expression represents a crucial difference to other immunotherapies not relying on target internalization. With ATPPs, persisting antigen turnover will hence allow strikingly augmented delivery of immunogenic epitopes to cancer versus healthy cells and presumably result in a wider therapeutic window. Moreover, uncoupling of the targeting moiety and the T cell response-eliciting agent constitutes another important distinction to established technologies. Since antibodies can be loaded with differing amounts of peptide, there´s no predefined relation between target expression and T cell activation. As T cell activation depends on proper TCR clustering and hence requires a certain amount of peptide-MHC complexes on the cell surface, the possibility to selectively adapt the number of peptides delivered per antibody allows target-dependent modification, in order to achieve efficient lysis of cancer cells but sub-threshold delivery to healthy tissues.

Nevertheless, every target antigen will eventually require detailed investigation, as

the safety and efficacy profile surely significantly depends on the inherent properties of the target (expression levels, internalization efficacy, turnover), as well as on the characteristics of the utilized antibody (affinity, pharmacokinetics) and the conjugated peptide (affinity to MHC, T cell affinity to peptide-MHC complexes).

8.5. Further sophistication of conjugate design

Aside from the target antigen, the conjugate design decisively influences a drug´s efficacy and safety profile. For instance, the pharmacokinetic plays a critical role in defining these features. In this respect, IgG antibodies – that constitute the backbone of the utilized ATPP conjugates – have a half-life of up to 4 weeks, depending on the influence of target-mediated clearance. Yet, in theory, ATPPs could also be generated with scFv or Fab molecules, e.g. to achieve better tissue/tumor penetration owing to the reduced molecular size. The size of ATPP conjugates is mainly defined by the antibody part, as linkers and peptides are very small, hence not exceeding 150-160kDa. Given that microvascular permeability only varied 2-fold in the range of 25-160kDa as determined in a xenografted human colon adenocarcinoma model[237], the usage of antibody fragments lacking the Fc-part may be counterproductive, as these molecules will have strikingly reduced half-lives (24-48h) due to missing FcRn binding and faster renal clearance[238-240]. Therefore, the usage of full-length antibody molecules seems favorable. The possible drawback of FcγR-mediated clearance has already been addressed in utilized ATPP conjugates by introducing the P329G LALA mutation into the Fc-part[195]. Moreover, the utilization of humanized antibodies in combination with the simple design of ATPP conjugates will help to reduce the risk for anti-drug antibodies that mediate enhanced clearance in kidney and liver[239].

On the molecular basis, targeted peptide conjugation should be applied, in order to reduce intermolecular heterogeneity between ATPP conjugates. ATPPs utilized in this study, were generated by randomly conjugating SPDP-linked peptides to lysine residues on the antibodies, hence precluding a defined antibody-peptide-ratio, which represents an important regulatory element to fine-tune therapeutic efficacy and safety. In this respect, site-specific conjugation has already been reported to not only preclude drug heterogeneity, but to simultaneously improve conjugate stability, pharmacokinetics as well as to potentially enlarge the therapeutic window[241]. Moreover, random conjugation could theoretically affect antibody affinity or even

specificity e.g. when binding within complementarity determining regions (CDRs). Although we could not detect differences in target binding or internalization, the applied conjugation process represents a potential drawback.

With respect to the utilized SPDP linker, it remains to be confirmed that these conjugates are stable in circulating blood of patients. Though, in theory, other linker formats could be tested[241]. Nevertheless, it will be of major importance that the peptides are released in the correct intracellular compartment that allows transfer on recycling MHC molecules.

Further on, clinical applicability of the ATPP technology requires generation of immunoconjugates that allow treatment of a broad patient population. Therefore, the delivered peptide epitopes should be selected relating to the frequency of respective HLA genes and the abundance of peptide-specific T cells. In addition, differing binding affinities of peptides to the respective MHC molecules or varying TCR affinities for the cognate peptide-MHC complex may play important roles in determining the therapeutic potential.

In the performed experiments we have chosen immunodominant epitopes that bind to the high frequency HLA allotypes HLA-A2:01 and HLA-A1:01[242,243] and derive from viruses with high seroprevalence (EBV[244-246], Influenza A[247,248]). Moreover, it is well known that $CD8^+$ cytotoxic T cells against these viruses are maintained at high frequencies in the circulation of healthy persons and cancer patients and can be functionally reactivated upon antigen rechallenge[249-251]. Nevertheless, a combinatorial approach by conjugating multiple, varying peptide epitopes per antibody seems reasonable, in order to increase the pool of activated T cells and to allow treatment of a larger patient population. Along this line, the utilization of additional antigenic epitopes, against which memory T cells exists in the majority of the human population (e.g. CMV[252,253] or from vaccines against polio or hepatitis viruses), may be favorable. As mentioned above, specific vaccinations could additionally be applied prior to ATPP treatment, in order to induce or boost the respective effector memory pool. Besides increasing the therapeutic coverage of the patient population, employing various peptides with different HLA-restrictions may additionally counteract the emergence of tumor escape variants that e.g. downregulate or lose expression of certain HLA molecules.

In terms of feasibility, usage of the biotin-streptavidin system, conjugating Abs and peptide linkers in a two-step process, may even help to achieve personalized

therapeutics. Although streptavidin has been shown to elicit significant immune responses in humans, in turn limiting its utility, recent approaches of targeted mutagenesis have generated promising data in reducing its immunogenicity while preserving the core functions of biotin binding[254,255].

Taking together, our data demonstrate that ATPPs can trigger T cell activation against cancer cells from multiple cancer types by targeting different surface antigens and delivering immunogenic peptide epitopes with varying HLA restrictions. These immunoconjugates efficiently mediated lysis of targeted cancer cells *in vitro* and *in* vivo, hence providing evidence for a broad therapeutic applicability. Fundamental differences in the biological functionality of the ATPP technology compared to existing immunotherapies may open new avenues for therapeutic applications, possibly also in cancers that resist or escape current treatment strategies. As proven by the presented data, combined treatment with existing immunotherapies, especially with checkpoint inhibitors, suggests great potential for cancer therapy. Further pre-clinical and clinical research is required, especially with respect to the target antigen, in order to further advance this innovative and promising approach towards clinical development.

9. Supplemental Figures

a

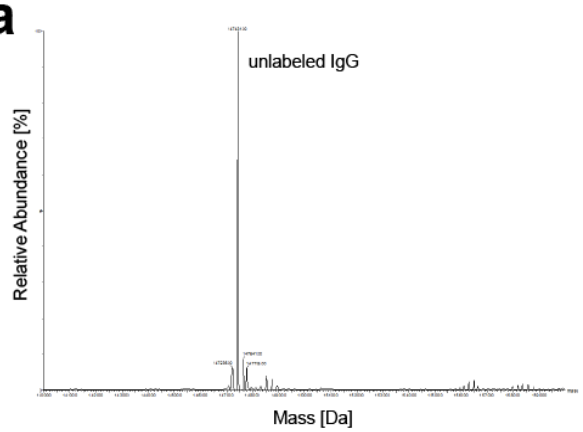

b

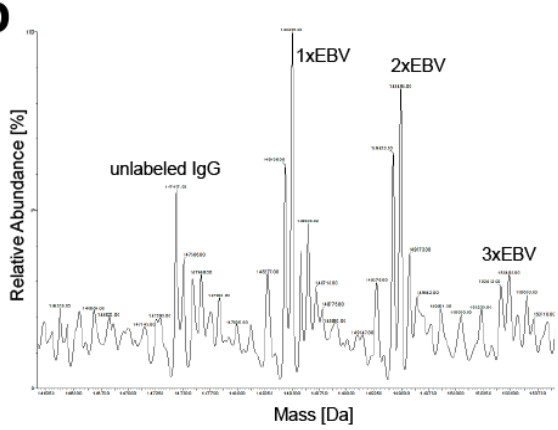

c

Mass [Da]	Rel. intensity [%]	Form
147437	14	IgG
148433	42	IgG(SPDP-EBV)
149423	36	$IgG(SPDP\text{-}EBV)_2$
150413	8	$IgG(SPDP\text{-}EBV)_3$
mean labeling rate: 1,38 peptides/IgG		

d

ATPP conjugate	Average peptides per Ab
αCDCP1-CLG	1.38
αCDCP1-GLC	1.83
αCDCP1-CTEL	5.35
αCDCP1-YGP	0.60
αCDCP1-CLG non-cleavable	1.95
αCD22-CLG	2.44
αCD79b-CLG	2.81
αCD138-CLG	1.66

Supplemental Figure 9.1 Mass spectrometric analysis of peptide labeling rates of ATPP immunoconjugates.
Mean peptide labeling rates of ATPP conjugates were determined by HPLC-MS after deglycosylation using N-glycosidase F. (**a**) ESI-MS spectrum of unlabeled αCDCP1 Ab. (**b**) ESI-MS spectrum of αCDCP1-CLG ATPP with SPDP linker and EBV_CLG peptide. (**c**) Calculation of mean peptide labeling rate of the αCDCP1-CLG ATPP as derived from (b). (**d**) Mean peptide labeling rates of all utilized ATPP conjugates. Data were generated by Dominic Knoblauch in the laboratory of Gloria Tabares (Protein Chemistry, Roche Diagnostics GmbH, Penzberg).

10. References

1. Siegel, R. L., Miller, K. D. & Jemal, A. Cancer statistics, 2016. *CA: A Cancer Journal for Clinicians* **66,** 7–30 (2016).
2. Siegel, R., Naishadham, D. & Jemal, A. Cancer statistics, 2012. *CA: A Cancer Journal for Clinicians* **62,** 10–29 (2012).
3. Hanahan, D. D. & Weinberg, R. A. R. The hallmarks of cancer. *Cell* **100,** 57–70 (2000).
4. Hanahan, D. & Weinberg, R. A. Hallmarks of cancer: the next generation. *Cell* **144,** 646–674 (2011).
5. Slamon, D. J. *et al.* Human breast cancer: correlation of relapse and survival with amplification of the HER-2/neu oncogene. *Science* **235,** 177–182 (1987).
6. Perona, R. Cell signalling: growth factors and tyrosine kinase receptors. *Clin Transl Oncol* **8,** 77–82 (2006).
7. Witsch, E., Sela, M. & Yarden, Y. Roles for growth factors in cancer progression. *Physiology (Bethesda)* **25,** 85–101 (2010).
8. Croce, C. M. Oncogenes and cancer. *New Engl J Med* **358,** 502–511 (2008).
9. Pylayeva-Gupta, Y., Grabocka, E. & Bar-Sagi, D. RAS oncogenes: weaving a tumorigenic web. *Nature Publishing Group* **11,** 761–774 (2011).
10. Markowitz, S. *et al.* Inactivation of the type II TGF-beta receptor in colon cancer cells with microsatellite instability. *Science* **268,** 1336–1338 (1995).
11. Schutte, M. *et al.* DPC4 gene in various tumor types. *Cancer Res.* **56,** 2527–2530 (1996).
12. Evan, G. & Littlewood, T. A matter of life and cell death. *Science* **281,** 1317–1322 (1998).
13. Green, D. R. & Evan, G. I. A matter of life and death. *Cancer Cell* **1,** 19–30 (2002).
14. Adams, J. M. & Cory, S. The Bcl-2 apoptotic switch in cancer development and therapy. *Oncogene* **26,** 1324–1337 (2007).
15. Hayflick, L. Mortality and immortality at the cellular level. A review. *Biochemistry* **62,** 1180–1190 (1997).
16. Burkhart, D. L. & Sage, J. Cellular mechanisms of tumour suppression by the retinoblastoma gene. *Nature Publishing Group* **8,** 671–682 (2008).
17. Collado, M. & Serrano, M. Senescence in tumours: evidence from mice and humans. *Nature Publishing Group* **10,** 51–57 (2010).
18. Zhang, H., Herbert, B.-S., Pan, K.-H., Shay, J. W. & Cohen, S. N. Disparate effects of telomere attrition on gene expression during replicative senescence of human mammary epithelial cells cultured under different conditions. *Oncogene* **23,** 6193–6198 (2004).
19. Sherr, C. J. & DePinho, R. A. Cellular senescence: mitotic clock or culture shock? *Cell* **102,** 407–410 (2000).
20. Counter, C. M. *et al.* Telomere shortening associated with chromosome instability is arrested in immortal cells which express telomerase activity. *The EMBO Journal* **11,** 1921–1929 (1992).
21. Bryan, T. M. & Cech, T. R. Telomerase and the maintenance of chromosome ends. *Curr. Opin. Cell Biol.* **11,** 318–324 (1999).
22. Shay, J. W. & Wright, W. E. Role of telomeres and telomerase in cancer. *Seminars in Cancer Biology* **21,** 349–353 (2011).

23. Ziyad, S. & Iruela-Arispe, M. L. Molecular mechanisms of tumor angiogenesis. *Genes Cancer* **2,** 1085–1096 (2011).
24. Welti, J., Loges, S., Dimmeler, S. & Carmeliet, P. Recent molecular discoveries in angiogenesis and antiangiogenic therapies in cancer. *J. Clin. Invest.* **123,** 3190–3200 (2013).
25. Cavallaro, U. & Christofori, G. Cell adhesion and signalling by cadherins and Ig-CAMs in cancer. *Nat. Rev. Cancer* **4,** 118–132 (2004).
26. Polyak, K. & Weinberg, R. A. Transitions between epithelial and mesenchymal states: acquisition of malignant and stem cell traits. *Nat. Rev. Cancer* **9,** 265–273 (2009).
27. Balkwill, F. & Mantovani, A. Inflammation and cancer: back to Virchow? *Lancet* **357,** 539–545 (2001).
28. Mantovani, A., Allavena, P., Sica, A. & Balkwill, F. Cancer-related inflammation. *Nature* **454,** 436–444 (2008).
29. Smyth, M. J., Godfrey, D. I. & Trapani, J. A. A fresh look at tumor immunosurveillance and immunotherapy. *Nat. Immunol.* **2,** 293–299 (2001).
30. Dunn, G. P., Bruce, A. T., Ikeda, H., Old, L. J. & Schreiber, R. D. Cancer immunoediting: from immunosurveillance to tumor escape. *Nat. Immunol.* **3,** 991–998 (2002).
31. Dunn, G. P., Old, L. J. & Schreiber, R. D. The immunobiology of cancer immunosurveillance and immunoediting. *Immunity* **21,** 137–148 (2004).
32. Boon, T. & Kellermann, O. Rejection by syngeneic mice of cell variants obtained by mutagenesis of a malignant teratocarcinoma cell line. *Proc. Natl. Acad. Sci. U.S.A.* **74,** 272–275 (1977).
33. Boon, T. & Van Pel, A. Teratocarcinoma cell variants rejected by syngeneic mice: protection of mice immunized with these variants against other variants and against the original malignant cell line. *Proc. Natl. Acad. Sci. U.S.A.* **75,** 1519–1523 (1978).
34. Van Pel, A., Georlette, M. & Boon, T. Tumor cell variants obtained by mutagenesis of a Lewis lung carcinoma cell line: immune rejection by syngeneic mice. *Proc. Natl. Acad. Sci. U.S.A.* **76,** 5282–5285 (1979).
35. Kaplan, D. H. *et al.* Demonstration of an interferon gamma-dependent tumor surveillance system in immunocompetent mice. *Proc. Natl. Acad. Sci. U.S.A.* **95,** 7556–7561 (1998).
36. Shankaran, V. *et al.* IFNgamma and lymphocytes prevent primary tumour development and shape tumour immunogenicity. *Nature* **410,** 1107–1111 (2001).
37. Smyth, M. J. *et al.* Perforin-mediated cytotoxicity is critical for surveillance of spontaneous lymphoma. *J. Exp. Med.* **192,** 755–760 (2000).
38. Street, S. E., Cretney, E. & Smyth, M. J. Perforin and interferon-gamma activities independently control tumor initiation, growth, and metastasis. *Blood* **97,** 192–197 (2001).
39. Bach, E. A., Aguet, M. & Schreiber, R. D. The IFN gamma receptor: a paradigm for cytokine receptor signaling. *Annu. Rev. Immunol.* **15,** 563–591 (1997).
40. Kawasaki, A., Shinkai, Y., Yagita, H. & Okumura, K. Expression of perforin in murine natural killer cells and cytotoxic T lymphocytes in vivo. *Eur J Immunol* **22,** 1215–1219 (1992).
41. Voskoboinik, I., Dunstone, M. A., Baran, K., Whisstock, J. C. & Trapani, J. A. Perforin: structure, function, and role in human immunopathology. *Immunol*

Rev **235,** 35–54 (2010).
42. Smyth, M. J., Crowe, N. Y. & Godfrey, D. I. NK cells and NKT cells collaborate in host protection from methylcholanthrene-induced fibrosarcoma. *Int Immunol* **13,** 459–463 (2001).
43. Shinkai, Y. *et al.* RAG-2-deficient mice lack mature lymphocytes owing to inability to initiate V(D)J rearrangement. *Cell* **68,** 855–867 (1992).
44. Girardi, M. *et al.* The distinct contributions of murine T cell receptor (TCR)gammadelta+ and TCRalphabeta+ T cells to different stages of chemically induced skin cancer. *J. Exp. Med.* **198,** 747–755 (2003).
45. Gao, Y. *et al.* Gamma delta T cells provide an early source of interferon gamma in tumor immunity. *J. Exp. Med.* **198,** 433–442 (2003).
46. Diefenbach, A., Jamieson, A. M., Liu, S. D., Shastri, N. & Raulet, D. H. Ligands for the murine NKG2D receptor: expression by tumor cells and activation of NK cells and macrophages. *Nat. Immunol.* **1,** 119–126 (2000).
47. Cerwenka, A., Baron, J. L. & Lanier, L. L. Ectopic expression of retinoic acid early inducible-1 gene (RAE-1) permits natural killer cell-mediated rejection of a MHC class I-bearing tumor in vivo. *Proc. Natl. Acad. Sci. U.S.A.* **98,** 11521–11526 (2001).
48. Diefenbach, A., Jensen, E. R., Jamieson, A. M. & Raulet, D. H. Rae1 and H60 ligands of the NKG2D receptor stimulate tumour immunity. *Nature* **413,** 165–171 (2001).
49. Terabe, M. & Berzofsky, J. A. The role of NKT cells in tumor immunity. *Adv. Cancer Res.* **101,** 277–348 (2008).
50. Silva-Santos, B., Serre, K. & Norell, H. γδ T cells in cancer. *Nat. Rev. Immunol.* **15,** 683–691 (2015).
51. Knuth, A., Danowski, B., Oettgen, H. F. & Old, L. J. T-cell-mediated cytotoxicity against autologous malignant melanoma: analysis with interleukin 2-dependent T-cell cultures. *Proc. Natl. Acad. Sci. U.S.A.* **81,** 3511–3515 (1984).
52. van der Bruggen, P. *et al.* A gene encoding an antigen recognized by cytolytic T lymphocytes on a human melanoma. *Science* **254,** 1643–1647 (1991).
53. Bailey, J. M. *et al.* p53 mutations cooperate with oncogenic Kras to promote adenocarcinoma from pancreatic ductal cells. *Oncogene* **35,** 4282–4288 (2015).
54. Goh, A. M., Coffill, C. R. & Lane, D. P. The role of mutant p53 in human cancer. *J. Pathol.* **223,** 116–126 (2011).
55. Jančík, S., Drábek, J., Radzioch, D. & Hajdúch, M. Clinical relevance of KRAS in human cancers. *J. Biomed. Biotechnol.* **2010,** 150960 (2010).
56. Hernandez, C., Huebener, P. & Schwabe, R. F. Damage-associated molecular patterns in cancer: a double-edged sword. *Oncogene* **35,** 5931–5941 (2016).
57. Lu, Y. C. *et al.* Efficient Identification of Mutated Cancer Antigens Recognized by T Cells Associated with Durable Tumor Regressions. *Clinical Cancer Research* **20,** 3401–3410 (2014).
58. Robbins, P. F. *et al.* Mining exomic sequencing data to identify mutated antigens recognized by adoptively transferred tumor-reactive T cells. *Nat. Med.* **19,** 747–752 (2013).
59. Rosenberg, S. A. & Restifo, N. P. Adoptive cell transfer as personalized immunotherapy for human cancer. *Science* **348,** 62–68 (2015).

60. Sharma, P. & Allison, J. P. The future of immune checkpoint therapy. *Science* **348,** 56–61 (2015).
61. Strønen, E. *et al.* Targeting of cancer neoantigens with donor-derived T cell receptor repertoires. *Science* **352,** 1337–1341 (2016).
62. Sims, G. P., Rowe, D. C., Rietdijk, S. T., Herbst, R. & Coyle, A. J. HMGB1 and RAGE in inflammation and cancer. *Annu. Rev. Immunol.* **28,** 367–388 (2010).
63. Guerra, N. *et al.* NKG2D-deficient mice are defective in tumor surveillance in models of spontaneous malignancy. *Immunity* **28,** 571–580 (2008).
64. Anguille, S. *et al.* Dendritic Cells as Pharmacological Tools for Cancer Immunotherapy. *Pharmacol. Rev.* **67,** 731–753 (2015).
65. Bhadra, R., Cobb, D. A. & Khan, I. A. CD40 signaling to the rescue: A CD8 exhaustion perspective in chronic infectious diseases. *Crit. Rev. Immunol.* **33,** 361–378 (2013).
66. Hoffmann, T. K., Meidenbauer, N., Müller-Berghaus, J., Storkus, W. J. & Whiteside, T. L. Proinflammatory Cytokines and CD40 Ligand Enhance Cross-Presentation and Cross-Priming Capability of Human Dendritic Cells Internalizing Apoptotic Cancer Cells. *J. Immunother.* **24,** 162–171 (2001).
67. Katakam, A. K. *et al.* Dendritic cells require NIK for CD40-dependent cross-priming of CD8+ T cells. *Proceedings of the National Academy of Sciences* **112,** 14664–14669 (2015).
68. Clark, W. H. *et al.* Model predicting survival in stage I melanoma based on tumor progression. *J. Natl. Cancer Inst.* **81,** 1893–1904 (1989).
69. Clemente, C. G. *et al.* Prognostic value of tumor infiltrating lymphocytes in the vertical growth phase of primary cutaneous melanoma. *Cancer* **77,** 1303–1310 (1996).
70. Naito, Y. *et al.* CD8+ T cells infiltrated within cancer cell nests as a prognostic factor in human colorectal cancer. *Cancer Res.* **58,** 3491–3494 (1998).
71. Zhang, L. *et al.* Intratumoral T cells, recurrence, and survival in epithelial ovarian cancer. *New Engl J Med* **348,** 203–213 (2003).
72. Unitt, E. *et al.* Tumour lymphocytic infiltrate and recurrence of hepatocellular carcinoma following liver transplantation. *Journal of Hepatology* **45,** 246–253 (2006).
73. Fridman, W.-H., Pagès, F., Sautès-Fridman, C. & Galon, J. The immune contexture in human tumours: impact on clinical outcome. *Nat. Rev. Cancer* **12,** 298–306 (2012).
74. Pages, F. *et al.* Effector memory T cells, early metastasis, and survival in colorectal cancer. *N. Engl. J. Med.* **353,** 2654–2666 (2005).
75. Galon, J. *et al.* Type, density, and location of immune cells within human colorectal tumors predict clinical outcome. *Science* **313,** 1960–1964 (2006).
76. Sato, E. *et al.* Intraepithelial CD8+ tumor-infiltrating lymphocytes and a high CD8+/regulatory T cell ratio are associated with favorable prognosis in ovarian cancer. *Proc. Natl. Acad. Sci. U.S.A.* **102,** 18538–18543 (2005).
77. Badoual, C. *et al.* Prognostic value of tumor-infiltrating CD4+ T-cell subpopulations in head and neck cancers. *Clin. Cancer Res.* **12,** 465–472 (2006).
78. Tosolini, M. *et al.* Clinical impact of different classes of infiltrating T cytotoxic and helper cells (Th1, th2, treg, th17) in patients with colorectal cancer. *Cancer Res.* **71,** 1263–1271 (2011).

79. Birkeland, S. A. *et al.* Cancer risk after renal transplantation in the Nordic countries, 1964-1986. *Int. J. Cancer* **60,** 183–189 (1995).
80. Andrés, A. Cancer incidence after immunosuppressive treatment following kidney transplantation. *Crit Rev Oncol Hematol* **56,** 71–85 (2005).
81. Penn, I. Sarcomas in organ allograft recipients. *Transplantation* **60,** 1485–1491 (1995).
82. Penn, I. Malignant melanoma in organ allograft recipients. *Transplantation* **61,** 274–278 (1996).
83. Alexandrov, L. B. *et al.* Signatures of mutational processes in human cancer. *Nature* **500,** 415–421 (2013).
84. Dunn, G. P., Old, L. J. & Schreiber, R. D. The three Es of cancer immunoediting. *Annu. Rev. Immunol.* **22,** 329–360 (2004).
85. Schreiber, R. D., Old, L. J. & Smyth, M. J. Cancer immunoediting: integrating immunity's roles in cancer suppression and promotion. *Science* **331,** 1565–1570 (2011).
86. Algarra, I., Cabrera, T. & Garrido, F. The HLA crossroad in tumor immunology. *Hum. Immunol.* **61,** 65–73 (2000).
87. Restifo, N. P. *et al.* Identification of human cancers deficient in antigen processing. *J. Exp. Med.* **177,** 265–272 (1993).
88. Seliger, B., Maeurer, M. J. & Ferrone, S. Antigen-processing machinery breakdown and tumor growth. *Immunol. Today* **21,** 455–464 (2000).
89. Khong, H. T. & Restifo, N. P. Natural selection of tumor variants in the generation of ‘tumor escape’ phenotypes. *Nat. Immunol.* **3,** 999–1005 (2002).
90. Zaid Siddiquee, Al, K. & Turkson, J. STAT3 as a target for inducing apoptosis in solid and hematological tumors. *Cell Res.* **18,** 254–267 (2008).
91. Medema, J. P., de Jong, J., van Hall, T., Melief, C. J. & Offringa, R. Immune escape of tumors in vivo by expression of cellular FLICE-inhibitory protein. *J. Exp. Med.* **190,** 1033–1038 (1999).
92. Hersey, P. & Zhang, X. D. How melanoma cells evade trail-induced apoptosis. *Nat. Rev. Cancer* **1,** 142–150 (2001).
93. Dong, H. *et al.* Tumor-associated B7-H1 promotes T-cell apoptosis: a potential mechanism of immune evasion. *Nat. Med.* **8,** 793–800 (2002).
94. Tripathi, P. & Agrawal, S. Non-classical HLA-G antigen and its role in the cancer progression. *Cancer Invest.* **24,** 178–186 (2006).
95. Derré, L. *et al.* Expression and release of HLA-E by melanoma cells and melanocytes: potential impact on the response of cytotoxic effector cells. *J Immunol* **177,** 3100–3107 (2006).
96. O'Connell, J., O'Sullivan, G. C., Collins, J. K. & Shanahan, F. The Fas counterattack: Fas-mediated T cell killing by colon cancer cells expressing Fas ligand. *J. Exp. Med.* **184,** 1075–1082 (1996).
97. Uyttenhove, C. *et al.* Evidence for a tumoral immune resistance mechanism based on tryptophan degradation by indoleamine 2,3-dioxygenase. *Nat. Med.* **9,** 1269–1274 (2003).
98. Munn, D. H. *et al.* GCN2 kinase in T cells mediates proliferative arrest and anergy induction in response to indoleamine 2,3-dioxygenase. *Immunity* **22,** 633–642 (2005).
99. Cederbaum, S. D. *et al.* Arginases I and II: do their functions overlap? *Mol. Genet. Metab.* **81 Suppl 1,** S38–44 (2004).
100. Bronte, V. & Zanovello, P. Regulation of immune responses by L-arginine metabolism. *Nat. Rev. Immunol.* **5,** 641–654 (2005).

101. XU, W., LIU, L. Z., Loizidou, M., Ahmed, M. & Charles, I. G. The role of nitric oxide in cancer. *Cell Res.* **12,** 311–320 (2002).
102. Singer, K., Gottfried, E., Kreutz, M. & Mackensen, A. Suppression of T-cell responses by tumor metabolites. *Cancer Immunol. Immunother.* **60,** 425–431 (2011).
103. Fallarino, F. *et al.* The combined effects of tryptophan starvation and tryptophan catabolites down-regulate T cell receptor zeta-chain and induce a regulatory phenotype in naive T cells. *J Immunol* **176,** 6752–6761 (2006).
104. Lee, G. K. *et al.* Tryptophan deprivation sensitizes activated T cells to apoptosis prior to cell division. *Immunology* **107,** 452–460 (2002).
105. Blesson, S. *et al.* Analysis of the mechanisms of human cytotoxic T lymphocyte response inhibition by NO. *Int Immunol* **14,** 1169–1178 (2002).
106. Groh, V., Wu, J., Yee, C. & Spies, T. Tumour-derived soluble MIC ligands impair expression of NKG2D and T-cell activation. *Nature* **419,** 734–738 (2002).
107. Villablanca, E. J. *et al.* Tumor-mediated liver X receptor-alpha activation inhibits CC chemokine receptor-7 expression on dendritic cells and dampens antitumor responses. *Nat. Med.* **16,** 98–105 (2010).
108. Radoja, S., Rao, T. D., Hillman, D. & Frey, A. B. Mice bearing late-stage tumors have normal functional systemic T cell responses in vitro and in vivo. *J Immunol* **164,** 2619–2628 (2000).
109. Rubtsov, Y. P. *et al.* Regulatory T Cell-Derived Interleukin-10 Limits Inflammation at Environmental Interfaces. *Immunity* **28,** 546–558 (2008).
110. Shevach, E. M. Mechanisms of foxp3+ T regulatory cell-mediated suppression. *Immunity* **30,** 636–645 (2009).
111. Yokosuka, T. *et al.* Programmed cell death 1 forms negative costimulatory microclusters that directly inhibit T cell receptor signaling by recruiting phosphatase SHP2. *J. Exp. Med.* **209,** 1201–1217 (2012).
112. Yokosuka, T. *et al.* Spatiotemporal basis of CTLA-4 costimulatory molecule-mediated negative regulation of T cell activation. *Immunity* **33,** 326–339 (2010).
113. Wing, K. *et al.* CTLA-4 control over Foxp3+ regulatory T cell function. *Science* **322,** 271–275 (2008).
114. Qureshi, O. S. *et al.* Trans-Endocytosis of CD80 and CD86: A Molecular Basis for the Cell-Extrinsic Function of CTLA-4. *Science* **332,** 600–603 (2011).
115. Walker, L. S. K. & Sansom, D. M. Confusing signals: recent progress in CTLA-4 biology. *Trends Immunol.* **36,** 63–70 (2015).
116. Sakaguchi, S., Yamaguchi, T., Nomura, T. & Ono, M. Regulatory T Cells and Immune Tolerance. *Cell* **133,** 775–787 (2008).
117. Turk, M. J. *et al.* Concomitant tumor immunity to a poorly immunogenic melanoma is prevented by regulatory T cells. *J. Exp. Med.* **2011,** 771–782 (2004).
118. Antony, P. A. *et al.* CD8+ T cell immunity against a tumor/self-antigen is augmented by CD4+ T helper cells and hindered by naturally occurring T regulatory cells. *J Immunol* **174,** 2591–2601 (2005).
119. Li, X., Kostareli, E., Suffner, J., Garbi, N. & Hämmerling, G. J. Efficient Treg depletion induces T-cell infiltration and rejection of large tumors. *Eur J Immunol* **40,** 3325–3335 (2010).
120. Quezada, S. A., Peggs, K. S., Simpson, T. R. & Allison, J. P. Shifting the

equilibrium in cancer immunoediting: from tumor tolerance to eradication. *Immunol Rev* **241,** 104–118 (2011).
121. Lin, E. Y. *et al.* Macrophages Regulate the Angiogenic Switch in a Mouse Model of Breast Cancer. *Cancer Res.* **66,** 11238–11246 (2006).
122. Qian, B. *et al.* A Distinct Macrophage Population Mediates Metastatic Breast Cancer Cell Extravasation, Establishment and Growth. *PLoS ONE* **4,** e6562 (2009).
123. Gabrilovich, D. I., Ostrand-Rosenberg, S. & Bronte, V. Coordinated regulation of myeloid cells by tumours. *Nat. Rev. Immunol.* **12,** 253–268 (2012).
124. Lindau, D., Gielen, P., Kroesen, M., Wesseling, P. & Adema, G. J. The immunosuppressive tumour network: myeloid-derived suppressor cells, regulatory T cells and natural killer T cells. *Immunology* **138,** 105–115 (2013).
125. Motz, G. T. *et al.* Tumor endothelium FasL establishes a selective immune barrier promoting tolerance in tumors. *Nat. Med.* **20,** 607–615 (2014).
126. Huang, B. *et al.* Gr-1+CD115+ immature myeloid suppressor cells mediate the development of tumor-induced T regulatory cells and T-cell anergy in tumor-bearing host. *Cancer Res.* **66,** 1123–1131 (2006).
127. Schlecker, E. *et al.* Tumor-Infiltrating Monocytic Myeloid-Derived Suppressor Cells Mediate CCR5-Dependent Recruitment of Regulatory T Cells Favoring Tumor Growth. *J Immunol* **189,** 5602–5611 (2012).
128. Grohmann, U. *et al.* CTLA-4–Ig regulates tryptophan catabolism in vivo. *Nat. Immunol.* **3,** 1097–1101 (2002).
129. Han, Y. *et al.* Human CD14 +CTLA-4 +regulatory dendritic cells suppress T-cell response by cytotoxic T-lymphocyte antigen-4-dependent IL-10 and indoleamine-2,3-dioxygenase production in hepatocellular carcinoma. *Hepatology* **59,** 567–579 (2013).
130. Nagaraj, S. *et al.* Altered recognition of antigen is a mechanism of CD8+ T cell tolerance in cancer. *Nat. Med.* **13,** 828–835 (2007).
131. Kusmartsev, S., Nefedova, Y., Yoder, D. & Gabrilovich, D. I. Antigen-specific inhibition of CD8+ T cell response by immature myeloid cells in cancer is mediated by reactive oxygen species. *J Immunol* **172,** 989–999 (2004).
132. Schmielau, J. & Finn, O. J. Activated granulocytes and granulocyte-derived hydrogen peroxide are the underlying mechanism of suppression of t-cell function in advanced cancer patients. *Cancer Res.* **61,** 4756–4760 (2001).
133. Sektioglu, I. M. *et al.* Macrophage-derived nitric oxide initiates T-cell diapedesis and tumor rejection. *OncoImmunology* **5,** e1204506 (2016).
134. Atkins, M. B. *et al.* High-dose recombinant interleukin 2 therapy for patients with metastatic melanoma: analysis of 270 patients treated between 1985 and 1993. *J. Clin. Oncol.* **17,** 2105–2116 (1999).
135. Cole, B. F. *et al.* Quality-of-life-adjusted survival analysis of interferon alfa-2b adjuvant treatment of high-risk resected cutaneous melanoma: an Eastern Cooperative Oncology Group study. *J. Clin. Oncol.* **14,** 2666–2673 (1996).
136. Jochems, C. *et al.* The IDO1 selective inhibitor epacadostat enhances dendritic cell immunogenicity and lytic ability of tumor antigen-specific T cells. *Oncotarget* **7,** 37762–37772 (2016).
137. Muller, A. J. & Scherle, P. A. Targeting the mechanisms of tumoral immune tolerance with small-molecule inhibitors. *Nat. Rev. Cancer* **6,** 613–625 (2006).
138. Reff, M. E. *et al.* Depletion of B cells in vivo by a chimeric mouse human

monoclonal antibody to CD20. *Blood* **83,** 435–445 (1994).
139. Rituximab The First Monoclonal Antibody Approved for the Treatment of Lymphoma. *Curr Pharm Biotechnol.* **1,** 1–9 (2000).
140. Horowitz, M. M. *et al.* Graft-versus-leukemia reactions after bone marrow transplantation. *Blood* **75,** 555–562 (1990).
141. Gnjatic, S. *et al.* Survey of naturally occurring CD4+ T cell responses against NY-ESO-1 in cancer patients: correlation with antibody responses. *Proc. Natl. Acad. Sci. U.S.A.* **100,** 8862–8867 (2003).
142. Jager, E. *et al.* Monitoring CD8 T cell responses to NY-ESO-1: Correlation of humoral and cellular immune responses. *Proceedings of the National Academy of Sciences* **97,** 4760–4765 (2000).
143. Carreno, B. M. *et al.* A dendritic cell vaccine increases the breadth and diversity of melanoma neoantigen-specific T cells. *Science* **348,** 803–808 (2015).
144. Khalil, D. N., Smith, E. L., Brentjens, R. J. & Wolchok, J. D. The future of cancer treatment: immunomodulation, CARs and combination immunotherapy. *Nat Rev Clin Oncol* **13,** 273–290 (2016).
145. Peggs, K. S., Quezada, S. A. & Allison, J. P. Cancer immunotherapy: co-stimulatory agonists and co-inhibitory antagonists. *Clin Exp Immunol* **157,** 9–19 (2009).
146. Pardoll, D. M. The blockade of immune checkpoints in cancer immunotherapy. *Nat. Rev. Cancer* **12,** 252–264 (2012).
147. Quezada, S. A. & Peggs, K. S. Exploiting CTLA-4, PD-1 and PD-L1 to reactivate the host immune response against cancer. *Br J Cancer* **108,** 1560–1565 (2013).
148. Barber, D. L. *et al.* Restoring function in exhausted CD8 T cells during chronic viral infection. *Nature* **439,** 682–687 (2006).
149. Shi, F. *et al.* PD-1 and PD-L1 upregulation promotes CD8(+) T-cell apoptosis and postoperative recurrence in hepatocellular carcinoma patients. *Int. J. Cancer* **128,** 887–896 (2011).
150. Schietinger, A. & Greenberg, P. D. Tolerance and exhaustion: defining mechanisms of T cell dysfunction. *Trends Immunol.* **35,** 51–60 (2014).
151. Said, E. A. *et al.* Programmed death-1-induced interleukin-10 production by monocytes impairs CD4+ T cell activation during HIV infection. *Nat. Med.* **16,** 452–459 (2010).
152. Hodi, F. S. *et al.* Improved survival with ipilimumab in patients with metastatic melanoma. *New Engl J Med* **363,** 711–723 (2010).
153. Peggs, K. S., Quezada, S. A., Chambers, C. A., Korman, A. J. & Allison, J. P. Blockade of CTLA-4 on both effector and regulatory T cell compartments contributes to the antitumor activity of anti-CTLA-4 antibodies. *J. Exp. Med.* **206,** 1717–1725 (2009).
154. Simpson, T. R. *et al.* Fc-dependent depletion of tumor-infiltrating regulatory T cells co-defines the efficacy of anti-CTLA-4 therapy against melanoma. *J. Exp. Med.* **210,** 1695–1710 (2013).
155. Robert, C. *et al.* Anti-programmed-death-receptor-1 treatment with pembrolizumab in ipilimumab-refractory advanced melanoma: a randomised dose-comparison cohort of a phase 1 trial. *Lancet* **384,** 1109–1117 (2014).
156. Powles, T. *et al.* MPDL3280A (anti-PD-L1) treatment leads to clinical activity in metastatic bladder cancer. *Nature* **515,** 558–562 (2014).
157. Garon, E. B. *et al.* Pembrolizumab for the treatment of non-small-cell lung

cancer. *New Engl J Med* **372,** 2018–2028 (2015).
158. Nguyen, L. T. & Ohashi, P. S. Clinical blockade of PD1 and LAG3--potential mechanisms of action. *Nat. Rev. Immunol.* **15,** 45–56 (2015).
159. Curti, B. D. *et al.* OX40 is a potent immune-stimulating target in late-stage cancer patients. *Cancer Res.* **73,** 7189–7198 (2013).
160. Makkouk, A., Chester, C. & Kohrt, H. E. Rationale for anti-CD137 cancer immunotherapy. *Eur J Cancer* **54,** 112–119 (2016).
161. Bartkowiak, T. & Curran, M. A. 4-1BB Agonists: Multi-Potent Potentiators of Tumor Immunity. *Front Oncol* **5,** 117 (2015).
162. Wolchok, J. D. *et al.* Nivolumab plus ipilimumab in advanced melanoma. *New Engl J Med* **369,** 122–133 (2013).
163. Chen, S. *et al.* Combination of 4-1BB agonist and PD-1 antagonist promotes antitumor effector/memory CD8 T cells in a poorly immunogenic tumor model. *Cancer Immunol Res* **3,** 149–160 (2015).
164. Guo, Z. *et al.* PD-1 blockade and OX40 triggering synergistically protects against tumor growth in a murine model of ovarian cancer. *PLoS ONE* **9,** e89350 (2014).
165. Rizvi, N. A. *et al.* Mutational landscape determines sensitivity to PD-1 blockade in non-small cell lung cancer. *Science* **348,** 124–128 (2015).
166. Van Allen, E. M. *et al.* Genomic correlates of response to CTLA-4 blockade in metastatic melanoma. *Science* **350,** 207–211 (2015).
167. Snyder, A. *et al.* Genetic basis for clinical response to CTLA-4 blockade in melanoma. *New Engl J Med* **371,** 2189–2199 (2014).
168. Ruf, P. *et al.* Pharmacokinetics, immunogenicity and bioactivity of the therapeutic antibody catumaxomab intraperitoneally administered to cancer patients. *Br J Clin Pharmacol* **69,** 617–625 (2010).
169. Heiss, M. M. *et al.* The trifunctional antibody catumaxomab for the treatment of malignant ascites due to epithelial cancer: Results of a prospective randomized phase II/III trial. *Int. J. Cancer* **127,** 2209–2221 (2010).
170. Bargou, R. *et al.* Tumor regression in cancer patients by very low doses of a T cell-engaging antibody. *Science* **321,** 974–977 (2008).
171. Herrmann, I. *et al.* Highly efficient elimination of colorectal tumor-initiating cells by an EpCAM/CD3-bispecific antibody engaging human T cells. *PLoS ONE* **5,** e13474 (2010).
172. Sanford, M. Blinatumomab: first global approval. *Drugs* **75,** 321–327 (2015).
173. Topp, M. S. *et al.* Phase II trial of the anti-CD19 bispecific T cell-engager blinatumomab shows hematologic and molecular remissions in patients with relapsed or refractory B-precursor acute lymphoblastic leukemia. *J. Clin. Oncol.* **32,** 4134–4140 (2014).
174. Bacac, M. *et al.* A Novel Carcinoembryonic Antigen T-Cell Bispecific Antibody (CEA TCB) for the Treatment of Solid Tumors. *Clin. Cancer Res.* **22,** 3286–3297 (2016).
175. Srivastava, S. & Riddell, S. R. Engineering CAR-T cells: Design concepts. *Trends Immunol.* **36,** 494–502 (2015).
176. Davila, M. L. *et al.* Efficacy and toxicity management of 19-28z CAR T cell therapy in B cell acute lymphoblastic leukemia. *Sci Transl Med* **6,** 224ra25 (2014).
177. Maude, S. L. *et al.* Chimeric antigen receptor T cells for sustained remissions in leukemia. *New Engl J Med* **371,** 1507–1517 (2014).
178. Robbins, P. F. *et al.* Tumor regression in patients with metastatic synovial

cell sarcoma and melanoma using genetically engineered lymphocytes reactive with NY-ESO-1. *J. Clin. Oncol.* **29,** 917–924 (2011).
179. Rapoport, A. P. *et al.* NY-ESO-1-specific TCR-engineered T cells mediate sustained antigen-specific antitumor effects in myeloma. *Nat. Med.* **21,** 914–921 (2015).
180. Adusumilli, P. S. *et al.* Regional delivery of mesothelin-targeted CAR T cell therapy generates potent and long-lasting CD4-dependent tumor immunity. *Sci Transl Med* **6,** 261ra151 (2014).
181. Bonifant, C. L., Jackson, H. J., Brentjens, R. J. & Curran, K. J. Toxicity and management in CAR T-cell therapy. *Mol Ther Oncolytics* **3,** 16011 (2016).
182. Goebeler, M.-E. *et al.* Bispecific T-Cell Engager (BiTE) Antibody Construct Blinatumomab for the Treatment of Patients With Relapsed/Refractory Non-Hodgkin Lymphoma: Final Results From a Phase I Study. *J. Clin. Oncol.* **34,** 1104–1111 (2016).
183. Viardot, A. *et al.* Phase 2 study of the bispecific T-cell engager (BiTE) antibody blinatumomab in relapsed/refractory diffuse large B-cell lymphoma. *Blood* **127,** 1410–1416 (2016).
184. Grupp, S. A. *et al.* Chimeric antigen receptor-modified T cells for acute lymphoid leukemia. *New Engl J Med* **368,** 1509–1518 (2013).
185. Casar, B. *et al.* In vivo cleaved CDCP1 promotes early tumor dissemination via complexing with activated β1 integrin and induction of FAK/PI3K/Akt motility signaling. *Oncogene* **33,** 255–268 (2014).
186. Scherl-Mostageer, M. *et al.* Identification of a novel gene, CDCP1, overexpressed in human colorectal cancer. *Oncogene* **20,** 4402–4408 (2001).
187. Hooper, J. D. *et al.* Subtractive immunization using highly metastatic human tumor cells identifies SIMA135/CDCP1, a 135 kDa cell surface phosphorylated glycoprotein antigen. *Oncogene* **22,** 1783–1794 (2003).
188. Ikeda, J. I. *et al.* Expression of CUB domain containing protein (CDCP1) is correlated with prognosis and survival of patients with adenocarcinoma of lung. *Cancer Science* **100,** 429–433 (2009).
189. Miyazawa, Y. *et al.* CUB domain-containing protein 1, a prognostic factor for human pancreatic cancers, promotes cell migration and extracellular matrix degradation. *Cancer Res.* **70,** 5136–5146 (2010).
190. Kollmorgen, G. *et al.* Antibody mediated CDCP1 degradation as mode of action for cancer targeted therapy. *Mol Oncol* **7,** 1142–1151 (2013).
191. Yang, J., Chen, H., Vlahov, I. R., Cheng, J.-X. & Low, P. S. Evaluation of disulfide reduction during receptor-mediated endocytosis by using FRET imaging. *Proc. Natl. Acad. Sci. U.S.A.* **103,** 13872–13877 (2006).
192. Neefjes, J., Jongsma, M. L. M., Paul, P. & Bakke, O. Towards a systems understanding of MHC class I and MHC class II antigen presentation. *Nat. Rev. Immunol.* **11,** 823–836 (2011).
193. Gromme, M. *et al.* Recycling MHC class I molecules and endosomal peptide loading. *Proc. Natl. Acad. Sci. U.S.A.* **96,** 10326–10331 (1999).
194. Lizée, G. *et al.* Control of dendritic cell cross-presentation by the major histocompatibility complex class I cytoplasmic domain. *Nat. Immunol.* **4,** 1065–1073 (2003).
195. Baehner, M., Jenewein, S., Kubbies, M., Moessner, E. & Schlothauer, T. Antibody fc variants. *U.S. patent WO/2012/130831* (2013).
196. Overdijk, M. B. *et al.* Crosstalk between human IgG isotypes and murine

effector cells. *J Immunol* **189,** 3430–3438 (2012).
197. Klages, K. *et al.* Selective depletion of Foxp3+ regulatory T cells improves effective therapeutic vaccination against established melanoma. *Cancer Res.* **70,** 7788–7799 (2010).
198. Mattarollo, S. R. *et al.* Transient Foxp3(+) regulatory T-cell depletion enhances therapeutic anticancer vaccination targeting the immune-stimulatory properties of NKT cells. *Immunol. Cell Biol.* **91,** 105–114 (2013).
199. Iezzi, G. *et al.* The immunogenicity of experimental tumors is strongly biased by the expression of dominant viral cytotoxic T-lymphocyte epitopes. *Cancer Res.* **57,** 2564–2568 (1997).
200. Uhr, J. W. & Pantel, K. Controversies in clinical cancer dormancy. *Proceedings of the National Academy of Sciences* **108,** 12396–12400 (2011).
201. Rubinstein, M. P. *et al.* Converting IL-15 to a superagonist by binding to soluble IL-15R{alpha}. *Proc. Natl. Acad. Sci. U.S.A.* **103,** 9166–9171 (2006).
202. Mueller, K., Schweier, O. & Pircher, H. Efficacy of IL-2- versus IL-15-stimulated CD8 T cells in adoptive immunotherapy. *Eur J Immunol* **38,** 2874–2885 (2008).
203. Porgador, A., Yewdell, J. W., Deng, Y., Bennink, J. R. & Germain, R. N. Localization, quantitation, and in situ detection of specific peptide-MHC class I complexes using a monoclonal antibody. *Immunity* **6,** 715–726 (1997).
204. Cesson, V. *et al.* Active antiviral T-lymphocyte response can be redirected against tumor cells by antitumor antibody x MHC/viral peptide conjugates. *Clin. Cancer Res.* **12,** 7422–7430 (2006).
205. Ogg, G. S. *et al.* Sensitization of tumour cells to lysis by virus-specific CTL using antibody-targeted MHC class I/peptide complexes. *Br J Cancer* **82,** 1058–1062 (2000).
206. Robert, B., Guillaume, P., Luescher, I., Romero, P. & Mach, J.-P. Antibody-conjugated MHC class I tetramers can target tumor cells for specific lysis by T lymphocytes. *Eur J Immunol* **30,** 3165–3170 (2000).
207. Savage, P. *et al.* Induction of viral and tumour specific CTL responses using antibody targeted HLA class I peptide complexes. *Br J Cancer* **86,** 1336–1342 (2002).
208. Mous, R. *et al.* Redirection of CMV-specific CTL towards B-CLL via CD20-targeted HLA/CMV complexes. *Leukemia* **20,** 1096–1102 (2006).
209. Weir, C. *et al.* Streptavidin: a novel immunostimulant for the selection and delivery of autologous and syngeneic tumor vaccines. *Cancer Immunol Res* **2,** 469–479 (2014).
210. Lev, A., Novak, H., Segal, D. & Reiter, Y. Recruitment of CTL activity by tumor-specific antibody-mediated targeting of single-chain class I MHC-peptide complexes. *J Immunol* **169,** 2988–2996 (2002).
211. Lev, A. *et al.* Tumor-specific Ab-mediated targeting of MHC-peptide complexes induces regression of human tumor xenografts in vivo. *Proc. Natl. Acad. Sci. U.S.A.* **101,** 9051–9056 (2004).
212. Oved, K., Lev, A., Noy, R., Segal, D. & Reiter, Y. Antibody-mediated targeting of human single-chain class I MHC with covalently linked peptides induces efficient killing of tumor cells by tumor or viral-specific cytotoxic T lymphocytes. *Cancer Immunol. Immunother.* **54,** 867–879 (2005).
213. Novak, H. *et al.* Selective antibody-mediated targeting of class I MHC to EGFR-expressing tumor cells induces potent antitumor CTL activity in vitro and in vivo. *Int. J. Cancer* **120,** 329–336 (2007).

214. Schmittnaegel, M. *et al.* Committing Cytomegalovirus-Specific CD8 T Cells to Eliminate Tumor Cells by Bifunctional Major Histocompatibility Class I Antibody Fusion Molecules. **3,** 764–776 (2015).
215. King, B. C. *et al.* Antibody-peptide-MHC fusion conjugates target non-cognate T cells to kill tumour cells. *Cancer Immunol. Immunother.* **62,** 1093–1105 (2013).
216. Lanzavecchia, A., Iezzi, G. & Viola, A. From TCR engagement to T cell activation: a kinetic view of T cell behavior. *Cell* **96,** 1–4 (1999).
217. Korb, L. C., Mirshahidi, S., Ramyar, K., Sadighi Akha, A. A. & Sadegh-Nasseri, S. Induction of T cell anergy by low numbers of agonist ligands. *J Immunol* **162,** 6401–6409 (1999).
218. Yu, X. *et al.* Antigen-armed antibodies targeting B lymphoma cells effectively activate antigen-specific CD4+ T cells. *Blood* **125,** 1601–1610 (2015).
219. Blum, J. S., Wearsch, P. A. & Cresswell, P. Pathways of antigen processing. *Annu. Rev. Immunol.* **31,** 443–473 (2013).
220. Kang, T. H., Ma, B., Wang, C., Wu, T. C. & Hung, C.-F. Targeted coating with antigenic peptide renders tumor cells susceptible to CD8(+) T cell-mediated killing. *Mol. Ther.* **21,** 542–553 (2013).
221. Thomas, G. Furin at the cutting edge: from protein traffic to embryogenesis and disease. *Nat Rev Mol Cell Biol* **3,** 753–766 (2002).
222. Kedl, R. M. & Mescher, M. F. Qualitative differences between naive and memory T cells make a major contribution to the more rapid and efficient memory CD8+ T cell response. *J Immunol* **161,** 674–683 (1998).
223. Sallusto, F., Lenig, D., Förster, R., Lipp, M. & Lanzavecchia, A. Two subsets of memory T lymphocytes with distinct homing potentials and effector functions. *Nature* **401,** 708–712 (1999).
224. Veiga-Fernandes, H., Walter, U., Bourgeois, C., McLean, A. & Rocha, B. Response of naïve and memory CD8+ T cells to antigen stimulation in vivo. *Nat. Immunol.* **1,** 47–53 (2000).
225. Wortmann, A., He, Y., Deryugina, E. I., Quigley, J. P. & Hooper, J. D. The cell surface glycoprotein CDCP1 in cancer--insights, opportunities, and challenges. *IUBMB Life* **61,** 723–730 (2009).
226. Yang, L. *et al.* Dysregulated expression of cell surface glycoprotein CDCP1 in prostate cancer. *Oncotarget* **6,** 43743–43758 (2015).
227. Hammarström, S. The carcinoembryonic antigen (CEA) family: structures, suggested functions and expression in normal and malignant tissues. *Seminars in Cancer Biology* **9,** 67–81 (1999).
228. Zhou, H., Stanners, C. P. & Fuks, A. Specificity of anti-carcinoembryonic antigen monoclonal antibodies and their effects on CEA-mediated adhesion. *Cancer Res.* **53,** 3817–3822 (1993).
229. Ross, J. S. & Fletcher, J. A. The HER-2/neu oncogene in breast cancer: prognostic factor, predictive factor, and target for therapy. *Stem Cells* **16,** 413–428 (1998).
230. Nicholson, R. I., Gee, J. M. & Harper, M. E. EGFR and cancer prognosis. *Eur J Cancer* **37 Suppl 4,** S9–15 (2001).
231. Kersemaekers, A.-M. F. *et al.* Oncogene Alterations in Carcinomas of the Uterine Cervix: Overexpression of the Epidermal Growth Factor Receptor Is Associated with Poor Prognosis. *Clinical Cancer Research* **5,** 577–586 (1999).
232. Argani, P. *et al.* Mesothelin is overexpressed in the vast majority of ductal

adenocarcinomas of the pancreas: identification of a new pancreatic cancer marker by serial analysis of gene expression (SAGE). *Clin. Cancer Res.* **7,** 3862–3868 (2001).
233. Frierson, H. F. *et al.* Large-scale molecular and tissue microarray analysis of mesothelin expression in common human carcinomas. *Hum. Pathol.* **34,** 605–609 (2003).
234. Ordóñez, N. G. Value of mesothelin immunostaining in the diagnosis of mesothelioma. *Mod Pathol* **16,** 192–197 (2003).
235. Mosesson, Y., Mills, G. B. & Yarden, Y. Derailed endocytosis: an emerging feature of cancer. *Nature Publishing Group* **8,** 835–850 (2008).
236. Mellman, I. & Yarden, Y. Endocytosis and cancer. *Cold Spring Harb Perspect Biol* **5,** a016949 (2013).
237. Yuan, F. *et al.* Vascular Permeability in a Human Tumor Xenograft: Molecular Size Dependence and Cutoff Size. *Cancer Res.* **55,** 3752–3756 (1995).
238. Keizer, R. J., Huitema, A. D. R., Schellens, J. H. M. & Beijnen, J. H. Clinical pharmacokinetics of therapeutic monoclonal antibodies. *Clin Pharmacokinet* **49,** 493–507 (2010).
239. Vugmeyster, Y., Xu, X., Theil, F.-P., Khawli, L. A. & Leach, M. W. Pharmacokinetics and toxicology of therapeutic proteins: Advances and challenges. *World J Biol Chem* **3,** 73–92 (2012).
240. Deslandes, A. Comparative clinical pharmacokinetics of antibody-drug conjugates in first-in-human Phase 1 studies. *MAbs* **6,** 859–870 (2014).
241. Panowski, S., Bhakta, S., Raab, H., Polakis, P. & Junutula, J. R. Site-specific antibody drug conjugates for cancer therapy. *MAbs* **6,** 34–45 (2014).
242. Solberg, O. D. *et al.* Balancing selection and heterogeneity across the classical human leukocyte antigen loci: a meta-analytic review of 497 population studies. *Hum. Immunol.* **69,** 443–464 (2008).
243. Takeshita, L. Y. C., Jones, A. R., Gonzalez-Galarza, F. F. & Middleton, D. Allele Frequencies Database. *Transfus Med Hemother* **41,** 10–10 (2014).
244. Balfour, H. H. *et al.* Age-specific prevalence of Epstein-Barr virus infection among individuals aged 6-19 years in the United States and factors affecting its acquisition. *J. Infect. Dis.* **208,** 1286–1293 (2013).
245. Dowd, J. B., Palermo, T., Brite, J., McDade, T. W. & Aiello, A. Seroprevalence of Epstein-Barr Virus Infection in U.S. Children Ages 6-19, 2003-2010. *PLoS ONE* **8,** e64921 (2013).
246. Linton, M. S., Kroeker, K., Fedorak, D., Dieleman, L. & Fedorak, R. N. Prevalence of Epstein-Barr Virus in a population of patients with inflammatory bowel disease: a prospective cohort study. *Aliment Pharmacol Ther* **38,** 1248–1254 (2013).
247. Sauerbrei, A. *et al.* Prevalence of antibodies against influenza A and B viruses in children in Germany, 2008 to 2010. *Euro Surveill.* **19,** (2014).
248. Khan, S. U., Anderson, B. D., Heil, G. L., Liang, S. & Gray, G. C. A Systematic Review and Meta-Analysis of the Seroprevalence of Influenza A(H9N2) Infection Among Humans. *J. Infect. Dis.* **212,** 562–569 (2015).
249. Kaech, S. M. *et al.* Selective expression of the interleukin 7 receptor identifies effector CD8 T cells that give rise to long-lived memory cells. *Nat. Immunol.* **4,** 1191–1198 (2003).
250. Dunne, P. J. *et al.* Epstein-Barr virus-specific CD8(+) T cells that re-express CD45RA are apoptosis-resistant memory cells that retain replicative potential. *Blood* **100,** 933–940 (2002).

251. Wahid, R., Cannon, M. J. & Chow, M. Virus-specific CD4+ and CD8+ cytotoxic T-cell responses and long-term T-cell memory in individuals vaccinated against polio. *J. Virol.* **79,** 5988–5995 (2005).
252. Cannon, M. J., Schmid, D. S. & Hyde, T. B. Review of cytomegalovirus seroprevalence and demographic characteristics associated with infection. *Rev. Med. Virol.* **20,** 202–213 (2010).
253. Snyder, C. M. Buffered memory: a hypothesis for the maintenance of functional, virus-specific CD8(+) T cells during cytomegalovirus infection. *Immunol. Res.* **51,** 195–204 (2011).
254. Meyer, D. L. *et al.* Reduced antibody response to streptavidin through site-directed mutagenesis. *Protein Sci.* **10,** 491–503 (2001).
255. Yumura, K. *et al.* Mutations for decreasing the immunogenicity and maintaining the function of core streptavidin. *Protein Science* **22,** 213–221 (2013).

11. Acknowledgements / Danksagung

An erster Stelle möchte ich mich bei meinem Erstgutachter Prof. Dr. Rienk Offringa für die große Unterstützung und akademische Betreuung über den gesamten Zeitraum der Doktorarbeit sowie die freundliche Aufnahme in seine Arbeitsgruppe während des Praktikums am DKFZ bedanken. Zudem danke ich ihm sowie Prof. Dr. Viktor Umansky und Prof. Dr. Philipp Beckhove für die produktiven wissenschaftlichen Diskussionen und Ratschläge im Rahmen der Zwischenberichte. Des Weiteren danke ich Prof. Dr. Ana Martin-Villalba und Dr. Adelheid Cerwenka für ihre Bereitschaft, als Mitglieder der Prüfungskommission zu fungieren.

Ein großer Dank geht an Dr. Alexander Lifke für die Initiierung des Projektes und die Aufnahme in seine Arbeitsgruppe. Ein besonderer Dank geht auch an Dr. Valeria Lifke, welche mich zu einem späten Zeitpunkt freundlich in ihre Arbeitsgruppe integriert hat. Ich danke sowohl Alexander als auch Valeria für die Einführung in die projektspezifische Thematik sowie für die große Unterstützung jeglicher Art, insbesondere für die äußerst hilfreichen wissenschaftlichen Diskussionen.

Ich möchte mich nochmals speziell bei Prof. Dr. Rienk Offringa, Dr. Alexander Lifke und Dr. Valeria Lifke bedanken, die diese Arbeit Korrektur gelesen haben.

Ein weiterer, besonderer Dank gilt Dr. Lars Hillringhaus und seinen Mitarbeitern, welche die Kopplung und Aufreinigung der ATPP Konjugate durchgeführt haben.

Herzlich bedanken möchte ich mich auch bei Dr. Frank Herting, welcher mich in vielerlei Hinsicht unterstützt und mir mit Rat zur Seite gestanden hat. Bei ihm möchte ich mich zudem für die Unterstützung bei der Planung der *in vivo* Experimente bedanken.

Ein herzlicher Dank gilt Karin Mann und Ildiko Wünsche für die exzellente technische Unterstützung bei diversen Experimenten. Insbesondere möchte ich mich für die große Hilfsbereitschaft bedanken, Experimente oder Zellkulturen weiterzuführen falls ich verhindert war. An dieser Stelle danke ich auch Franz Osl, der meine T Zellkulturen des Öfteren gerettet hat.

Ich möchte zudem Dr. Olaf Mundigl und seiner Arbeitsgruppe, insbesondere Heike Seul und Doris Ziegler-Landesberger, für die Unterstützung bei den FRET- und Timelapse-Experimenten danken.

Ich danke auch Dominique Ostler und Fabian Birzele für die Hilfe bei der Zelltypisierung/-charakterisierung, sowie Theresia Manger-Harasim und Saskia Asmussen für die Unterstützung bei der Zellkultur.

Zudem möchte ich mich herzlich bei Dr. Alexander Lifke, Dr. Valeria Lifke, Franz Osl, Theresia Manger-Harasim und Saskia Asmussen für die Unterstützung und kompetente Hilfestellung bei den *in vivo* Arbeiten bedanken.

Ein weiterer Dank gilt Dr. Gloria Tabares und ihrem Mitarbeiter Dominic Knoblauch für die Analyse der ATPP-Konjugate mittels Massenspektrometrie.

Außerdem danke ich Dr. Christian Lehmann für die freundliche Aufnahme in sein Labor nach der Umstrukturierung.

Ein besonderer Dank gebührt zudem Wilma Ganslmeier und Brigitta Reger für Ihre außerordentliche Hilfsbereitschaft und Motivation, die sie tagtäglich aufbringen, um die Arbeitsabläufe für ihre Kollegen so angenehm und unkompliziert wie möglich zu gestalten.

Des Weiteren möchte ich mich bei Dr. Maria Mertes für die patentrechtliche Überprüfung der Arbeit und ihre Hilfsbereitschaft sowie ihr Verständnis bedanken.

Ein großer, genereller Dank geht an alle Mitarbeiter von Roche pRED, die - vielleicht ohne es zu wissen - einen Beitrag zum Gelingen dieser Arbeit geleistet haben: sei es durch die Inspiration durch wissenschaftliche Diskussionen oder Vorträge, die freundliche Atmosphäre, die stete Hilfsbereitschaft oder die Bereitstellung der vorhandenen Technologien.

Abschließend gilt mein größter Dank meiner Familie und insbesondere meinen Eltern, die mich auf meinem bisherigen Weg stets unterstützt und motiviert haben. Ohne diese Unterstützung wäre diese Arbeit niemals zustande gekommen.

Selbiges gilt für Lisa Stegner, die mir immer zur Seite stand und wohl am meisten unter den Umständen der Promotion (Zeitmangel, Stress und Frustration) leiden musste.